

**ADULT BONE MARROW MESENCHYMAL STEM CELLS PRIMED FOR
THE REPAIR OF DAMAGED CARDIAC TISSUE AFTER MYOCARDIAL
INFARCTION**

by

Edward D. Marks

A dissertation submitted to the Faculty of the University of Delaware in partial fulfillment of the requirements for the degree of Doctor of Philosophy in Medical Sciences

Spring 2017

© 2017 Marks
All Rights Reserved

**ADULT BONE MARROW MESENCHYMAL STEM CELLS PRIMED FOR
THE REPAIR OF DAMAGED CARDIAC TISSUE AFTER MYOCARDIAL
INFARCTION**

by

Edward D. Marks

Approved: _____
Esther Biswas-Fiss, Ph.D.
Chair of the Department of Medical Laboratory Sciences

Approved: _____
Kathleen Matt, Ph.D.
Dean of the College of Health Sciences

Approved: _____
Ann L. Ardis, Ph.D.
Senior Vice Provost for Graduate and Professional Education

I certify that I have read this dissertation and that in my opinion it meets the academic and professional standard required by the University as a dissertation for the degree of Doctor of Philosophy.

Signed:

Arun Kumar, Ph.D.
Professor in charge of dissertation

I certify that I have read this dissertation and that in my opinion it meets the academic and professional standard required by the University as a dissertation for the degree of Doctor of Philosophy.

Signed:

Michael Stillabower, M.D.
Member of dissertation committee

I certify that I have read this dissertation and that in my opinion it meets the academic and professional standard required by the University as a dissertation for the degree of Doctor of Philosophy.

Signed:

William Farquhar, Ph.D.
Member of dissertation committee

I certify that I have read this dissertation and that in my opinion it meets the academic and professional standard required by the University as a dissertation for the degree of Doctor of Philosophy.

Signed:

X. Lucas Lu, Ph.D.
Member of dissertation committee

I certify that I have read this dissertation and that in my opinion it meets the academic and professional standard required by the University as a dissertation for the degree of Doctor of Philosophy.

Signed:

John Rabolt, Ph.D.
Member of dissertation committee

ACKNOWLEDGMENTS

I would like to thank my advisor, Dr. Arun Kumar, and my committee members, Drs. William Farquhar, Lucas Lu, John Rabolt, and Michael Stillabower, for providing me guidance, advice, and humility throughout this endeavor. I would like to also thank the Medical Laboratory Sciences department, specifically Dr. MaryAnn McLane, for providing extensive support and reassurance during this entire period. I would like to thank Lauren Singer, for being a rock with which I can always moor my boat during choppy seas. And finally, I must thank my family, Robyn, David, and Samantha, for their unwavering support and kindness, and for asking insightful questions that taught me how to broadcast my research to a global audience; I could not have finished without you.

TABLE OF CONTENTS

LIST OF TABLES.....	ix
LIST OF FIGURES	x
ABSTRACT.....	xiv

Chapter

1	THE BURDEN OF CARDIOVASCULAR DISEASE AND THE NEED FOR NEW TREATMENT	1
1.1	Introduction.....	1
1.2	Left ventricular remodeling	2
1.3	Patient treatment options	3
1.4	Stem cell treatment options	4
1.5	Mesenchymal stem cells in cardiac repair	5
1.6	Specific aims.....	8
1.6.1	Specific Aim 1: Develop an adjustable rat model of myocardial infarction using multi-dose injections of isoproterenol.	8
1.6.2	Specific Aim 2: Characterize human bone marrow stem cell differentiation on nanofiber scaffolds.....	8
1.6.3	Specific Aim 3: Assess the response of a given infarct to an optimized differentiated hBMSC/nanoscaffold delivery platform.....	8
2	MATERIALS AND METHODS.....	10
2.1	PCL solution formulation	10
2.2	Electrospinning of nanoscaffold	10
2.3	IR nanoscaffold characterization	11
2.4	UV nanoscaffold characterization	11
2.5	Microscopic nanoscaffold characterization	11
2.6	Nanoscaffold preparation.....	11
2.7	Coating degradation from nanoscaffolds.....	12
2.8	Cell culture.....	12
2.9	Nanoparticle preparation	13

2.10	Scanning topographical analysis.....	14
2.11	Microscopic analysis.....	14
2.12	Animals.....	15
2.13	Statistics.....	17
3	DEVELOP AN ADJUSTABLE RAT MODEL OF MYOCARDIAL INFARCTION USING MULTI-DOSE INJECTIONS OF ISOPROTERENOL.....	19
3.1	Abstract.....	19
3.2	Background.....	19
3.3	Methods.....	26
3.3.1	Animals.....	26
3.3.2	Statistics.....	28
3.4	Results.....	30
3.4.1	Isoproterenol injections.....	30
3.4.2	Cardiac damage.....	33
3.4.3	Therapeutic injection optimization.....	34
3.5	Discussion.....	39
4	CHARACTERIZE HUMAN BONE MARROW STEM CELL DIFFERENTIATION ON NANOFIBER SCAFFOLDS.....	42
4.1	Abstract.....	42
4.2	Background.....	43
4.3	Methods.....	45
4.3.1	PCL solution formulation.....	45
4.3.2	Electrospinning of nanoscaffold.....	45
4.3.3	IR nanoscaffold characterization.....	45
4.3.4	UV nanoscaffold characterization.....	46
4.3.5	Microscopic nanoscaffold characterization.....	46
4.3.6	Nanoscaffold preparation.....	46
4.3.7	Coating degradation from nanoscaffolds.....	47
4.3.8	Cell culture.....	47
4.3.9	Scanning topographical analysis.....	48
4.3.10	Microscopic analysis.....	49
4.3.11	Statistics.....	49
4.4	Results.....	51

4.4.1	Nanofiber visualization.....	51
4.4.2	FTIR and UV/Vis characterization.....	53
4.4.3	Cell viability on PCL nanoscaffold.....	55
4.4.4	Coating of nanofiber.....	57
4.4.5	Small molecule WNT pathway modifiers.....	59
4.4.6	Combinatorial differentiation.....	62
4.4.7	Cell maturation.....	64
4.4.8	Extra: Experimental PCL gel formulation.....	66
4.5	Discussion.....	69
5	ASSESS THE RESPONSE OF A GIVEN INFARCT TO AN OPTIMIZED DIFFERENTIATED hBMSC/NANOSCAFFOLD DELIVERY PLATFORM.....	73
5.1	Abstract.....	73
5.2	Background.....	74
5.3	Materials and Methods.....	75
5.3.1	PCL solution formulation.....	75
5.3.2	Electrospinning of nanoscaffold.....	75
5.3.3	Nanoscaffold preparation.....	76
5.3.4	Cell culture.....	76
5.3.5	Nanoparticle preparation.....	77
5.3.6	Microscopic analysis.....	77
5.3.7	Animals.....	77
5.3.8	Statistics.....	80
5.4	Results.....	82
5.4.1	Development of adjustable MI model.....	82
5.4.2	hBMSCs engraft to the myocardium.....	84
5.4.3	Therapeutic benefit of injections is dependent on cardiac damage.....	86
5.5	Discussion.....	89
6	CONCLUSION AND FUTURE DIRECTIONS.....	93
6.1	Background.....	93
6.2	Specific Aim 1.....	94
6.2.1	Conclusion.....	94
6.2.2	Future directions.....	95

6.3	Specific Aim 2	96
6.3.1	Conclusion	96
6.3.2	Future directions	97
6.4	Specific Aim 3	100
6.4.1	Conclusion	100
6.4.2	Future directions	101
6.5	Overall conclusion	104
	REFERENCES	106
Appendix		
	INSTITUTIONAL ANIMAL CARE AND USE COMMITTEE PROTOCOL APPROVAL	126

LIST OF TABLES

Table 1.1:	Animal measurements taken over the full two week study period. No significance was noted at baseline in any animal group. N=4 animals per test; *p<0.05, **p<0.01, ***p<0.001, NS=no significance of samples compared to PBS control; data are mean±SEM. LVIDd, left ventricular internal diameter during diastole; LVIDs, left ventricular internal diameter during systole; LVEDV, left ventricular end diastolic volume; LVESV, left ventricular end systolic volume; FS, fractional shortening; EF, ejection fraction.	87
------------	---	----

LIST OF FIGURES

Figure 1.1:	General strategy for BMSC differentiation and intracardiac injections. ...	9
Figure 3.1:	Tying off the LAD results in downstream ischemia and necrosis.	22
Figure 3.2:	Subcutaneous administration of isoproterenol results in left ventricular accumulation of isoproterenol and catecholamines, leading to uncontrolled metabolism and cardiomyocyte contraction, and eventually ischemia.	25
Figure 3.3:	Evidence for adjustable MI model. Increasing myocardial damage can be seen both in H&E tissue staining (left images) and ultrasound details (right images) as the concentration of isoproterenol increases. ...	29
Figure 3.4:	Comparison of small (10mg/kg), medium (100mg/kg), and large (150mg/kg) doses of isoproterenol on cardiac metrics and scar formation. Arrows show points of collagen scar formation. LVESV, left ventricular end systolic volume; FS, fractional shortening; EF, ejection fraction.	32
Figure 3.5:	Attempted strategies for intracardiac injections using endoscope visualization. A. Intraperitoneal injections allowed for apex visualization through the diaphragm. B. Intrathoracic injections allowed direct visualization of the left ventricle and atria of the heart. ...	36
Figure 3.6:	Ultrasound guided intracardiac injection. Schematic (left) of the hypothesis, and direct ultrasound image (right) of the actual therapeutic injection.	38
Figure 4.1:	Microscopic visualization of PCL nanoscaffold. A. Linear aligned PCL. Scale bar=200um. B. Randomly aligned PCL. Scale bar=200um. C. AFM visualization of a nanofiber bundle, showing fiber width averaged 257 ± 48 nm.	50

Figure 4.2:	IR/UV characterization of nanoscaffold. A. FTIR of PCL (inset) with characteristic peaks labeled. B-D. PCL mixed with 0.1mg/mL Evan's blue as UV contrast. B. Pure PCL dissolved in DMSO; major peak at 600nm. C. Pure PCL and pure gelatin, both dissolved in DMSO, run separately. Major peak changes at 600nm. D. Pure PCL and pure gelatin, both dissolved in DMF, run separately. Gelatin peak stays at 600nm, but PCL blueshifts to 430nm.	52
Figure 4.3:	Cell viability on a strengthening nanoscaffold. A. Fluorescent images of cells on linear and random nanoscaffolds. Red, actin; blue, DAPI. Scale bar=200um. B. SEM close-up of individual cells. Scale bar=10um. C. Lengthening of cells across the nanoscaffold. Linear nanoscaffolds usually held significantly less cell mass. Scale bar=50um (linear), 100um (random). D/E. Topographical analysis of cells covering random nanoscaffold. Cells tended to clump in certain areas (red), leading to gaps in other areas (dark blue). F. Cells contributed to increasing strength of the nanoscaffold over time, indicated with uniaxial strength test.	54
Figure 4.4:	Effect of Tβ4 on cell growth and differentiation. Nanoscaffold coating with Tβ4 produces combined peaks from the protein component (inset) and underlying nanoscaffold architecture. Tβ4 produces minimal differentiation of hBMSCs to the cardiac lineage after one week. Both hBMSC growth and cardiac biomarker expression are significantly enhanced when grown on nanoscaffolds coated with Tβ4 compared to control. *p<0.05; **p<0.01; Scale bar=200um. Graphs adapted from Kumar, et al. 2014 ¹⁰⁰	56

- Figure 4.5: Proposed hypothesis of hBMSC differentiation mechanism of action via WNT-effecting small molecules. Importantly for cardiomyocyte differentiation, the noncanonical pathway causes surges in intracellular Ca²⁺, resulting in cytoskeletal rearrangement, inhibition of βcat translocation (thus blocking the canonical pathway), and upregulation of the PKC and NF-AT pathways. Dvl 1/2/3 also significantly increases MAPK signaling, promoting cell survival to insults such as osmotic stress and proinflammatory cytokines, and increasing gene expression for tasks such as proliferation, differentiation, and mitosis. Pathways shortened for clarity. Pcn, porcupine; Wnt, wingless; LRP, lipoprotein receptor-related protein; Dvl, disheveled; GSK, glycogen synthase kinase; APC, adenomatous polyposis coli; βcat, β-catenin; TCF, transcription factor 7 variant; PCP, planar cell polarity; PLC, phospholipase C; PKC, protein kinase 3; NF-AT, nuclear factor of activated T-cells; CamKII, Ca²⁺/calmodulin-dependent protein kinase II; NLK, nemo-like kinase; MAPK, mitogen activated protein kinases.....58
- Figure 4.6: Comparing WNT effectors IWP-2 and CHIR99021. A. FTIR output of nanoscaffold coated in 20um IWP-2. B. FTIR output of nanoscaffold coated in 20um CHIR. Note the distinct peaks between the two small molecules, but the same peaks for the underlying PCL nanoscaffold. C. Coating efficiency of various concentrations of Tβ4 and small molecules. D. The amount of degradation per week of concentrations of Tβ4 and small molecules, calculated from FTIR peaks of remaining material. E. Total time until complete degradation of each of the small molecules and Tβ4 per week, calculated from D. F. Molecular staining of β-catenin (top) and RhoA (bottom) demonstrating targeted effects on the WNT pathway. G. Calculations of positive staining area in F.61
- Figure 4.7: Synergistic effects of IWP-2 vs CHIR99021 in BMSC differentiation. IWP-2/Tβ4 significantly outperforms CHIR99021/Tβ4 in differentiating BMSCs to the cardiac lineage, as demonstrated by cardiac biomarker staining for α-actinin, troponin I, and desmin. Cell survival was also significantly increased. Scale bar=200um; *p<0.05; **p<0.01; ***p<0.001.....63
- Figure 4.8: Evidence of BMSC cardiac maturation with IWP-2. A/B. Decreasing ANP staining over time indicates the transition from atrial to ventricular cardiomyocytes. C. Positive Cnx43 staining, allowing hBMSCs to communicate with native cardiomyocytes via ion channels. D. Positive tropomyosin staining.....65

Figure 4.9: Experimental PCL gel. A-C. Coating a stained paper towel in PCL gel resulted in far less stain dissolving into dH ₂ O. D. dH ₂ O solutions after paper towel soaking. PCL gel (yellow) had significantly decreased stain peaks compared to control (green). E. Troponin differentiation indicated. Scale bar=200um. F. No positive desmin staining was found. Scale bar=200um.	68
Figure 5.1: Representative ultrasounds. Arrows show left ventricular interior diameter during systole (small arrow) and diastole (large arrow), which are used to calculate cardiac metrics.	81
Figure 5.2: NP formulation and addition to cells. A. TEM of NPs showing uniform size. B. DLS graph(s) of NPs formulation. Washing and rinsing through 0.1um pore sized filters resulted in consistent sub-100nm particles. C. Rinsed nanoparticles were transfected to BMSCs in culture. No effect was seen on differentiation potential.	83
Figure 5.3: Cellular injections stayed in the heart after 2weeks. A. Schematic image demonstrating injection strategy. B. Positive staining for SRY protein (green, indicated by white arrowheads) and NPs (navy, indicated by blue arrowheads) in the same area shows cells stayed in the heart. C. Injected cells spread through spaces in myocardial tissue caused by increasing cardiac damage allowing collections of cells to be found beneath the epicardial membrane despite being injected into the ventricle. Blue, nanoparticles/cells; red, cardiac actinin; e, epicardium.	85
Figure 5.4: Therapeutic injections prevent LV remodeling and improve cardiac function. Despite lack of statistical significance, therapeutic injections increased FS and EF over PBS control in all cases (see graphs). N=4 animals per test; red line= control sample means; *p<0.05, **p<0.01, ***p<0.001 of samples compared to PBS control ; data are mean±SEM. LVESV, left ventricular end systolic volume; FS, fractional shortening; EF, ejection fraction.	88

ABSTRACT

The burden of cardiovascular disease around the world is growing, despite improvements in hospital care and time to treatment. As more people survive an initial myocardial infarction (MI), the decompensated heart tissue is strained, leading to heart failure (HF) and an increased risk for a second MI. While extensive progress has been made in treating the symptoms after MI, including HF and angina, little success has come from repairing the damaged heart tissue to alleviate the progression to these end-stage symptoms. One promising area of regenerative research has been the use of adult stem cells, particularly from the bone marrow (BMSCs). These cells can differentiate towards the cardiac cell lineage in vitro while producing trophic factors that can repair damaged tissue. When placed in the heart after MI though, BMSCs have mixed results, producing profound changes in some patients but zero or even negative effects in others. In this report, we used BMSCs as a stem cell base for a regenerative medicine system for the repair of damaged cardiac tissue. These cells are seeded on a polycaprolactone nanoscaffolding support system, which provides a growth substrate for in vitro work, as well as a housing system for protected in vivo delivery. When the nanoscaffold is pre-coated with a novel combination of a cardiac protein, thymosin β 4 (T β 4), and a small molecule effector of the WNT protein pathway, IWP-2, BMSCs differentiated towards the cardiac lineage in as little as 24hours. When injected into rat hearts that have been given an ischemic MI, the nanoscaffolding system slowly dissolves, leaving the cells in place of the damaged cardiac tissue. After two weeks of

monitoring, BMSCs are present within the damaged hearts, as evidenced by immunofluorescence and nanoparticle tracking. Injections of the nanoscaffolding/cell system led to robust healing of the rat hearts that had been given small- and medium-damage heart attacks, outperforming PBS sham and cell culture media injections. Significant improvements in cardiac metrics, including ejection fraction and left ventricular end systolic volume, were seen compared to untreated animals, and were comparable to healthy controls. To our knowledge this is the first side-by-side comparison of cell culture media and stem cells to heal a predefined range of MI damage. We believe this simple, inexpensive treatment option is a new beneficial step towards healing damaged patient tissue after MI.

Chapter 1

THE BURDEN OF CARDIOVASCULAR DISEASE AND THE NEED FOR NEW TREATMENT

1.1 Introduction

The circulatory system, first described in English physician William Harvey's seminal work "On the Motion Of the Heart and Blood In Animals" published in 1628, pumps approximately 5 liters of blood per minute around the body (termed cardiac output, CO). As the heart beats faster through such physiological drivers as exercise or stress, CO can significantly increase and over time the heart muscle cells (cardiomyocytes) begin to hypertrophy to compensate for the increased pressure against which the heart pumps. This natural process of cardiac hypertrophy is beneficial for many athletes, but hypertrophy can also be of genetic or pathological origin. For example, autosomal dominant inheritance of the gene causing familial hypertrophic cardiomyopathy can lead a healthy athlete's heart muscle to appear clinically similar to someone who has had a massive heart attack¹. In young athletes, this condition can lead to sudden cardiac death (SCD), where the increased strain on the heart from exercise causes the individual to die on the playing field, despite defibrillation.

In pathological hypertrophy, the heart is compensating for an issue that is usually slow growing. For example, progressive hypertension as a result of increased arterial stiffness leads to increased left ventricular (LV) pressure; this forces cardiomyocytes to increase contractile forces that can ultimately lead to their

hypertrophy. These hallmark symptoms of heart disease coupled with arterial plaque buildup often lead to myocardial infarctions (MI), in which the body is unable to pump oxygenated blood to sections of the heart muscle tissue^{2,3}. As the cardiomyocytes lose their blood supply during ischemic MI, they begin to die. Reperfusion of the cardiac tissue can decrease the extent of dead cardiomyocytes, but only if performed ≤ 2 hrs after symptom onset⁴; this is very difficult considering transport times from first medical contact to surgical intervention.

1.2 Left ventricular remodeling

The resulting ventricular remodeling leading to lack of contractile tissue after MI is due to the extremely slow proliferation rate of cardiomyocytes. As shown by Bergman, et al.⁵, cardiomyocytes mainly derive from division of preexisting cardiomyocytes, meaning cell death as a result of MI decreases the progenitor pool from which proliferation can occur. Even with surgical intervention within 24hrs of symptom onset, the heart begins the process of fibrotic scar tissue formation⁶. Following the initial ischemic event in which the cardiomyocytes do not receive ample blood supply for proper contractile function, the heart moves into the necrotic phase. This is indicated pathologically by intracellular edema, evidenced by wavy active fibers within cardiomyocytes, then dead muscle cell clearance by the action of matrix metalloproteinases^{7,8}. Infarct area increases as immune cells clear more dead tissue, and longitudinal and circumferential ventricular stiffness increase as the beginnings of a collagen scar are laid in place of the removed contractile tissue⁹. Risk of ventricular rupture is highest at this point, as the increasing cardiac pressure may overload the nascent scar.

Collagen deposition leads the heart to the fibrotic stage of healing. Here, fibroblast-derived collagen type III lays a foundational scaffold for much larger, thicker, anisotropically aligned collagen type I¹⁰; ventricular stiffness increases linearly with the increased deposition of collagen¹¹. This non-contractile collagen scar decreases compliance (“stretch”) of the LV resulting in decreased chamber filling and impaired functions of the non-infarcted (healthy) myocardium¹².

The final and longest stage of healing after an infarct is the remodeling phase. This usually begins approximately 6 weeks after the initial infarct (in humans; rats are closer to 1 week), and can extend indefinitely, as the scar tissue is biologically active and thus constantly in flux¹³. Depressed diastolic function due to poor scar compliance (brought on by increased collagen cross-linking^{14, 15}) eventually leads to cardiac dysfunction as the remaining contractile cardiomyocytes become hypertrophic; particularly in large infarcts, this pathology eventually presents as heart failure (HF)¹⁶.

1.3 Patient treatment options

There is a notable dearth in the options available to patients at risk of cardiac disease. New biologics such as Praluent (alirocumab; Sanofi, Regeneron) and Repatha (evolocumab; Amgen) decrease heart attack risk by blocking the PCSK9 gene, significantly decreasing blood cholesterol and thus the buildup of arterial plaques^{17, 18}. Standard of care for HF has remained fairly stable over time; the most recent improvement has been the approval of Entresto (sacubitril and valsartan; Novartis), a combination neprilysin inhibitor/angiotensin II receptor blocker for patients in chronic HF with ejection fraction (EF) <35% (about half the normal EF)¹⁹.

Combined with diet and exercise, pharmacological cardiac medicine is preventative, not reparative. PCSK9 inhibitors prevent further MI, and Entresto or

diuretics prevent further myocardial deterioration by decreasing the pressure on the left ventricle. There are currently no drugs or treatments available to increase regrowth of contractile cells^{20,21}, or to prevent infarct expansion following MI. As of 2015, 735,000 people in the United States had a heart attack annually³, leading cardiovascular disease (CVD) to be the nation's top cause of death. In 12 major European countries, heart disease has only very recently been overtaken by cancer as the number one killer²²; still, over 4million people in Europe die of CVD each year, and CVD causes the most deaths worldwide.

1.4 Stem cell treatment options

To combat the issues of increasing patient deaths and a lack of immediate reparative care for MI, research has begun investigating the therapeutic, regenerative value of stem cells. Stem cells fall into three main groups: embryonic; adult, including mesenchymal and cKit+; and more recently induced pluripotent (iPSCs). Embryonic stem cells and iPSCs are useful because they can turn into any cell type from the three embryonic germ layers, significantly improving their therapeutic potential. These properties allow researchers to model diseases of any cell type in vitro without having to move through costly and time consuming animal experiments. iPSCs are especially useful for disease model development, as the stem cells are derived from patient tissue, meaning diseases such as cardiac congenital malformations can be recapitulated on a genetic and cellular level.

There are drawbacks to these cell types. Embryonic stem cells come with ethical baggage, having formerly led to a moratorium on new embryonic stem cell line development in the early 2000s²³. Both embryonic and iPSCs currently take months to differentiate to the cell type of interest, and then need to be purified to ensure only

differentiated cells are given to patients. If purification is done incorrectly (or not at all), undifferentiated stem cells injected into animals may form teratomas after interacting with and receiving signals from in vivo tissue²⁴. While extremely promising, neither of these cell types are currently ready for therapeutic human use.

For this reason, adult stem cells have become the cell type of choice for cardiac clinical trials aimed at repairing damaged cardiomyocytes and improving cardiac function in patients after MI or during HF²⁵. Most adult stem cells can be extracted easily from patients and provide a large enough starting cell population to expand into treatments for multiple patients. Adult stem cells can also be recruited endogenously from the peripheral system or from a target organ, particularly in the heart, liver, and kidneys, which all have resident stem cell populations²⁶. For example, Ellison, et al., building on an initial report by Orlic from 2001²⁷, recently proved in a mouse model that the adult heart contains resident cKit⁺ cardiac stem cells that can repair damaged tissue and prevent progression to HF after myocardial stunning²⁸ (a small ischemic event, most often in the LV, that causes little damage initially but can be fatal if recurring). The group is currently searching for small molecules that may be able to recruit these endogenous cells in humans.

1.5 Mesenchymal stem cells in cardiac repair

By far the most common cell type translated into clinical trials is the mesenchymal stem cell (MSC), with 493 clinical trials ongoing or completed as of 2015²⁹. MSCs are found throughout the body, including the bone marrow, adipose tissue, and skeletal muscle. They are multipotent, in that they can turn into multiple cell types derived from the mesoderm, including muscle, bone, and fat. They have also been found to be immune evasive, meaning they subvert notice by the immune system

by developing a protective microenvironment in vivo³⁰, and exogenous human bone marrow stem cells (hBMSCs) in particular increase cytotoxic T cells without inducing tissue damage, while decreasing lymphocytes and other antigen-presenting cells^{31, 32}. This immune subversion is thought to convert the cardiac microenvironment to a non-inflammatory state by decreasing the M1:M2 macrophage ratio, preventing scar expansion and sparing healthy myocardium from immune attack.

There is still much debate concerning the role of MSCs in cardiac repair, and whether the term “repair” is even warranted. Numerous studies demonstrate improved cardiac function after intravenous infusion of MSCs or injections directly into the LV wall³³⁻³⁶, but a recent meta analysis claimed that most positive clinical effects are unfounded, resulting from poor statistical work or outright fraud³⁷. Delivery is also an issue as MSCs are much larger than small molecules and proteins and can become compacted within vessels or catheter tubes^{36, 38}; for IV delivery, the highest payload to reach inflamed tissue has not exceeded 25% of injected cells³⁹. Finally, there is debate on how the MSCs exert a therapeutic benefit, since research has both confirmed^{40, 41} and rejected⁴² the hypothesis that MSCs differentiate to functioning cardiomyocytes in vivo. It has long been known through in vitro biomarker studies that MSCs can differentiate to the cardiac lineage but cannot become fully differentiated cardiomyocytes⁴³.

Because of their superior safety profile, ease of use, and potential efficacy, MSCs are continuously studied and used as a potential therapy for MI. Two main reasons are keeping the hope alive for MSCs as a future therapy: paracrine factors; and scaffolding technology.

MSCs, particularly from the bone marrow (BMSCs), are recruited to sites of inflammation and injury through chemokine signaling^{26, 38, 44}. In certain instances such as cartilage and bone injury the BMSCs can differentiate directly in to the tissue of interest to repair some portions of the damaged area. In other injured organs such as the brain and heart BMSCs cannot permanently bind to the tissue of interest and then differentiate, but they stick around long enough to release paracrine factors that recruit cells to heal the organ. For example, BMSCs recruited to damaged heart tissue release paracrine factors to induce an environmental change from an inflammatory to “resolving” environment (M1 to M2 macrophage shift), and promote the heart’s release of factors like thymosin β 4 which increase neovascularization^{45, 46}. There is little evidence that BMSCs stay in the target organ after they have induced this environmental inflammatory shift, but if BMSCs are blocked from the target area of inflammation repair is delayed and resulting tissue loss and scar formation is significantly increased⁴⁷.

Because the biological proof of BMSC retention within organ systems is tenuous at best, researchers have more recently sought to synthetically manage the transit time and staying power of BMSCs within organ systems. As an example, congenital cardiac defects affect ~5% of children born within the United States each year. These issues range from mild cardiomyopathy to immense malformations of atria or ventricles⁴⁸. No amount of endogenous BMSC recruitment will stimulate repair of these defects, so researchers have used solid gel materials as a form of plug within the fetal heart to cap holes between atria and/or ventricles. One type of plug, made of biologically soluble chitosan and polycaprolactone (PCL), slowly dissolves to release BMSCs or pre-differentiated cardiac cells and stimulatory factors; the cells

seed the surrounding tissue to lessen the hole, and the stimulatory factors recruit new BMSCs and immune cells to help repair the damage⁴⁹. Other research, including results presented herein, demonstrate the ability of BMSCs to grow on and within biocompatible nanoscaffolding for weeks at a time. When the nanoscaffolding/cell matrix is transplanted to damaged tissue, these cells still release their healing factors but do not get swept away and released as the environment changes. This continued presence of BMSCs significantly increases healing of the target organ⁵⁰⁻⁵².

1.6 Specific aims

With these facts and considerations in mind, we chose to explore the hypothesis that BMSCs housed within a nanoscaffolding system can efficiently repair a rat heart that has suffered a myocardial infarction. Additionally, because of the discrepancies in the field, we sought to determine at what level of cardiac damage the stem cell/nanoscaffolding system provides the greatest therapeutic benefit. Three main obstacles within the study design became three Specific Aims that form the basis for this dissertation:

1.6.1 Specific Aim 1: Develop an adjustable rat model of myocardial infarction using multi-dose injections of isoproterenol.

1.6.2 Specific Aim 2: Characterize human bone marrow stem cell differentiation on nanofiber scaffolds.

1.6.3 Specific Aim 3: Assess the response of a given infarct to an optimized differentiated hBMSC/nanoscaffold delivery platform.

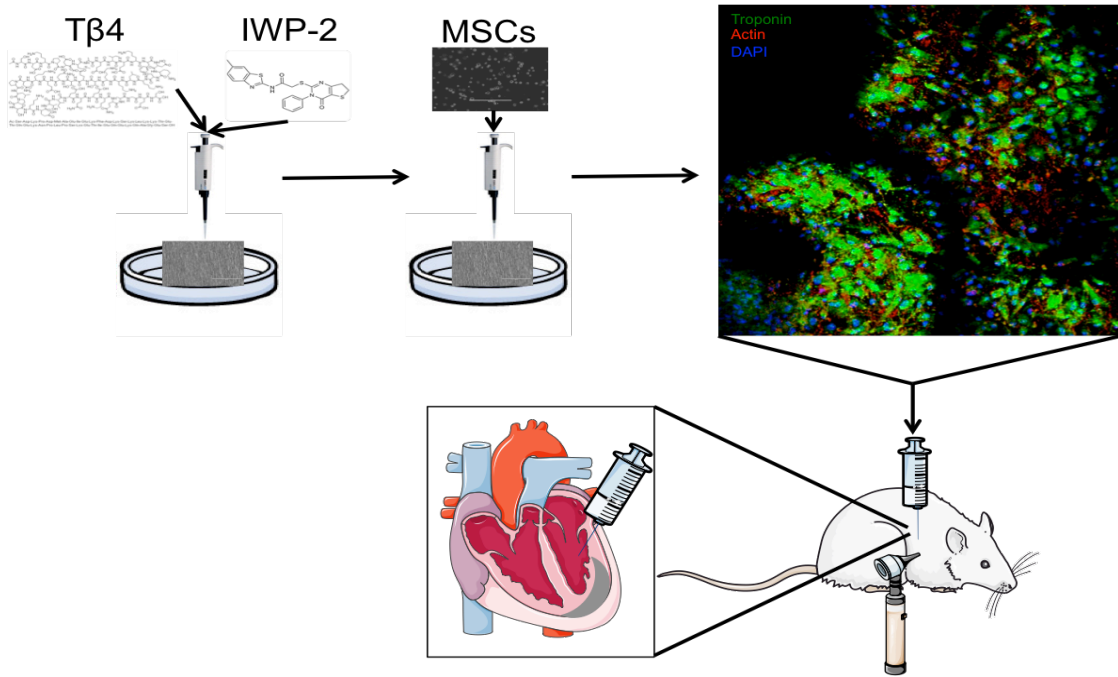


Figure 1.1: General strategy for BMSC differentiation and intracardiac injections.

Chapter 2

MATERIALS AND METHODS

2.1 PCL solution formulation

PCL tablets were purchased from Sigma Aldrich (Missouri, USA). Dichloromethane (DCM) and N,N-dimethylformamide (DMF) were purchased from Acros Organics (Geel, Belgium). PCL tablets weighing 1.5g were dissolved in a solvent mixture containing a 1:4 ratio of DCM to DMF. This combination was sonicated for 1hr to ensure tablets were fully dissolved.

2.2 Electrospinning of nanoscaffold

The DCM/DCF/PCL solution was suctioned into a syringe and attached to a flow rate controller (Thermo Fisher Scientific, Massachusetts, USA). The solution was pumped at a flow rate of 0.5mL/h. A Voltmeter lead was attached to the syringe needle and another lead was attached to a rolling drum (Oriental Motor, Tokyo, Japan) that housed an aluminum sheet. The rolling drum was mounted on an E7 Limo easy linear motion controller (Oriental Motor) for linear and rotational fiber distribution. The Human Machine Interface (Omron, Kyoto, Japan) was set at a 3hr run time, a starting position of 105mm, and a rolling drum speed of 630RPM. A potential of 12kV was applied between the spinneret and grounded collector located 12cm below the spinneret to pull the solution from the syringe and accurately align the fibers to the rolling drum mounted on the E7 Limo.

2.3 IR nanoscaffold characterization

A Nicolet iS5 spectrometer with an iD1 Transmission adapter (Thermo Fisher Scientific, Massachusetts, USA) was used to perform Fourier transform infrared spectroscopy (FTIR). Fiber bundles were measured to determine characteristic peaks relating to bond stretching and rocking, using air as a background. The FTIR analysis was performed over a wave number range between 4,000 and 400 cm^{-1} at a 2 cm^{-1} resolution.

2.4 UV nanoscaffold characterization

An Evolution 220 UV-Vis Spectrophotometer (Thermo Fisher Scientific, Massachusetts, USA) was used to determine absorption peaks along the UV spectrum. Samples were dissolved in DMSO or DMF, and mixed with concentrations of Evan's blue (see Chapters for specific ratios) for purity assessment.

2.5 Microscopic nanoscaffold characterization

A Bioscope Catalyst Atomic Force Microscope (Bruker, Massachusetts, USA) was used for nanofiber diameter measures. Samples were mounted in a petri dish and submerged in PBS. The AFM tip was placed on the sample with measurements of Vert -0.2 \rightarrow 0.3, and Horiz as close to 0 as possible. The tip was Navigated with onscreen software, and withdrawn and repositioned if necessary.

2.6 Nanoscaffold preparation

Electrospun PCL nanoscaffolds were adhered to square 20 mm^2 coverslips by adhesive silicon type A glue (NuSil Technology, California, USA). Cover slips with nanoscaffolds were transferred and attached to the base of 6- or 12-well culture plates (Thermo Fisher Scientific, Massachusetts, USA) with silicon glue. Nanoscaffolding

and cover slip were then sanitized as follows: 1mL bleach wash for 5min, rinse with ultrapure water (Millipore, Massachusetts, USA), repeat; 1mL ethanol wash for 5min, rinse with ultrapure water, repeat; nanoscaffolding was left under UV light to dry.

Confirmatory experiments (September 2013-April 2014): After drying, nanoscaffolds were coated with 0.1% polylysine aqueous solution for 4 to 6hrs prior to cell seeding. Treated nanoscaffolds were coated with thymosin β 4 (T β 4; PeproTech, New Jersey, USA) solutions at concentrations of 0.5-7.5% w/v.

Optimization experiments (May 2014-March 2015): 100 μ L of 2%, 4%, or 10% concentrations of T β 4 stock in ultrapure water were mixed with either 100 μ L of 20 μ M, 40 μ M, or 100 μ M concentrations of CHIR99021 or IWP-2 stocks (StemCell Technologies, Vancouver, Canada) in ultrapure water. Resulting 200 μ L solutions were used to coat the nanoscaffolds and allowed one hour to dry.

2.7 Coating degradation from nanoscaffolds

Coated nanoscaffolds were examined using FTIR to determine the rate of degradation of coated compounds (T β 4, CHIR99021, IWP-2) from acellular scaffolds. Dry uncoated PCL, cell culture media, and solutions of T β 4, CHIR99021, or IWP-2 were used as positive controls for FTIR peaks. Decreasing amine peaks in the 3500 cm^{-1} range were used to calculate compound degradation rates from the nanoscaffold.

2.8 Cell culture

Human bone marrow mesenchymal stem cells (hBMSCs) were purchased from StemCell Technologies (Vancouver, Canada) and passaged in MSC Basal Medium (StemCell Technologies) with MesenCult Stimulatory Supplements (StemCell Technologies) to prevent differentiation. hBMSCs were seeded at a concentration of

7.5-10×10⁴ cells/mL over nanoscaffolds coated with Tβ4 and/or CHIR99021 or IWP-2, and covered with MSC Basal Medium (StemCell Technologies) without supplementation to allow differentiation. Cells were incubated in a Forma SteriCycle CO₂ Incubator (Thermo Fisher Scientific, Massachusetts, USA) at 36.5°C and 5.0% CO₂. After 24hrs-1week, media was removed, cells were fixed in 4% paraformaldehyde in PBS for 18min, and washed 3x for 3min each in PBS. Cell differentiation was monitored with the Cardiomyocyte Characterization Kit (Millipore, Massachusetts, USA) using the following dilutions: anti-desmin Ab, 1:100; anti-troponin I Ab, 1:100; anti-α-actinin Ab, 1:200. Other antibodies used: anti-CD105 1:75; anti-ANP 1:200; anti- Cnx43 1:200; anti-β-catenin 1:200; anti-RhoA 1:200. Donkey anti-rabbit or anti-mouse 2^o Ab at 1:200 (Pierce Antibodies, Massachusetts, USA) was overlaid for protein visualization. Cells were counterstained for F-actin using ActinRed 555 Ready Probes (Life Technologies, California, USA) and nuclei with NucBlue Molecular Probes stain (Life Technologies), as per company protocol (2 drops stain for every 1mL PBS; incubate 20min). Cultures were washed in PBS and mounted in ProLong Gold Antifade mount (Thermo Fisher Scientific, Massachusetts, USA).

2.9 Nanoparticle preparation

0.5g Fe II was mixed with 1.0g Fe III in 6mL diH₂O and stirred for 1hr at 1200RPM. Supernatant was removed and particles washed in ethanol 3x. Ethanol was allowed to evaporate, particles were resuspended in PBS, and spun down. The supernatant was removed, particles were resuspended, and run through a 0.1µm filter. The filtrate was resuspended in 1-2mL PBS with a ratio of 1uL Lipofectamine:1mL of

cell culture media. NP/PBS/Lipofectamine was added to cell culture flasks 24hrs prior to seeding on nanoscaffolds.

2.10 Scanning topographical analysis

A ContourGT-X 3D Optical Microscope (Bruker, Massachusetts, USA) was used to scan a fiber area of $76,800\mu\text{m}^2$ ($320\mu\text{m} \times 240\mu\text{m}$). Average roughness values across the sample were used to produce a topographical output. The cover slip on which the nanoscaffold was mounted was used as a starting $0\mu\text{m}$ value, assuming a flush contact.

Scanning electron microscopy (SEM) was performed to examine acute topography. Fibers and cells were mounted on aluminum mount-M4 sample holders (Electron Microscopy Sciences, Pennsylvania, USA) and placed in a Denton Bench Top Turbo III vacuum chamber (Denton Vacuum, New Jersey, USA) for sputter coating with a 50:50 mix Au:Pd to aid visualization. Samples were placed into the SEM (Hitachi S4700, Hitachi High Technologies, Tokyo, Japan) and images were taken from 10x to 3000x.

2.11 Microscopic analysis

An EvosFL Cell Imaging System (Life Technologies, Carlsbad, CA) was used to monitor cell growth and determine preliminary cell counts. Cells were washed and stained as described, and placed on the microscope stage. An image was taken, and the Toolbar function was used to place a hemocytometer grid on the screen for cell counts.

For higher quality images, a Zeiss 5 LIVE DUO Highspeed/Spectral Confocal microscope (Zeiss, Gena, Germany) was used. 8x image averages were taken with

10x-25x lenses to produce a final image; Z-stack was performed periodically to determine the extent of cell infiltration within the nanoscaffold matrix.

2.12 Animals

IACUC: Initial Institutional Animal Care and Use Committee approval was given via protocol AUP#1273. Initial training was provided under preliminary non-survival protocols for heart attack induction, ultrasound, exploratory surgery, arthroscopic camera imaging, and cardiac injections. Final protocol (AUP#1301) was approved in late March 2016; experiments began on 2month old female Sprague Dawley rats (Envigo, Maryland, USA) in April 2016. No protocol was long enough to necessitate eye drops or a heating pad. No dietary manipulations were induced. Clinical parameters that necessitated euthanasia, including sluggishness that impedes eating or drinking, weight loss exceeding 20%, hunched posture, or serious infection, were used to determine if animals should not continue through the full course of experimentation.

Heart attack induction: Isoproterenol (ISO; Sigma Aldrich, Missouri, USA) was dissolved in PBS at concentrations ranging from 10mg ISO per kg rat body weight (mg/kg) to 150mg/kg, with lower concentrations corresponding to a less severe heart attack. ISO was dissolved in a sterile rubber capped vial at volumes dependent on number of animals in the protocol (no more than 5mL at any one time). Solutions were kept for no longer than 2weeks, as ISO is light sensitive. To induce the heart attack, rats were anesthetized with isoflurane through a nose cone, level 4 for induction, level 2 for maintenance. Injections of ~100uL (dependent on ISO concentration and rat weight) were made subcutaneously at the base of the neck. Long acting (72hr) buprenorphine was given directly following injection; short acting (24hr)

buprenorphine was given as needed for the remaining protocol period. Rats were monitored for 1hr after injection to ensure no adverse effects; subsequent checkups occurred 3x daily for 1week.

Ultrasound: Rats were anesthetized with isoflurane through a nose cone, level 4 for induction, level 2 for maintenance. The left thoracic region was shaved to aid visualization. Ultrasound gel was placed on the shaved area and on the ultrasound probe. The probe was placed parallel to the ribs with the rat laying on its right side. Standard images were taken in M-mode; blood flow images were taken using the Doppler setting. Rats were monitored for 1hr following ultrasound to ensure no side effects from prolonged anesthesia. Left ventricular interior diameter during diastole (LVIDd) and systole (LVIDs) were measured using ultrasound readouts. The following calculations were then performed to determine cardiac function (FS: fractional shortening; LVESV: left ventricular end systolic volume; LVEDV: left ventricular end diastolic volume; EF: ejection fraction):

$$FS\% = 100 * ((LVIDd - LVIDs) / LVIDs)$$

$$LVESV = (7 / (2.4 + LVIDs)) * (LVIDs^3)$$

$$EF\% = 100 * ((LVEDV - LVESV) / LVEDV)$$

Intra-cardiac injections: 48hrs after ISO injections, rats were anesthetized for standard ultrasound just prior to intra-cardiac injections. 1mL syringes (20-24G) were loaded with 100uL of either PBS, cell culture media only, or cell culture media + nanoscaffold containing hBMSCs. The heart was detected manually by feeling for the 4th intercostal space of a rat laying on its right side. Needle puncture occurred in the 2nd intercostal space and moved from the upper left hypochondriac region to the

middle epigastric region to puncture the left ventricle of the rat heart. Aspiration of pumping blood prior to injection ensured placement within the left ventricle and not the body cavity. The syringe contents were then slowly dispensed into the left ventricle cavity and the needle removed from the body. Rats were monitored directly for 1hr after injection to ensure no immediate adverse effects; subsequent checkups occurred 3x daily for 1week.

Euthanization: After 2weeks animals were euthanized via intraperitoneal injection of Euthazol solution. Death was confirmed by tail and toe pinch, and lack of breathing. Animals were then necropsied, with heart removed. Other organs, such as kidneys, liver, and lungs, were also removed.

Tissue imaging: Hearts were flash frozen in liquid nitrogen and stored at -80°C. Frozen hearts were placed in a Leica 3050 Cryostat (Leica, Wetzlar, Germany), sliced at 10µm, and mounted on glass slides. Slides were stained for immunofluorescence as described above (fixed in PFA, washed in PBS, 1^o anti-SRY at 1:200, 2^o donkey anti-mouse at 1:200) and imaged via Zeiss 5 LIVE DUO Highspeed/Spectral Confocal microscope (Zeiss, Gena, Germany). Slides were stained for nanoparticles using proprietary reagents from HEMATOGNOST Fe® kit (Millipore, Massachusetts, USA). Slides were stained with H&E as per DBI protocol. H&E and nanoparticle slides were imaged using Axioplan 2 Upright Light Microscope (Zeiss, Gena, Germany) with top-mounted AxioCam camera and software (Zeiss).

2.13 Statistics

The statistical significance of the results was determined using analysis of variance (ANOVA) and a multiple means comparison function (t-test) in

JMP/GraphPad Prism with an alpha level of 0.05. All error bars are reported in mean \pm standard error from the mean. N is dependent on experimental protocol.

Animal numbers: The statistics and pilot studies indicate approximately 120 animals were needed to complete the initial experiment. Attrition in the pilot studies necessitated an increase in the number of animals per group; the statistics indicated $n=4/\text{sample}$ with 4 samples/group = 16 rats/group, but we elected to increase by 0.66 to ensure enough rats for statistical viability in the results.

Chapter 3

DEVELOP AN ADJUSTABLE RAT MODEL OF MYOCARDIAL INFARCTION USING MULTI-DOSE INJECTIONS OF ISOPROTERENOL

3.1 Abstract

Myocardial infarction (MI) produces a highly ischemic environment resulting in extensive cardiomyocyte death and recruitment of pro-inflammatory immune cells, prior to left ventricular remodeling and scar tissue formation. Multiple animal models exist to recapitulate this process, each with their own advantages and disadvantages. With the therapeutic goal of being as non-invasive as possible, we have used subcutaneous injections of various doses of isoproterenol to induce an ischemic MI targeting the left ventricle of a rat heart. The injection volume and concentration were optimized to induce appropriate cardiac damage, and results were assessed via ultrasound and tissue staining. We were able to successfully induce variable damage within rat left ventricles, resulting in visible ultrasound changes, and evidence of intracellular edema and cell death in excised tissue samples. These results will guide our experimental process for upcoming therapeutic injections.

3.2 Background

As experimental quality has increased over the years, new methods have arisen to properly recapitulate the ischemic environment seen in the cardiac niche after a myocardial infarction (MI)⁵³. The complex combination of cell death, immune cell invasion, adrenergic signaling, and scar tissue formation in the days and weeks after

MI has proven difficult to model^{6,54}, and has resulted in the use of various ways to cut off blood flow to the left ventricle in various animal models. Hemorrhagic MI⁵⁵ is often secondary to the main cause of MI and can be attributed to reperfusion injury, as the vessels open but are unable to support the new blood flow, subsequently leaking contents to the interstitial space and preventing forceful heart contraction. This type of MI is rarely studied and will not be focused on herein.

By far the most common approach to inducing ischemic MI is surgical left anterior descending artery (LAD) ligation (Fig 3.1), which can be performed in any animal. The LAD is the major artery supplying blood flow to the left ventricle; tying off this artery for set periods of time allows for controlled ischemia specifically to the left ventricle. The procedure is very invasive: the chest is opened (4th intercostal space) and the ribs parted using a modified Finochietto retractor. The LAD is exposed and sutured, either for a set time period or permanently⁵⁶.

The extensive use of LAD ligation comes from the procedure's reproducibility, especially within the same lab or university. By tying off the same part of the artery for the same time period, between-group variability can be mitigated. Opening of the chest and tying off the artery can be done in minutes under experienced guidance, significantly decreasing the chances of infection or non-specific tissue damage⁵⁷. While reproducible, many variable procedures exist for LAD ligation. For example, the suture can be released after a certain time period, or left on for the duration of the experiment. Depending on the animal model and experimental goals, some therapies (i.e- stem cell injections to the infarct zone) are given at the same time as LAD ligation⁵⁸, while others are given weeks or months after⁵⁹. Even for straightforward therapeutic experiments duration of ischemia and time before injection can be

incredibly varied, decreasing the ability of outside researchers to draw definitive comparisons on therapeutic effectiveness. Further, the invasive nature of the procedure and time-to-treat is not clinically relevant, decreasing translational ability of the therapy and adding to the discrepancies already seen in large human trials of stem cell therapies for MI.

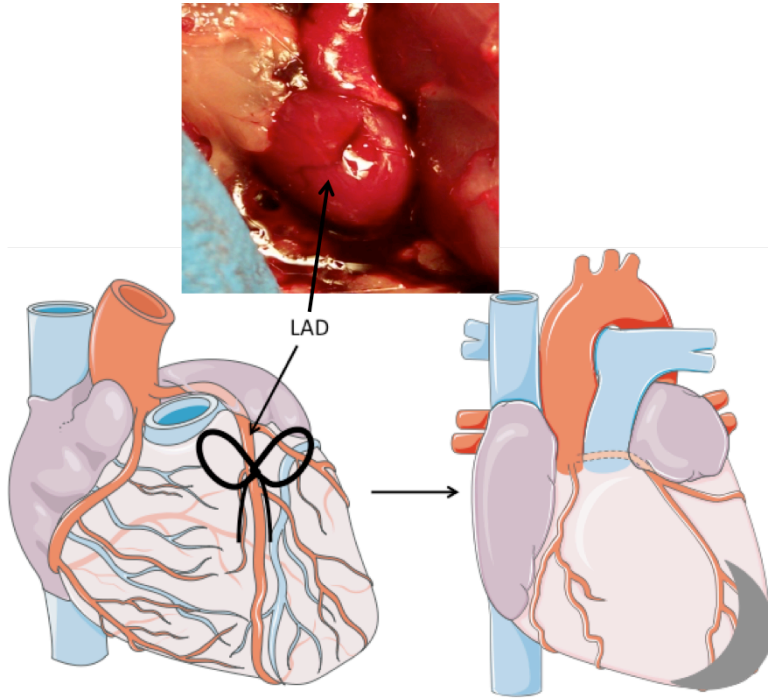


Figure 3.1: Tying off the LAD results in downstream ischemia and necrosis.

For these reasons, we have opted to use the beta-adrenergic receptor⁶⁰ agonist isoproterenol to induce ischemic MI in our rat model (Fig 3.2). By mimicking epinephrine/norepinephrine, isoproterenol works to increase cardiac muscle cell contraction via a signaling cascade beginning with receptor activation of adenylate cyclase, and ending with cyclic adenosine monophosphate (cAMP) activation of Protein Kinase A (PKA), a signaling protein for contractile cell gene transcription^{61, 62}.

Isoproterenol causes muscle cell contraction commensurate with its given dose: the higher the concentration of isoproterenol, the longer and harder the contractile cell beats. This effect can be tailored to induce focal ischemia in heavily contracting cells, particularly in the left ventricle. Small doses in rat models produce localized ischemia and induce some immune cell infiltration, while large doses induce extensive cardiomyocyte death^{63, 64}.

The issue with isoproterenol is the opposite of LAD ligation's strength: it is not entirely reproducible. Since isoproterenol is given as a subcutaneous injection, there is no guarantee the entire dose will travel systemically and thus be effective in inducing the desired level of cardiac damage. Also, because isoproterenol is not cell-specific, at higher doses it can induce damage in other contracting cells, including cardiac atria and skeletal muscle⁶⁵. Damage has also been reported in the liver and kidneys, but at concentrations that far exceed what is necessary to induce measured cardiac damage⁶⁶.

In our view, the ability to non-invasively damage the myocardium with isoproterenol in ways that mimic an ischemic MI outweigh the minimal benefits of using LAD ligation⁶⁷. Our use of isoproterenol thus needs to be extensively optimized to ensure as much reproducibility as possible, and to demonstrate an effective change

in myocardial damage and function as the concentration of isoproterenol increases between study groups. We need to also ensure that eventual injections of our stem cell/nanoscaffold therapy could be performed in a minimally invasive manner on a heart that had received a heart attack. In this chapter, we describe the successful use of various concentrations of isoproterenol in a rat to induce targeted degrees of myocardial damage. We further show that the damaged heart can withstand an injection of a therapeutic moiety, and that this injection can be performed in a non-invasive manner that will aid translation to further studies.

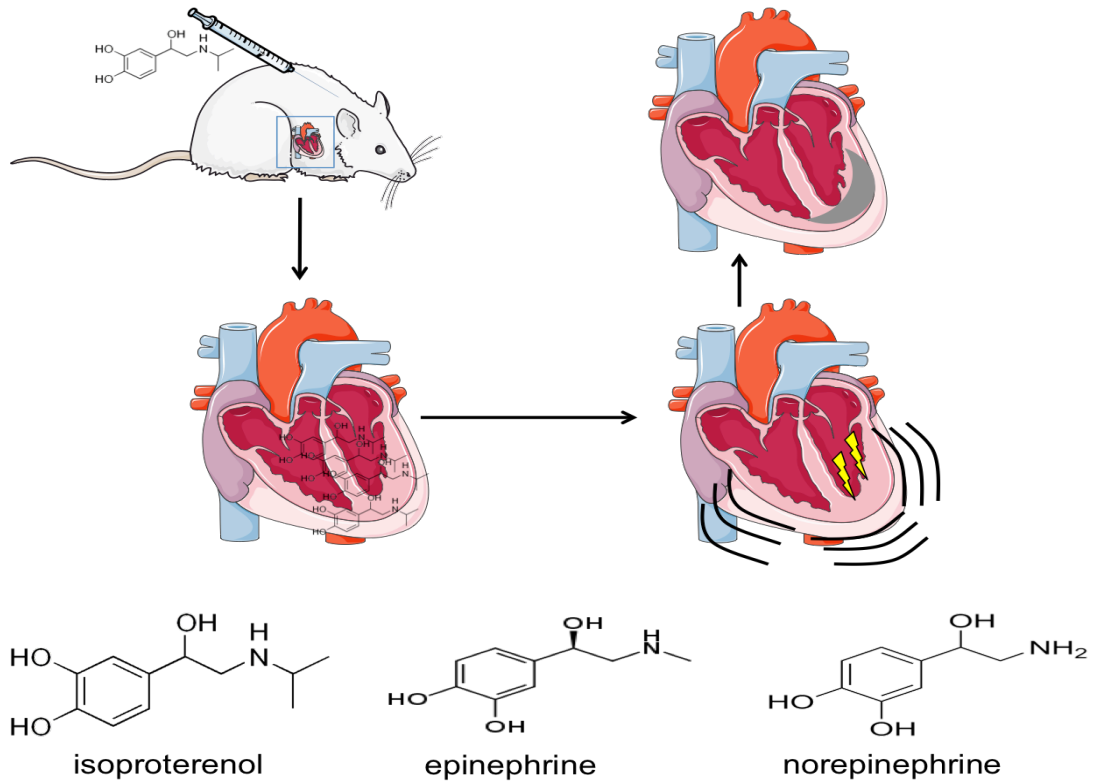


Figure 3.2: Subcutaneous administration of isoproterenol results in left ventricular accumulation of isoproterenol and catecholamines, leading to uncontrolled metabolism and cardiomyocyte contraction, and eventually ischemia.

3.3 Methods

3.3.1 Animals

IACUC: Initial Institutional Animal Care and Use Committee approval was given via protocol AUP#1273. Initial training was provided under preliminary non-survival protocols for heart attack induction, ultrasound, exploratory surgery, arthroscopic camera imaging, and cardiac injections. No protocol was long enough to necessitate eye drops or a heating pad. No dietary manipulations were induced. Clinical parameters that necessitated euthanasia, including sluggishness that impedes eating or drinking, weight loss exceeding 20%, hunched posture, or serious infection, were used to determine if animals should not continue through the full course of experimentation.

Heart attack induction: Isoproterenol (ISO; Sigma Aldrich, Missouri, USA) was dissolved in PBS at concentrations ranging from 10mg ISO per kg rat body weight (mg/kg) to 150mg/kg, with lower concentrations corresponding to a less severe heart attack. ISO was dissolved in a sterile rubber capped vial at volumes dependent on number of animals in the protocol (no more than 5mL at any one time). Solutions were kept for no longer than 2weeks, as ISO is light sensitive. To induce the heart attack, rats were anesthetized with isoflurane through a nose cone, level 4 for induction, level 2 for maintenance. Injections of ~100uL (dependent on ISO concentration and rat weight) were made subcutaneously at the base of the neck. Long acting (72hr) buprenorphine was given directly following injection; short acting (24hr) buprenorphine was given as needed for the remaining protocol period. Rats were monitored for 1hr after injection to ensure no adverse effects; subsequent checkups occurred 3x daily for 1week.

Ultrasound: Rats were anesthetized with isoflurane through a nose cone, level 4 for induction, level 2 for maintenance. The left thoracic region was shaved to aid visualization. Ultrasound gel was placed on the shaved area and on the ultrasound probe. The probe was placed parallel to the ribs with the rat laying on its right side. Standard images were taken in M-mode; blood flow images were taken using the Doppler setting. Rats were monitored for 1hr following ultrasound to ensure no side effects from prolonged anesthesia. Left ventricular interior diameter during diastole (LVIDd) and systole (LVIDs) were measured using ultrasound readouts. The following calculations were then performed to determine cardiac function (FS: fractional shortening; LVESV: left ventricular end systolic volume; LVEDV: left ventricular end diastolic volume; EF: ejection fraction):

$$FS\% = 100 * ((LVIDd - LVIDs) / LVIDs)$$

$$LVESV = (7 / (2.4 + LVIDs)) * (LVIDs^3)$$

$$EF\% = 100 * ((LVEDV - LVESV) / LVEDV)$$

Intra-cardiac injections: 48hrs after ISO injections, rats were anesthetized for standard ultrasound just prior to intra-cardiac injections. 1mL syringes (20-24G) were loaded with 100uL of either PBS, cell culture media only, or cell culture media + nanoscaffold containing hBMSCs. The heart was detected manually by feeling for the 4th intercostal space of a rat laying on its right side. Needle puncture occurred in the 2nd intercostal space and moved from the upper left hypochondriac region to the middle epigastric region to puncture the left ventricle of the rat heart. Aspiration of pumping blood prior to injection ensured placement within the left ventricle and not the body cavity. The syringe contents were then slowly dispensed into the left

ventricle cavity and the needle removed from the body. Rats were monitored directly for 1hr after injection to ensure no immediate adverse effects; subsequent checkups occurred 3x daily for 1week.

Euthanization: After 2weeks animals were euthanized via intraperitoneal injection of Euthasol solution. Death was confirmed by tail and toe pinch, and lack of breathing. Animals were then necropsied, with heart removed. Other organs, such as kidneys, liver, and lungs, were also removed.

Tissue imaging: Hearts were flash frozen in liquid nitrogen and stored at -80°C. Frozen hearts were placed in a Leica 3050 Cryostat (Leica, Wetzlar, Germany), sliced at 10µm, and mounted on glass slides. Slides were stained for immunofluorescence as described above (fixed in PFA, washed in PBS, 1^o anti-SRY at 1:200, 2^o donkey anti-mouse at 1:200) and imaged via Zeiss 5 LIVE DUO Highspeed/Spectral Confocal microscope (Zeiss, Gena, Germany). Slides were stained for nanoparticles using proprietary reagents from HEMATOGNOST Fe® kit (Millipore, Massachusetts, USA). Slides were stained with H&E as per DBI protocol. H&E and nanoparticle slides were imaged using Axioplan 2 Upright Light Microscope (Zeiss, Gena, Germany) with top-mounted AxioCam camera and software (Zeiss).

3.3.2 Statistics

The statistical significance of the results was determined using analysis of variance (ANOVA) and a multiple means comparison function (t-test) in JMP/GraphPad Prism with an alpha level of 0.05. All error bars are reported in mean ± standard error from the mean. N is dependent on experimental protocol.

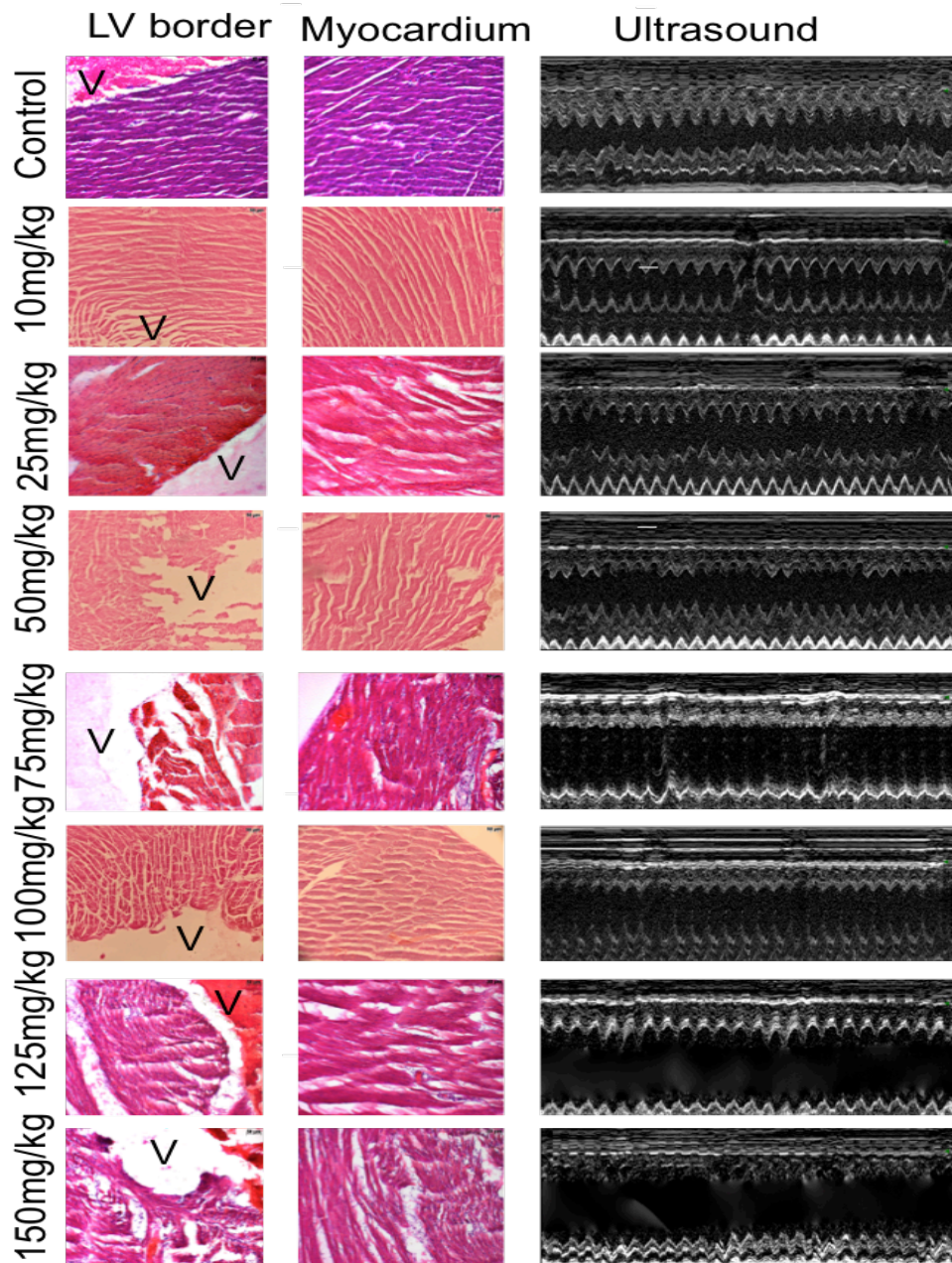


Figure 3.3: Evidence for adjustable MI model. Increasing myocardial damage can be seen both in H&E tissue staining (left images) and ultrasound details (right images) as the concentration of isoproterenol increases.

3.4 Results

3.4.1 Isoproterenol injections

Vial preparations: Stock concentrations of isoproterenol in sterile saline were prepared at concentrations of (X mg isoproterenol / Y kg rat weight): 10mg/kg (35.93mM); 25mg/kg (89.83mM); 50mg/kg (179.65mM); 75mg/kg (269.48mM); 100mg/kg (359.3mM); 125mg/kg (449.13mM); and 150mg/kg (538.95mM).

Subcutaneous injections: All animals were anesthetized with isoflurane prior to injection with isoproterenol (see Materials and Methods). 1mL syringes were filled with approximately 200uL isoproterenol solution at the desired dose. The skin at the base of the rat neck was pinched and lifted, and the contents of the needle were injected under this skin flap. Buprenorphine was given immediately following, also at the base of the neck.

Adverse events (AEs): Several immediate AEs were noted, given here in decreasing order of severity. One animal had a heart attack immediately after coming out from anesthesia (125mg/kg dose), and was deceased before a second dose of buprenorphine could be administered. Three animals (2 in 150mg/kg, 1 in 125mg/kg) were found deceased during following morning checkup; post-mortem tissue analysis showed cardiac damage consistent with massive heart attack (Fig 3.3). Malaise and sluggishness were noted in all animals above 50mg/kg, but none in the 25mg/kg group, and approximately half of the 50mg/kg group. Long-term AEs were more common. Animals in groups 75mg/kg-150mg/kg were often lethargic for the days following isoproterenol injection, but recovered. Some animals in the lower dose cohorts were subdued but could be roused fairly easily. Most animals developed injection site nodules that were between 1/3''-1/2'' in diameter; these did not seem to

cause the animals any distress and usually resolved themselves within a few days. One animal developed a skin infection at the injection site; this too did not seem to cause distress, and had healed on it's own accord after the first week.

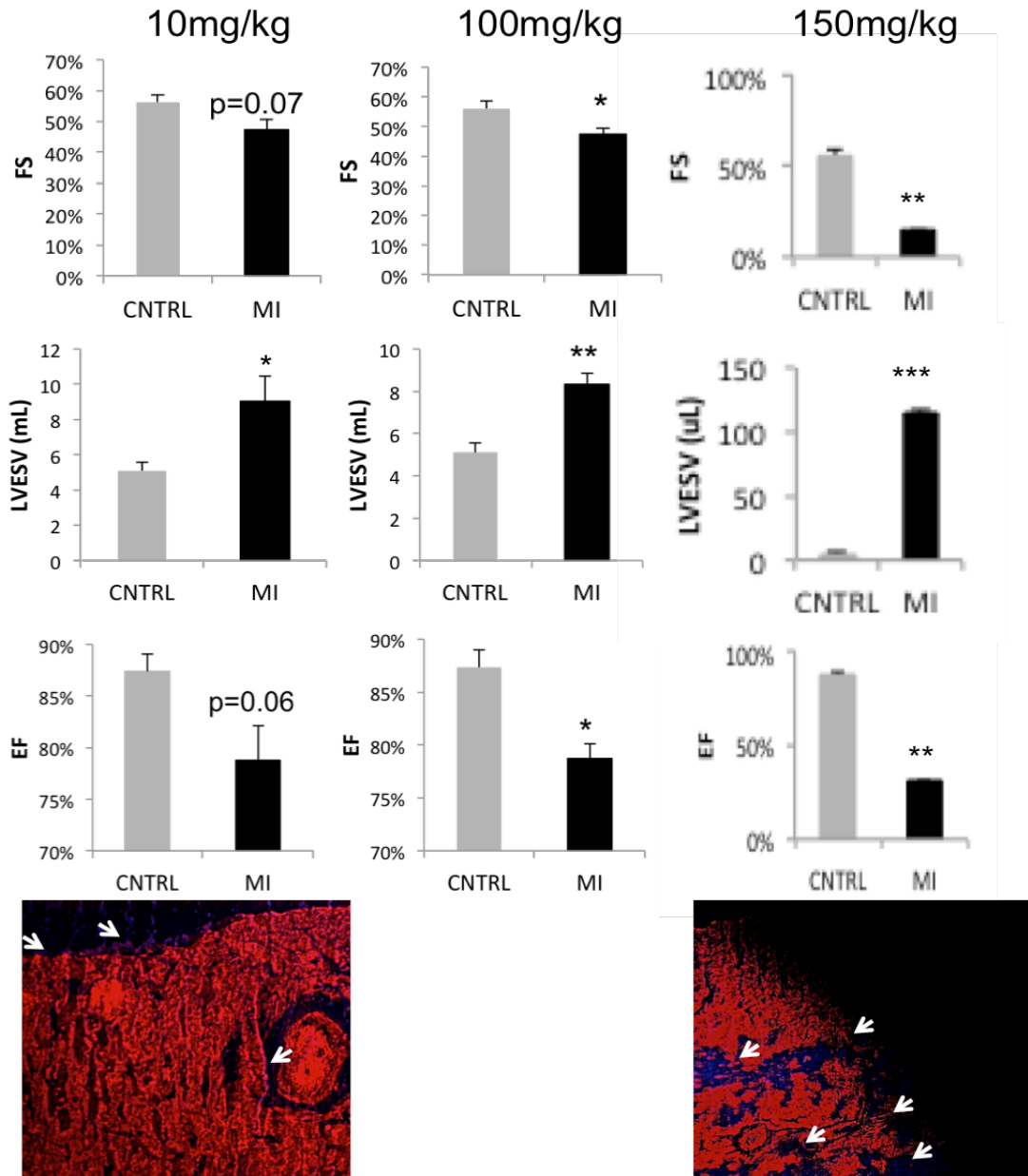


Figure 3.4: Comparison of small (10mg/kg), medium (100mg/kg), and large (150mg/kg) doses of isoproterenol on cardiac metrics and scar formation. Arrows show points of collagen scar formation. LVESV, left ventricular end systolic volume; FS, fractional shortening; EF, ejection fraction.

3.4.2 Cardiac damage

Ultrasound: Animals were anesthetized and ultrasounds were taken prior to isoproterenol injection, and then each day for up to 1 week after isoproterenol injection. Assessments of cardiac metrics (ejection fraction [EF], fractional shortening [FS], left ventricular end systolic volume [LVESV]) were made based on published results⁶⁸ (see also Materials and Methods). Increasing isoproterenol damage caused notable changes in the ultrasound readings (Fig 3.3; Fig 3.4). For the 10mg/kg group, LVESV was almost double the control values (5.08uL for control vs. 9.05uL for 10mg/kg; $p<0.05$). In the 150mg/kg group however, LVESV exceeded 20x control values (5.08uL for control vs. 114.67uL for 150mg/kg; $p<0.001$). This trend continued for EF and FS. EF for 10mg/kg (79%) was not significantly different from control (87%; $p=0.07$), but EF for 150mg/kg (31%) was highly significant compared to control ($p<0.01$). For FS, 10mg/kg (47% vs. 56% for control; $p=0.06$) was just shy of significant, while FS for 150mg/kg (15%) was again significantly lower than control ($p<0.001$) (Fig 3.4).

Tissue staining: Hematoxylin/Eosin staining was performed to observe the extent of cardiac damage on the cellular level (Fig 3.4). As expected, the control myocardium (receiving no isoproterenol) was comprised of linear cardiomyocytes and a distinct border zone between the ventricle wall and the open ventricular space. Aligned tissue can be seen in all damage levels (middle column, 'Myocardium'), but cells from hearts given higher isoproterenol doses were often separated from each other due to extensive interstitial edema. Cardiomyocytes also became "wavy" due to a breakdown of the internal actin cytoskeletal structure. The ventricle wall border broke down in doses exceeding 25mg/kg, leading to decreases in coordinated contraction around the open ventricle. Masson's Trichrome was used to determine

formation of a collagen scar after MI. Small amounts of collagen deposition can be seen in the 10mg/kg example, while extensive collagen scar formation has replaced contractile tissue in the 150mg/kg example (Fig 3.4, bottom, arrows).

3.4.3 Therapeutic injection optimization

After observing the damage seen and calculated in the previous results, we needed to ensure the affected rats could survive a procedure to inject our nanoscaffold directly to the heart. We hypothesized that a minimally- or non-invasive injection strategy would be ideal to increase rat survival (Fig 1.1). All injections and surgeries were performed on anesthetized animals in conjunction with IACUC approval (see Materials and Methods).

Intraperitoneal injection: Injection via the peritoneal cavity was believed to give us a proper view of the heart on the other side of the diaphragm (Fig 3.5A, labels). By injecting through the diaphragm we would be able to come up through the apex of the heart directly in to the left ventricle muscle. We were able to successfully inject into the heart, but were met with serious AEs. The hole put in the diaphragm by the needle (20G) was too large to self-heal, causing free air to leak in to the chest cavity. Attempts to stitch together the fragile diaphragm were unsuccessful, leading to suffocation of the rat. Further attempts were also unsuccessful, and the method was discontinued.

Intrathoracic injection: Surgical opening of the tissue surrounding the rib cage without separating the bones was thought to provide a perfect visual of the heart for an easy injection (Fig 3.5B, labels). After dissecting through the skin and pectoralis muscle between the 4th and 5th ribs, a purse-string suture was stitched around the incision. The exterior and interior intercostal muscles were then cut to expose the

thoracic cavity. The needle (22G) was pushed through the space and an injection made to the left ventricle. The purse string was closed around the needle, and free air within the cavity was drawn out prior to removing the needle. All animals survived the procedure. Temporarily strained breathing was only noted in one animal due to insufficient closing of the purse string suture; tightening and further suturing ameliorated this problem. No excessive bleeding was observed within the thoracic cavity during necropsy, indicating clean injections. We were unable to detect any cells or nanoscaffolding material within the left ventricle of the heart after heart excision and staining. Ex vivo analysis of LV thickness determined the needle bevel (20-22G) to be too thick to inject the therapy at a perpendicular angle to the myocardium. Because of minimal efficacy and comparatively invasive nature, this method was discontinued.

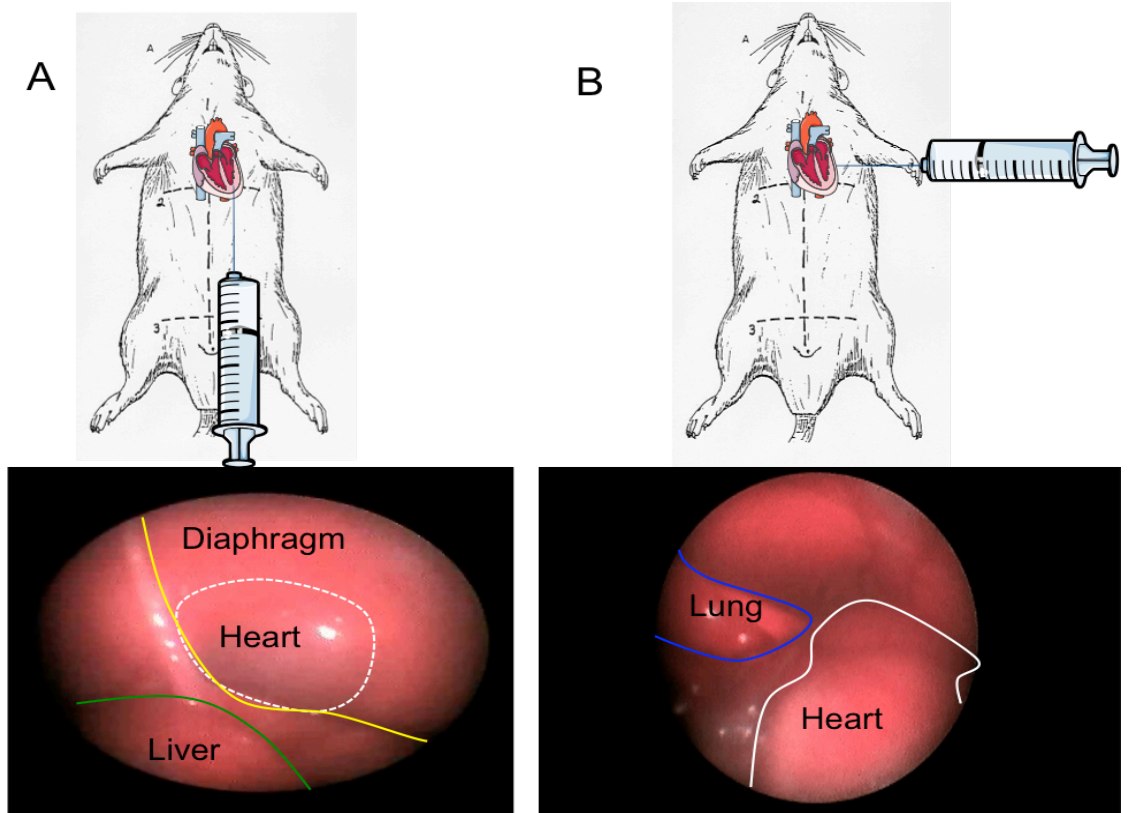


Figure 3.5: Attempted strategies for intracardiac injections using endoscope visualization. A. Intraperitoneal injections allowed for apex visualization through the diaphragm. B. Intrathoracic injections allowed direct visualization of the left ventricle and atria of the heart.

Ultrasound guided: Previous studies have successfully used ultrasound-guided injections in mice^{69,70}, so we attempted to repeat these results in our rat model. Rats were laid on their right side and an ultrasound probe was placed over the 4th/5th rib space to visualize the cardiac cavities. A needle (22G) was threaded between the 1st/2nd rib space to approach the heart from the left atrial section (Fig 3.6, schematic). The needle could be contrasted with the myocardium once it pierced the muscle (Fig 3.6, red dashed line), and the injected therapy could also be visualized (Fig 3.6, yellow box). No invasive surgical procedure was performed, and cardiac performance could also be monitored in real-time to ensure no adverse events occurred. Repeated injections to separate animals ensured this was a reproducible strategy for injecting our therapy to the left ventricle.

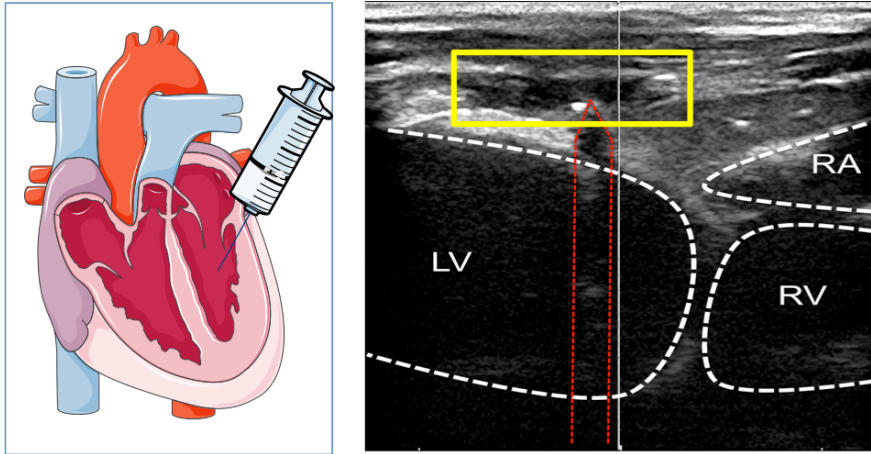


Figure 3.6: Ultrasound guided intracardiac injection. Schematic (left) of the hypothesis, and direct ultrasound image (right) of the actual therapeutic injection.

3.5 Discussion

We were able to successfully optimize an in vivo rat model of ischemic myocardial infarction. Optimization prior to attempting therapeutic intervention is crucial for ensuring reproducible, reliable results.

There are many ways to induce an ischemic MI in an animal model⁵³. We chose isoproterenol because of its ease of use, non-invasiveness, and customizability for inducing varying degrees of focal cardiac damage. Isoproterenol is less expensive than extracts of epinephrine/norepinephrine, while having a higher affinity for ligand binding⁷¹.

Despite being used for decades as one of the first methods for inducing MI^{53,72} isoproterenol is not yet fully understood mechanistically, though the effects are thought to occur through at least one of three pathways. First, ion gradient malfunction may occur through increased contractile signaling⁷³. As PKA signaling significantly increases through beta-adrenergic GPCR stimulation, chronotropic (+/-) signaling is stimulated via the ryanodine receptor 2 (RyR2), and inotropic (-/-) signaling is regulated via phospholamban (PLB). Both RyR2 and PLB function as modulators of Ca²⁺ pumps, and as signaling increases they have trouble maintaining ion balances (with K⁺) to assist in measured cell contraction. Sustained (+) states subsequently result in permanent damage to the signaling and regulatory mechanisms⁷³.

Second, catecholamine buildup within the cell may lead to acute toxicity⁷⁴. Catecholamines are a group of adrenergic agonists, including epinephrine, which can cause intracellular and systemic signaling effects. Principally in the case of isoproterenol-induced toxicity, there is a positive feedback loop whereby increased isoproterenol causes unrestrained release of acetylcholine and sympathetic nervous system activity. The resulting cascade leads cells to prioritize fatty acid oxidation over

glucose metabolism; the rate of consumption due to high sympathetic demand results in reactive oxygen species accumulation, mitochondrial dysfunction, and eventual cell death⁷⁴.

Third, it is thought the cells simply exhaust their terminal oxygen supply. Similar to the catecholamine cascade, overwork of the cells due to increased sympathetic signaling leads to an untenable rate of metabolism. Oxygen becomes increasingly scarce, producing an ischemic environment and cell death⁷⁵. In reality, the macro view (ischemic MI) is undoubtedly a combination of all three cascades, as cardiomyocyte contractile signaling and metabolism is immensely intertwined between these three hypotheses.

In our model, use of isoproterenol resulted in a dose dependent amount of cardiac damage. Developing different concentrations of isoproterenol allowed us to measure the amount of ischemic damage on a cellular and whole-heart level, through the use of defined tissue staining and ultrasound. At 10mg/kg (the lowest dose measured), we found mild cardiac damage with a trend toward significance in major metrics including increasing LVESV and decreasing EF and FS compared to control animals. Other studies have used doses as low as 5mg/kg, but this was mainly to induce an immune response and to recruit resident cardiac stem cells, not to measure the effects of a given therapy on ischemic MI²⁸. Still more studies have used concentrations upwards of 200-250mg/kg, purely as a means to measure what occurs during a massive ischemic event, but again not to test any given therapy⁷⁶.

We tested isoproterenol dose ranges from 0mg/kg (control) to 150mg/kg in this analysis. The increase in cardiac damage was very apparent between control and 150mg/kg, and indicated a measured increase in ischemic damage when compared to

results from the 10mg/kg cohort (Fig 3.4). Ventricular layers of myocardium are much more susceptible to ischemic damage, so this sub-endocardial to epicardial damage leads to the conclusion that we have successfully recapitulated an ischemic anterior infarct.

Cohorts above 100mg/kg were beset by severe adverse events, most notably death within the first 48hrs. After discussions with the IACUC review panel, it was advised we proceed with only dosages less than or equal to 100mg/kg. We agreed for two reasons: first, the change will decrease the necessary statistical power needed per animal cohort, as potential animal deaths will not need to be factored in to the calculations as heavily; and second, the 100mg/kg still provided damage that was significantly above the 10mg/kg and control cohorts (Fig 3.4), allowing for the continued increase in cardiac damage at the crux of this experiment.

Chapter 4

CHARACTERIZE HUMAN BONE MARROW STEM CELL DIFFERENTIATION ON NANOFIBER SCAFFOLDS

4.1 Abstract

After an ischemic cardiac event, proper treatment and care of the damaged tissue is crucial in restoring optimal cardiac function and preventing future cardiac events. Recently, thymosin β 4 (T β 4) has been found to play a vital role in cardiac cell health and development by regulating angiogenesis, inflammatory responses, and wound healing. We proposed that defined, electrospun poly(ϵ -caprolactone) (PCL) nanoscaffolds coated with T β 4 and a WNT pathway modifier could efficiently differentiate human bone marrow mesenchymal stem cells (hBMSCs) towards the cardiac cell lineage. hBMSCs were seeded on coated and uncoated nanoscaffolds and observed via fluorescent and electron microscopy. PCL nanoscaffolds coated with only T β 4 promoted growth and differentiation of hBMSCs compared to uncoated controls. The addition of a canonical WNT inhibitor significantly increased differentiation potential, while a canonical WNT promoter decreased differentiation and cell survival. The use of molecular targeting resulted in robust growth and differentiation of hBMSCs on coated nanoscaffolds compared with uncoated, showing potential for nanoscaffold-mediated cardiac cell replacement in vivo after a myocardial infarction or other cardiac event.

4.2 Background

Cardiac cell health post-myocardial infarction (MI) is imperative in the proper future functioning of the heart^{77, 78}. After MI, formation of fibrotic scar issue impairs the ability of the heart to properly function, leading to higher risk for a second cardiac event^{79, 80}. Developing new methods to repair and replace damaged cardiomyocytes is imperative.

Literature has shown that the 43-amino acid cardiac-specific protein thymosin β 4 (T β 4) effects actin-cytoskeletal organization necessary for cardiac cell motility, organogenesis, and other crucial cellular events necessary for cardiac repair by sequestering G-actin monomers⁸¹. The correlation between T β 4 and cardiac cells has been of great interest and debate worldwide⁸², but the overwhelming majority of studies have pointed to T β 4 having a positive therapeutic effect on ischemic cardiomyopathy. Gajzer et al.⁸³ and Smart, et al.⁸⁴ demonstrated in vivo that epicardium derived progenitor cells (EPDCs) primed with T β 4 differentiate into cardiomyocytes, and can be used to repair the myocardium after ischemic damage. Downregulation of T β 4 using a blocking antibody was shown to decrease survival of EPDC-derived cardiomyocytes, and this affect could be reversed by exogenous addition of T β 4⁸⁵. It has been widely demonstrated that T β 4 alone can promote cardiac cell migration^{81, 86, 87}, activate proliferation of cardiac fibroblasts and endothelial cells^{81, 83-85, 88}, and promote neoangiogenesis (development of new blood vessels)^{81, 86, 87, 89}.

Previous studies have used small molecule modifiers of the WNT pathway to differentiate human embryonic and induced pluripotent stem cells to beating cardiomyocytes⁹⁰⁻⁹² and to promote tissue healing^{93, 94}. The WNT pathways (canonical, noncanonical/ Ca^{2+} , and Planar Cell Polarity) are highly regulated during

fetal heart development, and play an extensive role throughout life by promoting cell proliferation, cytoskeletal rearrangement, differentiation, and survival⁹⁵, key aspects of stem cell growth. Small molecule therapeutics can control various aspects of the WNT pathway that can be unregulated in disease states⁹⁶, particularly CHIR99021, a GSK3 β inhibitor that increases intracellular β -catenin and promotes the canonical pathway; and IWP-2, a Porcupine inhibitor leading to sequestration of β -catenin, promoting the noncanonical/ Ca^{2+} and Planar Cell Polarity pathways.

We sought to use a nanoscaffold platform coated with the aforementioned small molecules, plus T β 4, to promote differentiation of hBMSCs towards the cardiac lineage in vitro. For biomedical applications these nanoscaffolds are made of naturally occurring, biocompatible materials such as collagen, starch, poly(L-lactide) and poly(ϵ -caprolactone) (PCL)⁹⁷ that will slowly and consistently dissolve in vivo. This dissolving can be used to deliver such things as therapeutic drugs⁹⁸ (such as T β 4) or bioactive molecules⁹⁹ (such as CHIR99021 or IWP-2). In this chapter, we show a robust differentiation of hBMSCs towards the cardiac cell lineage that is dependent on the addition of T β 4 to a PCL scaffold, and is further enhanced by canonical WNT pathway inhibition using IWP-2. Factors coated on nanoscaffolds dissolved at a linear rate as measured by FTIR analysis, and cell growth enhanced nanoscaffold strength 400% over two weeks. Future experiments will demonstrate whether this therapy can be translated in vivo to repair ischemic myocardium.

4.3 Methods

4.3.1 PCL solution formulation

PCL tablets were purchased from Sigma Aldrich (Missouri, USA). Dichloromethane (DCM) and N,N-dimethylformamide (DMF) were purchased from Acros Organics (Geel, Belgium). PCL tablets weighing 1.5g were dissolved in a solvent mixture containing a 1:4 ratio of DCM to DMF. This combination was sonicated for 1hr to ensure tablets were fully dissolved.

4.3.2 Electrospinning of nanoscaffold

The DCM/DCF/PCL solution was suctioned into a syringe and attached to a flow rate controller (Thermo Fisher Scientific, Massachusetts, USA). The solution was pumped at a flow rate of 0.5mL/h. A Voltmeter lead was attached to the syringe needle and another lead was attached to a rolling drum (Oriental Motor, Tokyo, Japan) that housed an aluminum sheet. The rolling drum was mounted on an E7 Limo easy linear motion controller (Oriental Motor) for linear and rotational fiber distribution. The Human Machine Interface (Omron, Kyoto, Japan) was set at a 3hr run time, a starting position of 105mm, and a rolling drum speed of 630RPM. A potential of 12kV was applied between the spinneret and grounded collector located 12cm below the spinneret to pull the solution from the syringe and accurately align the fibers to the rolling drum mounted on the E7 Limo.

4.3.3 IR nanoscaffold characterization

A Nicolet iS5 spectrometer with an iD1 Transmission adapter (Thermo Fisher Scientific, Massachusetts, USA) was used to perform Fourier transformed infrared spectroscopy (FTIR). Fiber bundles were measured to determine characteristic peaks

relating to bond stretching and rocking, using air as a background. The FTIR analysis was performed over a wave number range between 4,000 and 400 cm^{-1} at a 2 cm^{-1} resolution.

4.3.4 UV nanoscaffold characterization

An Evolution 220 UV-Vis Spectrophotometer (Thermo Fisher Scientific, Massachusetts, USA) was used to determine absorption peaks along the UV spectrum. Samples were dissolved in DMSO or DMF, and mixed with concentrations of Evan's blue (see Chapters for specific ratios) for purity assessment.

4.3.5 Microscopic nanoscaffold characterization

A Bioscope Catalyst Atomic Force Microscope (Bruker, Massachusetts, USA) was used for nanofiber diameter measures. Samples were mounted in a petri dish and submerged in PBS. The AFM tip was placed on the sample with measurements of Vert -0.2 \rightarrow 0.3, and Horiz as close to 0 as possible. The tip was Navigated with onscreen software, and withdrawn and repositioned if necessary.

4.3.6 Nanoscaffold preparation

Electrospun PCL nanoscaffolds were adhered to square 20 mm^2 coverslips by adhesive silicon type A glue (NuSil Technology, California, USA). Cover slips with nanoscaffolds were transferred and attached to the base of 6- or 12-well culture plates (Thermo Fisher Scientific, Massachusetts, USA) with silicon glue. Nanoscaffolding and cover slip were then sanitized as follows: 1mL bleach wash for 5min, rinse with ultrapure water (Millipore, Massachusetts, USA), repeat; 1mL ethanol wash for 5min, rinse with ultrapure water, repeat; nanoscaffolding was left under UV light to dry.

Confirmatory experiments (September 2013-April 2014): After drying, nanoscaffolds were coated with 0.1% polylysine aqueous solution for 4 to 6hrs prior to cell seeding. Treated nanoscaffolds were coated with thymosin β 4 (T β 4; PeproTech, New Jersey, USA) solutions at concentrations of 0.5-7.5% w/v.

Optimization experiments (May 2014-March 2015): 100 μ L of 2%, 4%, or 10% concentrations of T β 4 stock in ultrapure water were mixed with either 100 μ L of 20 μ M, 40 μ M, or 100 μ M concentrations of CHIR99021 or IWP-2 stocks (StemCell Technologies, Vancouver, Canada) in ultrapure water. Resulting 200 μ L solutions were used to coat the nanoscaffolds and allowed one hour to dry.

4.3.7 Coating degradation from nanoscaffolds

Coated nanoscaffolds were examined using FTIR to determine the rate of degradation of the coated compounds (T β 4, CHIR99021, IWP-2) from acellular scaffolds. Dry uncoated PCL, cell culture media, and solutions of T β 4, CHIR99021, or IWP-2 were used as positive controls for FTIR peaks. Decreasing amine peaks in the 3500 cm^{-1} range were used to calculate compound degradation rates from the nanoscaffold.

4.3.8 Cell culture

Human bone marrow mesenchymal stem cells (hBMSCs) were purchased from StemCell Technologies (Vancouver, Canada) and passaged in MSC Basal Medium (StemCell Technologies) with MesenCult Stimulatory Supplements (StemCell Technologies) to prevent differentiation. hBMSCs were seeded at a concentration of $7.5\text{-}10 \times 10^4$ cells/mL over nanoscaffolds coated with T β 4 and/or CHIR99021 or IWP-2, and covered with MSC Basal Medium (StemCell Technologies) without

supplementation to allow differentiation. Cells were incubated in a Forma SteriCycle CO₂ Incubator (Thermo Fisher Scientific, Massachusetts, USA) at 36.5°C and 5.0% CO₂. After 24hrs-1week, media were removed, cells were fixed in 4% paraformaldehyde in PBS for 18min, and washed 3x for 3min each in PBS. Cell differentiation was monitored with the Cardiomyocyte Characterization Kit (Millipore, Massachusetts, USA) using the following dilutions: anti-desmin Ab, 1:100; anti-troponin I Ab, 1:100; anti- α -actinin Ab, 1:200. Other antibodies used: anti-CD105 1:75; anti-ANP 1:200; anti- Cnx43 1:200; anti- β -catenin 1:200; anti-RhoA 1:200. Donkey anti-rabbit or anti-mouse 2^o Ab at 1:200 (Pierce Antibodies, Massachusetts, USA). Cells were counterstained for F-actin using ActinRed 555 Ready Probes (Life Technologies, California, USA) and nuclei with NucBlue Molecular Probes stain (Life Technologies), as per company protocol (2 drops stain for every 1mL PBS; incubate 20min). Cultures were washed in PBS and mounted in ProLong Gold Antifade mount (Thermo Fisher Scientific, Massachusetts, USA).

4.3.9 Scanning topographical analysis

A ContourGT-X 3D Optical Microscope (Bruker, Massachusetts, USA) was used to scan a fiber area of 76,800 μm^2 (320 μm x 240 μm). Average roughness values across the sample were used to produce a topographical output. The cover slip on which the nanoscaffold was mounted was used as a starting 0 μm value, assuming a flush contact.

Scanning electron microscopy (SEM) was performed to examine acute topography. Fibers and cells were mounted on aluminum mount-M4 sample holders (Electron Microscopy Sciences, Pennsylvania, USA) and placed in a Denton Bench Top Turbo III vacuum chamber (Denton Vacuum, New Jersey, USA) for sputter

coating with a 50:50 mix Au:Pd to aid visualization. Samples were placed into the SEM (Hitachi S4700, Hitachi High Technologies, Tokyo, Japan) and images were taken from 10x to 3000x.

4.3.10 Microscopic analysis

An EvosFL Cell Imaging System (Life Technologies, Carlsbad, CA) was used to monitor cell growth and determine preliminary cell counts. Cells were washed and stained as described, and placed on the microscope stage. An image was taken, and the Toolbar function was used to place a hemocytometer grid on the screen for cell counts.

For higher quality images, a Zeiss 5 LIVE DUO Highspeed/Spectral Confocal microscope (Zeiss, Gena, Germany) was used. 8x image averages were taken with 10x-25x lenses to produce a final image; Z-stack was performed periodically to determine the extent of cell infiltration within the nanoscaffold matrix.

4.3.11 Statistics

The statistical significance of the results was determined using analysis of variance (ANOVA) and a multiple means comparison function (t-test) in JMP/GraphPad Prism with an alpha level of 0.05. All error bars are reported in mean \pm standard error from the mean. N is dependent on experimental protocol.

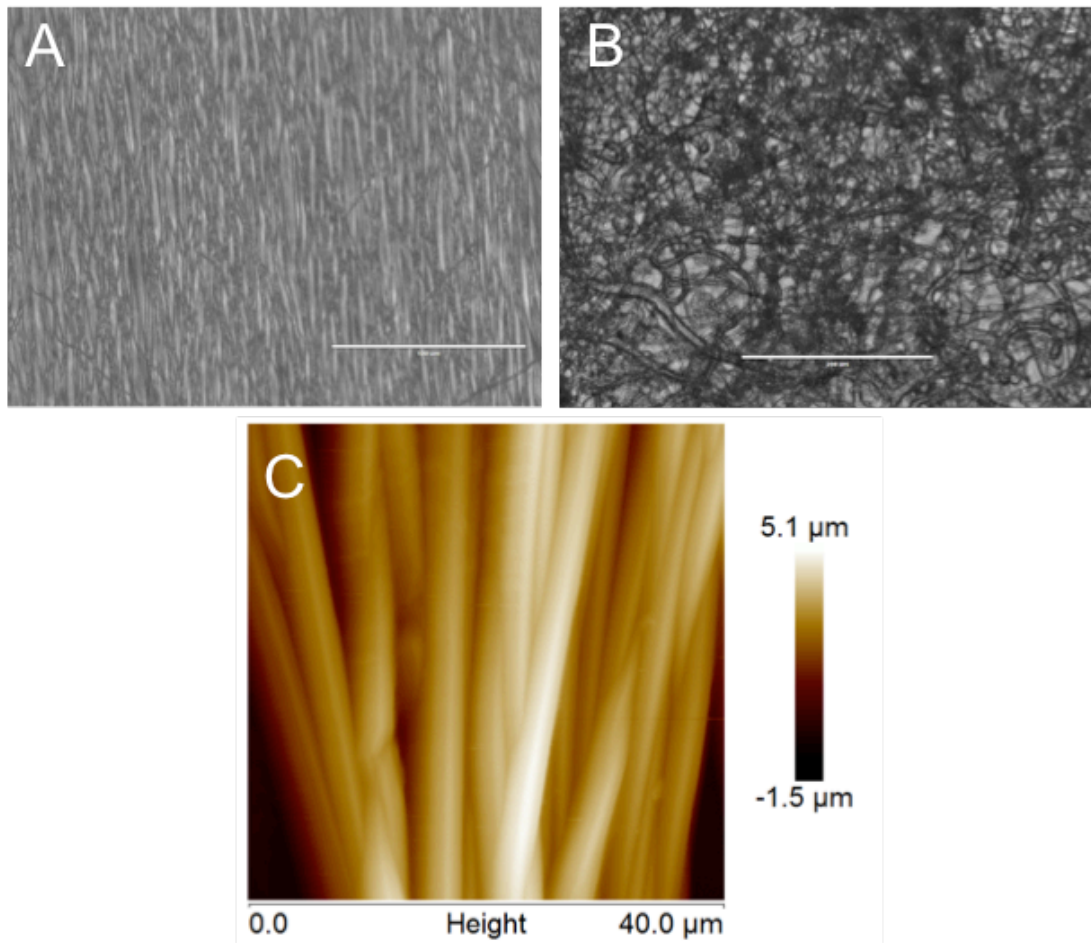


Figure 4.1: Microscopic visualization of PCL nanoscaffold. A. Linear aligned PCL. Scale bar=200μm. B. Randomly aligned PCL. Scale bar=200μm. C. AFM visualization of a nanofiber bundle, showing fiber width averaged 257 ± 48 nm.

4.4 Results

4.4.1 Nanofiber visualization

Evos FL and atomic force microscopy (AFM) images were taken to measure PCL nanoscaffold fiber assembly (Fig 4.1). Linear (Fig 4.1A) and randomly aligned (Fig 4.1B) nanoscaffolds showed expected morphology based on production method. AFM (Fig 4.1C) of specific nanofiber bundles showed fiber diameter averaged 257 ± 48 nm. Fibers containing beaded chunks of PCL were discarded prior to sampling.

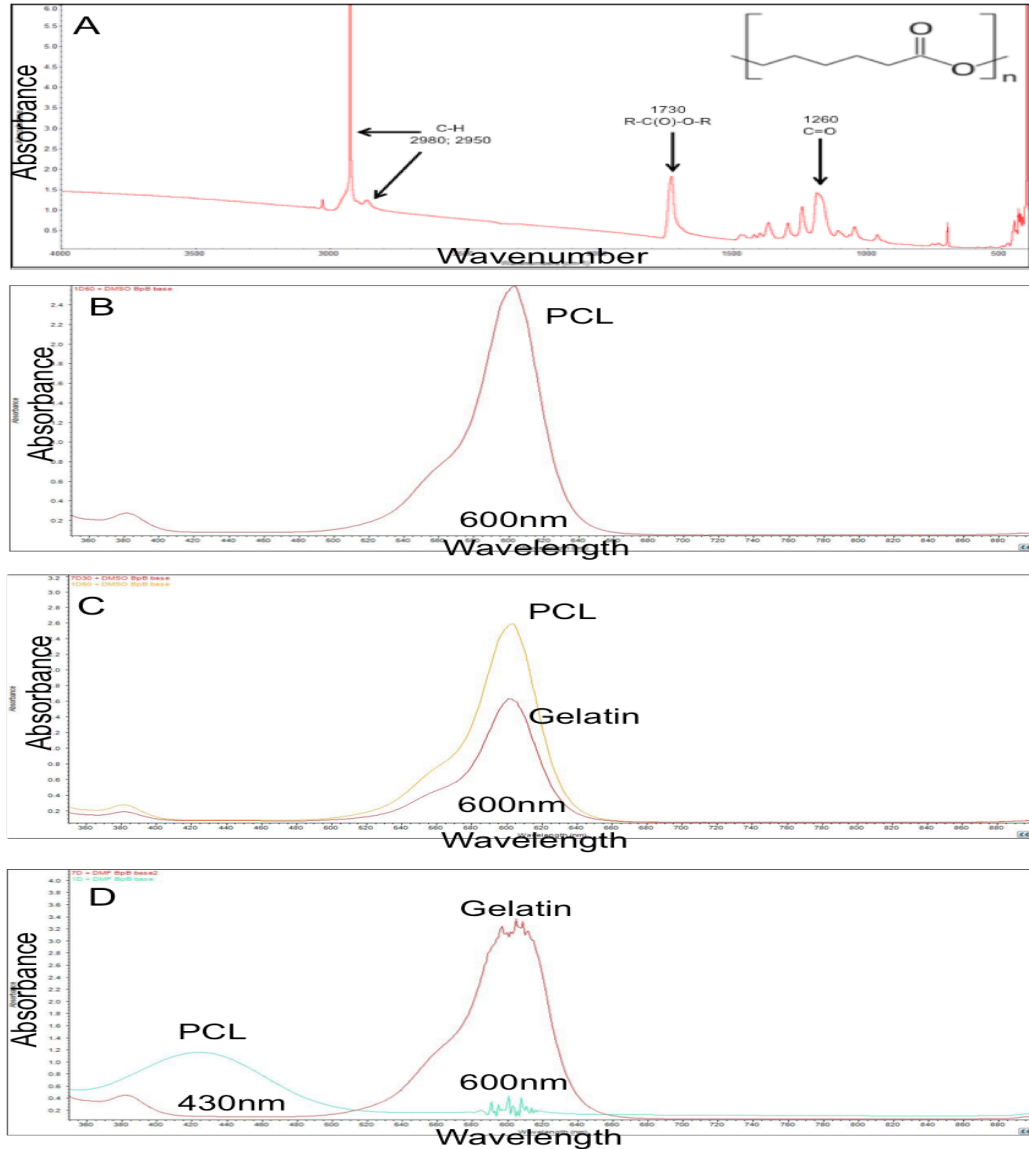


Figure 4.2: IR/UV characterization of nanoscaffold. A. FTIR of PCL (inset) with characteristic peaks labeled. B-D. PCL mixed with 0.1mg/mL Evan's blue as UV contrast. B. Pure PCL dissolved in DMSO; major peak at 600nm. C. Pure PCL and pure gelatin, both dissolved in DMSO, run separately. Major peak changes at 600nm. D. Pure PCL and pure gelatin, both dissolved in DMF, run separately. Gelatin peak stays at 600nm, but PCL blueshifts to 430nm.

4.4.2 FTIR and UV/Vis characterization

FTIR: Using the iD1 Transmission adapter we sought to determine the composition of the PCL nanoscaffold based on bond stretching and peak appearances (Fig 4.2A). PCL has a relatively long hydrocarbon chain in the repeating unit $[-(\text{CH}_2)_5-]$ before ending in an ester linkage $[-\text{R}_1-\text{CO}-\text{O}-\text{R}_2-]$ to the next repeat unit. Characteristic PCL ester stretching from the C=O bond occurred at 1260cm^{-1} , and the carbonyl stretch can be seen strongly at 1730cm^{-1} . A peak at 2980cm^{-1} and the accompanying shoulder at 2850cm^{-1} are indicative of extensive C-H α -groups.

UV/Vis: UV/Vis was used to further ensure the purity of the sample (Fig 4.2B-D). PCL in DMSO with Evan's blue (5g PCL/mL, 0.1mg Evan's blue/mL) demonstrated a strong peak at 600nm, and a smaller peak at 430nm (Fig 4.2B). The purity confirmation was determined when a mixture of gelatin in DMSO was overlaid to the PCL peak, indicating a strong difference in absorbance patterns (Fig 4.2C). To explore the blueshifted peak seen in Fig 4.2B, PCL was dissolved instead in DMF with Evan's blue at the same concentration. The 430nm peak was significantly increased, with a correspondingly sharp decrease in the 600nm peak (Fig 4.2D). DMF had no effect on the gelatin peak.

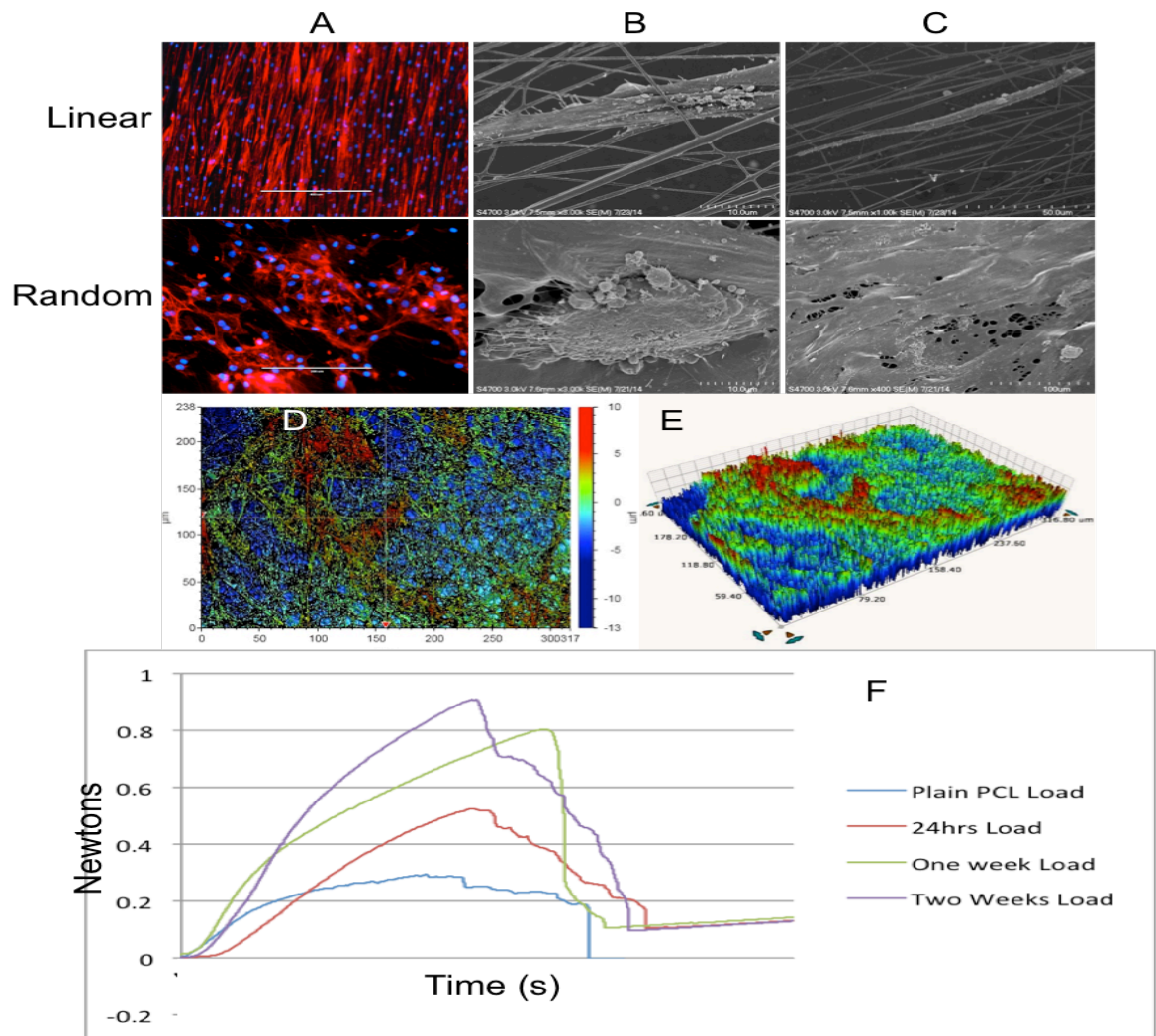


Figure 4.3: Cell viability on a strengthening nanoscaffold. A. Fluorescent images of cells on linear and random nanoscaffolds. Red, actin; blue, DAPI. Scale bar=200um. B. SEM close-up of individual cells. Scale bar=10um. C. Lengthening of cells across the nanoscaffold. Linear nanoscaffolds usually held significantly less cell mass. Scale bar=50um (linear), 100um (random). D/E. Topographical analysis of cells covering random nanoscaffold. Cells tended to clump in certain areas (red), leading to gaps in other areas (dark blue). F. Cells contributed to increasing strength of the nanoscaffold over time, indicated with uniaxial strength test.

4.4.3 Cell viability on PCL nanoscaffold

Prior to coating the nanoscaffold, it was imperative to corroborate the biocompatibility of our PCL nanoscaffold with the literature (Fig 4.3). Linear and randomly aligned nanoscaffolds showed strong cell adhesion and spreading (Fig 4.3A-C), with more concentrated cell growth on randomly aligned nanoscaffolds (Fig 4.3C). Cells tended to clump in certain areas of the nanoscaffold (Fig 4.3D/E), though this did not affect their growth. Finally, in a preliminary experiment, cells strengthened the nanoscaffold significantly over a period of two weeks as demonstrated by uniaxial mechanical testing (Fig 4.3F). Further work will determine whether nanoscaffold strengthening could lead to other biological applications of this system.

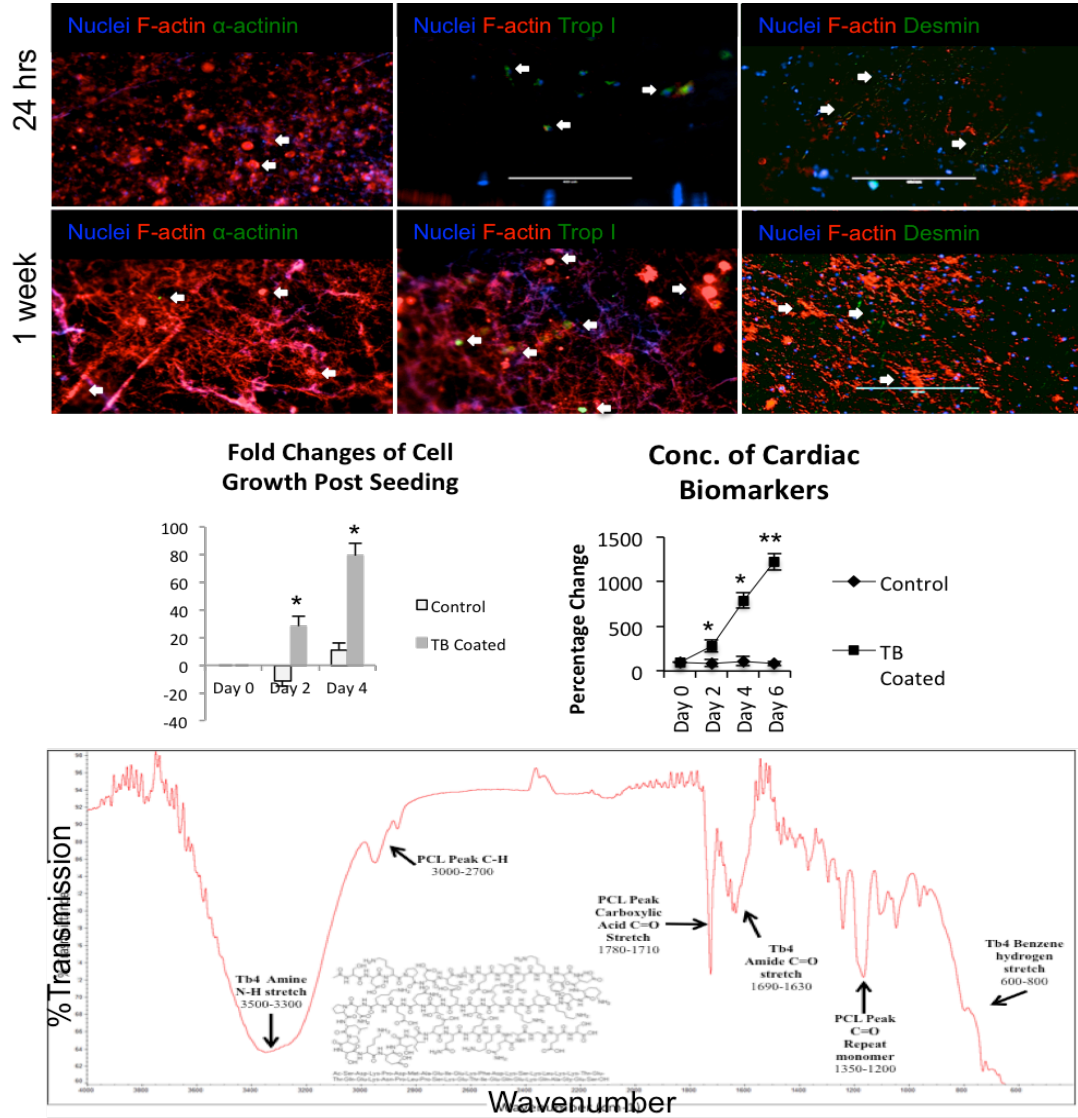


Figure 4.4: Effect of Tβ4 on cell growth and differentiation. Nanoscaffold coating with Tβ4 produces combined peaks from the protein component (inset) and underlying nanoscaffold architecture. Tβ4 produces minimal differentiation of hBMSCs to the cardiac lineage after one week. Both hBMSC growth and cardiac biomarker expression are significantly enhanced when grown on nanoscaffolds coated with Tβ4 compared to control. * $p < 0.05$; ** $p < 0.01$; Scale bar=200um. Graphs adapted from Kumar, et al. 2014¹⁰⁰.

4.4.4 Coating of nanofiber

As previously described¹⁰⁰ concentrations of 2% T β 4 w/v were used for nanoscaffold coating. As noted in Fig 4.4, amine (3500-3300cm⁻¹) and aromatic (860-680cm⁻¹) moieties appeared when the nanoscaffold was coated with the T β 4 protein, indicative of the notable amino acid structures within T β 4, while the PCL-specific peaks remained intact (Fig 2).

T β 4 coatings alone produced some differentiation of BMSCs to the cardiac lineage (Fig 4.4, top), shown via expression of the cardiac contractile biomarkers α -actinin (left), troponin I (middle), and desmin (right). In all cases, more differentiation was seen after one week compared to control samples. Importantly, T β 4 coating also significantly enhanced cell growth and survival on the nanoscaffolding system compared to uncoated (control) samples, ensuring extensive cell seeding for future in vivo experiments.

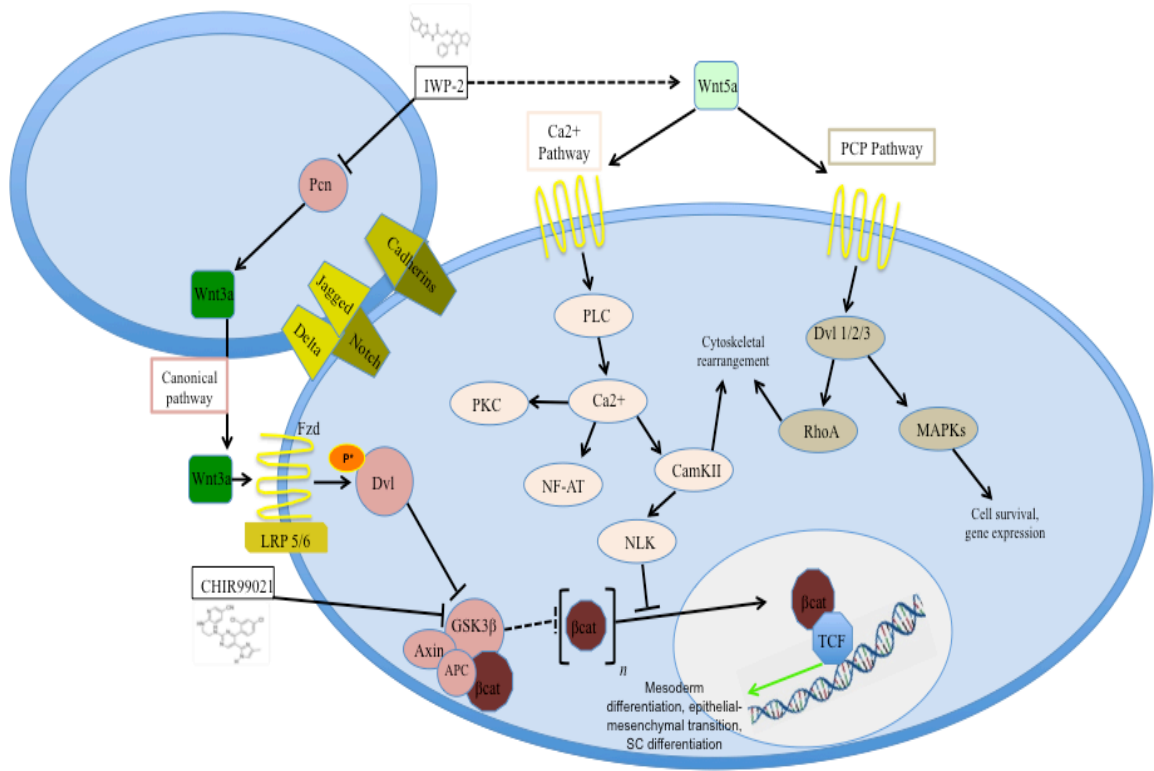


Figure 4.5: Proposed hypothesis of hBMSC differentiation mechanism of action via WNT-effecting small molecules. Importantly for cardiomyocyte differentiation, the noncanonical pathway causes surges in intracellular Ca²⁺, resulting in cytoskeletal rearrangement, inhibition of β cat translocation (thus blocking the canonical pathway), and upregulation of the PKC and NF-AT pathways. Dvl 1/2/3 also significantly increases MAPK signaling, promoting cell survival to insults such as osmotic stress and proinflammatory cytokines, and increasing gene expression for tasks such as proliferation, differentiation, and mitosis. Pathways shortened for clarity. Pcn, porcupine; Wnt, wingless; LRP, lipoprotein receptor-related protein; Dvl, disheveled; GSK, glycogen synthase kinase; APC, adenomatosis polyposis coli; β cat, β -catenin; TCF, transcription factor 7 variant; PCP, planar cell polarity; PLC, phospholipase C; PKC, protein kinase 3; NF-AT, nuclear factor of activated T-cells; CamKII, Ca²⁺/calmodulin-dependent protein kinase II; NLK, nemo-like kinase; MAPK, mitogen activated protein kinases.

4.4.5 Small molecule WNT pathway modifiers

It was hypothesized that the minimal hBMSC differentiation to the cardiac lineage seen in Fig 4.4 could be enhanced via targeting of specific molecular pathways (Fig 4.5). As described, in embryonic and induced pluripotent cell research the WNT pathway has been modified using small molecules as a way to enhance cells' differentiation towards beating cardiomyocytes. We sought to couple WNT pathway modifiers in our nanoscaffolding system to enhance our proven strategy of T β 4-based differentiation.

FTIR: We initially coated the nanoscaffold with either IWP-2, a WNT pathway inhibitor, or CHIR99021, a WNT pathway enhancer (Fig 4.6). As expected FTIR outputs of each coated nanoscaffold looked alike because of the molecules' similar side chains (i.e. C-H stretch at 3000-2700cm⁻¹), with two important differences: a C-N peak at 2400-2200cm⁻¹ in the CHIR99021 output; and a deeper amine stretch peak at 1690-1630cm⁻¹, owing to CHIR99021 having 3x as many N-H bonds as IWP-2 (Fig 4.6A/B, insets). Both small molecules sustained similar coating efficiencies (30.8% for IWP vs 26.5% for CHIR at 20uM), and degraded from the nanoscaffold at similar rates per week (17% for IWP vs 13.5% for CHIR at 20uM) (Fig 4.6C-E).

Cell signaling: Both small molecules acted as predicted on the molecular underpinnings of the WNT pathway (Fig 4.6F/G). IWP-2, an inhibitor of Porcupine, decreased β -catenin signaling compared to CHIR99021 (69% decrease, p<0.05); CHIR99021 sufficiently inhibited GSK3 β , leading to robust β -catenin signaling. In turn, IWP-2 increased RhoA signaling via induction of the Planar Cell Polarity pathway (83% increase compared to CHIR99021, p<0.01). T β 4 activates β -catenin expression, and CHIR99021 does not necessarily block RhoA signaling, leading to

isolated pockets of protein expression regardless of the inhibitors used (Fig 4.6F, arrows).

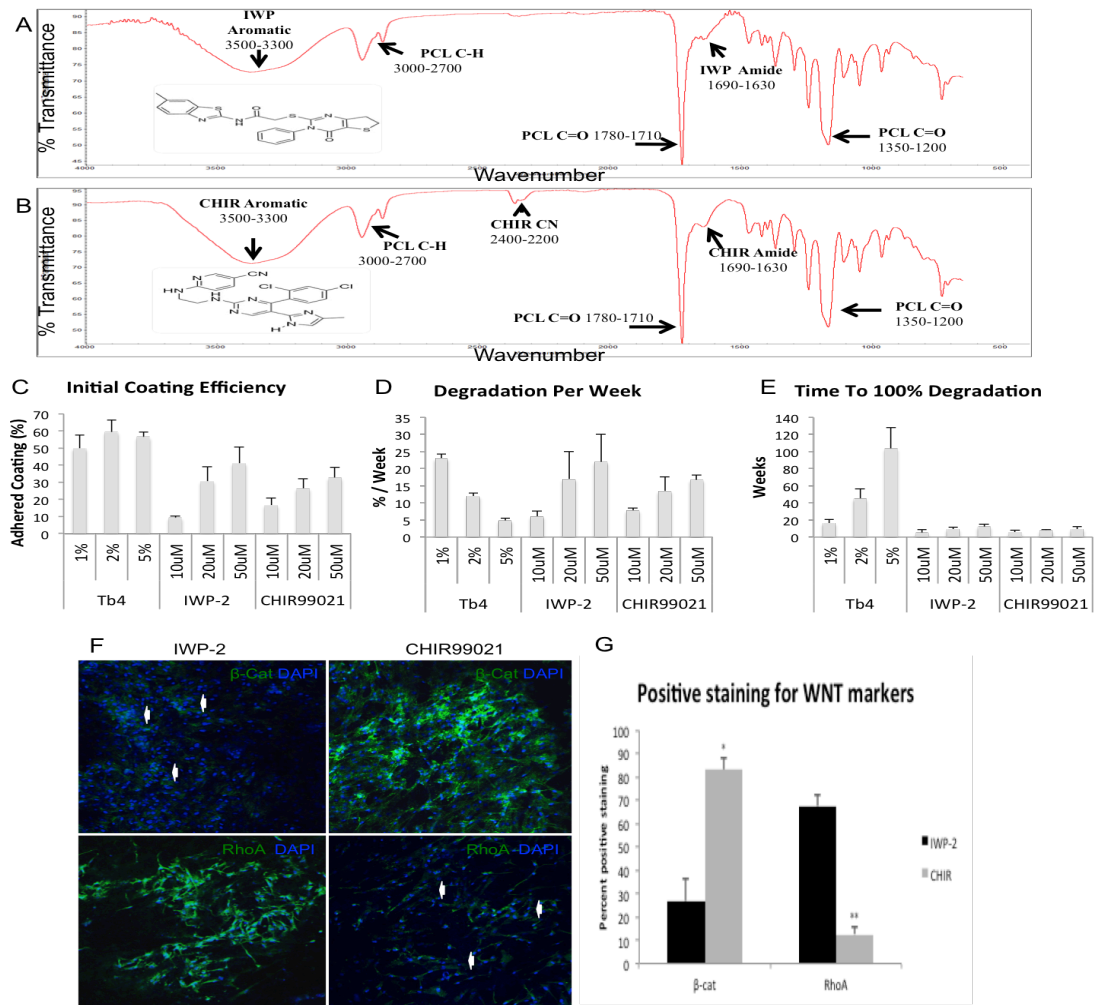


Figure 4.6: Comparing WNT effectors IWP-2 and CHIR99021. A. FTIR output of nanoscaffold coated in 20um IWP-2. B. FTIR output of nanoscaffold coated in 20um CHIR. Note the distinct peaks between the two small molecules, but the same peaks for the underlying PCL nanoscaffold. C. Coating efficiency of various concentrations of Tb4 and small molecules. D. The amount of degradation per week of concentrations of Tb4 and small molecules, calculated from FTIR peaks of remaining material. E. Total time until complete degradation of each of the small molecules and Tb4 per week, calculated from D. F. Molecular staining of β -catenin (top) and RhoA (bottom) demonstrating targeted effects on the WNT pathway. G. Calculations of positive staining area in F.

4.4.6 Combinatorial differentiation

We coated the nanoscaffolds with 20uM of either IWP-2 or CHIR99021 in a solution with 2% T β 4. Contrary to published reports on ESCs and iPSCs, we found the canonical promoter CHIR99021 significantly decreased hBMSC cell growth and differentiation compared to IWP-2, which induced robust growth and differentiation (Fig 4.7). After 24hrs, more cell growth was observed on nanoscaffolds coated with IWP-2/T β 4 compared to CHIR99021/T β 4 ($p < 0.001$) or T β 4 alone ($p < 0.01$). After 1 week, the IWP-2/T β 4 combination still showed remarkably better cell growth ($p < 0.001$ against both groups). Cells expressing cardiac biomarkers were also significantly more numerous in the IWP-2/T β 4 group compared to the two other combinations (Fig 4.7). In every case, T β 4 also outperformed CHIR99021 for cell growth and differentiation numbers, indicating CHIR99021 may have a detrimental effect on hBMSC proliferation.

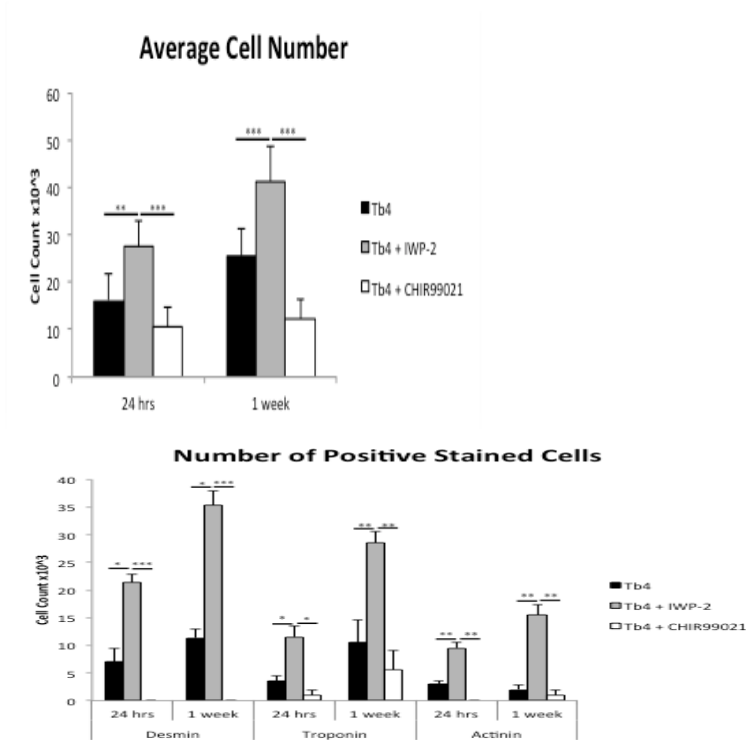
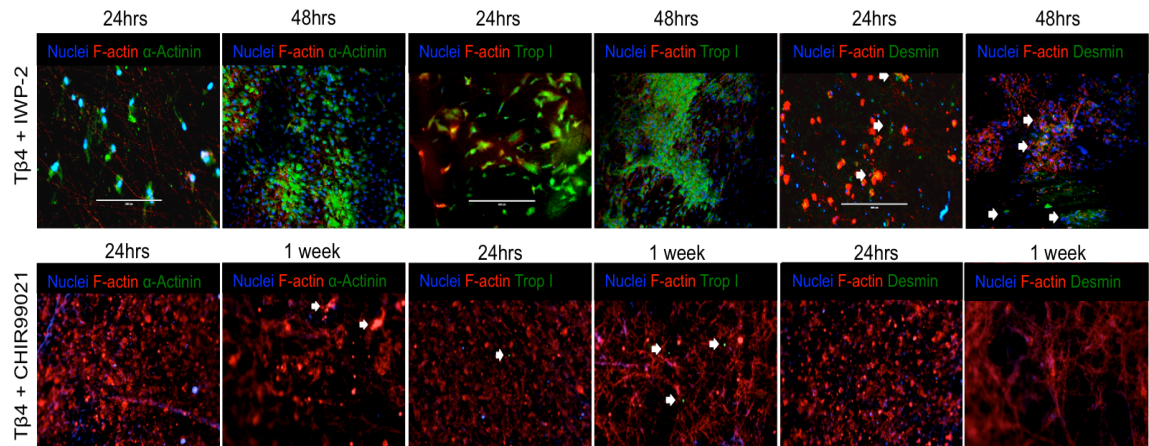


Figure 4.7: Synergistic effects of IWP-2 vs CHIR99021 in BMSC differentiation. IWP-2/Tβ4 significantly outperforms CHIR99021/Tβ4 in differentiating BMSCs to the cardiac lineage, as demonstrated by cardiac biomarker staining for α-actinin, troponin I, and desmin. Cell survival was also significantly increased. Scale bar=200um; *p<0.05; **p<0.01; ***p<0.001.

4.4.7 Cell maturation

With the success of the IWP-2/T β 4 combination, we sought to determine the extent and direction of differentiation by checking markers of ventricular cardiomyocyte maturation (Fig 4.8). Atrial natriuretic peptide (ANP) is fetally expressed in all cardiomyocytes but is not expressed in mature ventricular cardiomyocytes. We found in a time-course analysis that ANP expression decreases in our differentiating cells after 24hrs and continues to decrease until after 72hrs. We also found positive staining for other mature cardiomyocyte proteins: Connexin43, an ion channel protein used in cardiomyocyte cell-cell communication, and tropomyosin, a portion of the contractile apparatus (Fig 4.8).

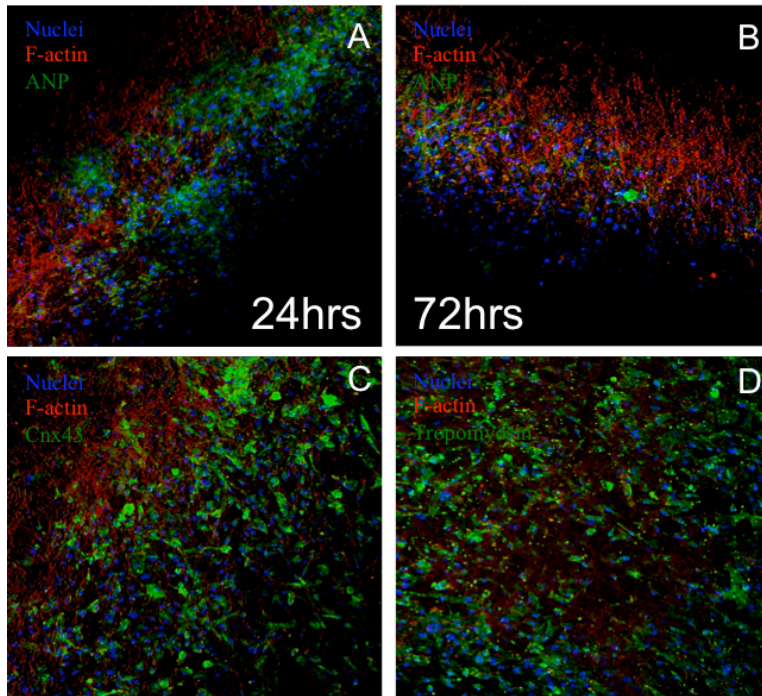


Figure 4.8: Evidence of BMSC cardiac maturation with IWP-2. A/B. Decreasing ANP staining over time indicates the transition from atrial to ventricular cardiomyocytes. C. Positive Cnx43 staining, allowing hBMSCs to communicate with native cardiomyocytes via ion channels. D. Positive tropomyosin staining.

4.4.8 Extra: Experimental PCL gel formulation

A separate experiment was performed to determine if a gel could be made from PCL beads. The rationale arrived from reading about thermoresponsive hydrogels that are injected to the heart. These gels “harden”, where they significantly increase their compressive modulus but are still pliable enough to not impede cardiac function. While these gels prevent cardiac remodeling, they are often acellular and implanted in an invasive manner^{50, 101, 102}, decreasing the translational value of the therapy. Our hypothesis then was that a biocompatible, injectable PCL gel could be made that would function the same as the PCL nanoscaffold (i.e- house factors and differentiate cells), and would therefore provide a secondary therapeutic for clinical use.

PCL beads were dissolved in DMSO and left to dry and harden under three conditions: spread thin in a petri dish, suctioned in a syringe, and deposited in a glass cylinder. Despite having the same concentration in each container (0.5mg/mL to 10mg/mL), only the cylindrical tubes produced a usable PCL gel. The petri dish produced a very papery PCL sheet that was weaker than the nanoscaffold; the syringe dried out so the PCL was crumbly on the inside and could not be rehydrated. Two experiments were then performed on the thicker, more gelatinous PCL produced in a glass tube.

PCL coating: Pieces of paper were dipped in Brilliant yellow dye and left to dry on the bench (Fig 4.9A/B). After drying, one paper was coated in PCL gel, the other left plain; both were then put in separate beakers of distilled water and allowed to leach their dye into solution (Fig 4.9C). After 2hrs, the fluid in the beakers was put into a UV/Vis machine to determine concentration of dye. Fig 4.9D shows a significant difference in color leaching; samples not coated in PCL had peaks 3x

higher than samples coated in PCL, demonstrating PCL produces a temporary water resistant coating that may be used for time-dependent particle delivery.

Cell growth: Because DMSO was used as a dissolving reagent, there needed to be assurance that after drying the gels were still biocompatible. To test this, we ran the same experiment described above (sterilize PCL; coat in 2% T β 4, 20uM IWP-2; seed with hBMSCs) and measured cell survival and differentiation (Fig 4.9E/F). Cells grew less readily on the PCL gel compared to the nanoscaffold, tending to favor thinner portions of the material; differentiation was also significantly reduced. This is a promising first step but further hBMSC work needs to be performed to determine whether and how best to translate this material in vivo.

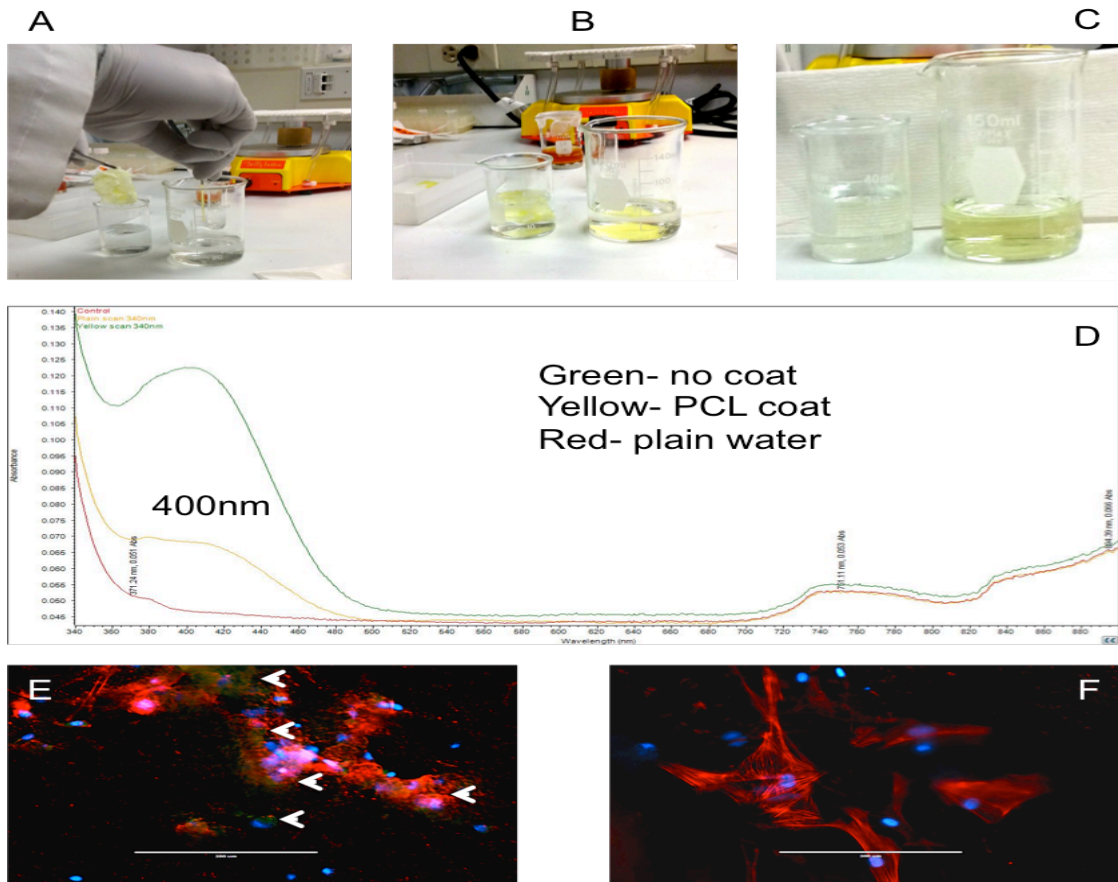


Figure 4.9: Experimental PCL gel. A-C. Coating a stained paper towel in PCL gel resulted in far less stain dissolving into dH₂O. D. dH₂O solutions after paper towel soaking. PCL gel (yellow) had significantly decreased stain peaks compared to control (green). E. Troponin differentiation indicated. Scale bar=200um. F. No positive desmin staining was found. Scale bar=200um.

4.5 Discussion

In this chapter we sought to outline the *in vitro* use of a poly(ϵ -caprolactone) (PCL) nanoscaffold on which to seed and differentiate human bone marrow mesenchymal stem cells (hBMSCs), for eventual use in repairing cardiac muscle after damaging cardiovascular events. Our study found PCL nanoscaffolds to be strong and biocompatible. hBMSC growth and differentiation was also aided by the addition of small molecule effectors of the WNT pathway, and the cardiac protein T β 4.

After fabrication any nanoscaffold construct can be subjected to coating, allowing the fiber to display novel researcher-selected properties such as hydrophobicity, bioactivity, or fluorescence¹⁰³. Bioactive coatings in particular can significantly enhance cell growth, cell signaling, and *in vivo* biocompatibility¹⁰⁴. Electrospinning allows nanoscaffolds produced to have extremely small diameters, creating a high surface area to volume ratio on which the cells can attach and proliferate⁸¹. Electrospun fibers also have topographical features that encourage cell adhesion, growth, and differentiation^{105, 106}. The electrospinning process produces fibers with a high porosity and interconnected pore structure, a crucial property that allows cells and nutrients to migrate from the exterior to the interior of the fibers^{107, 108}.

PCL has advantageous chemical properties that lends itself to biological applications. PCL is a biodegradable polymer with a slow rate of degradation¹⁰⁹ and low toxicity¹¹⁰. It also shows high anisotropy in cardiomyocyte cell culture when produced through electrospinning methods, and despite being a soft and flexible material PCL fibers are able to withstand the contraction force of a beating heart¹⁰⁹.

The ability of T β 4 to promote proliferation, differentiation, adhesion, and survival of cells has been used to enhance differentiation of stem cells towards the cardiac lineage, both *in vitro* and *in vivo*¹¹¹. T β 4 can be embedded within or used to

coat nanoscaffolds, on which cells are subsequently deposited. As these cells grow along the nanoscaffolding, extracellular phosphatidylinositol 3-kinase (PI3K) signaling is induced through interaction with T β 4, promoting an ILK-driven signaling cascade. Downstream activation of endothelial nitric oxide synthase 3 (eNOS) further increases cellular proliferation; in vivo, eNOS is crucial for regulation of vascular tone and promotion of angiogenesis, helping to explain how T β 4 increases vessel formation and stability^{112, 113}. Though there is still some speculation as to the surface receptor for T β 4, it is widely believed to be the purinergic receptor P2X4¹¹⁴, a receptor implicated in, among other biological processes, inflammasome activation after injury and ATP-stimulated electrical currents in ventricular cardiomyocytes^{115, 116}.

In vitro and in vivo cell differentiation studies have been performed using T β 4 as a primary or secondary differentiation factor. The Srivastava lab has worked extensively on characterizing T β 4 action for cell fate determination and differentiation as well as organogenesis. A recent paper by the lab¹¹⁷ shows cardiac fibroblasts can be differentiated to functional cardiomyocytes in vivo using the transcription factors Gata4, Mef2c and Tbx5, a process greatly enhanced by follow-up injection with T β 4. Injections of T β 4 into the injured heart also recruit resident cardiac stem cells to the site of injury where they differentiate into functional cardiomyocytes to aid in ventricular repair^{118, 119}, though whether T β 4 directly induces differentiation or whether induced changes in the cardiac microenvironment is the cause of differentiation is not yet clear⁸⁷. Qiu, et al.¹²⁰ used a transwell migration assay to show T β 4 is able to induce migration and differentiation of endothelial progenitor cells in vitro through the aforementioned ILK/eNOS pathway. Human umbilical vein endothelial cells, an in vitro cell model of angiogenesis, doubled vessel area and

formation when exposed to 100ng of Tβ4, with subsequent increases occurring in a concentration-dependent manner¹²¹. Our results using maximum 2% Tβ4 solutions are also comparable to previously described in vitro data where an overwhelming concentration of Tβ4 caused uncontrolled disassociations of actin bundles and cell death¹²². We therefore propose that lower and therefore less costly concentrations of Tβ4 could be efficiently used for cell differentiation.

To enhance cardiomyogenic differentiation we included IWP-2, a small molecule inhibitor of the canonical WNT pathway. Tβ4 and IWP-2 have synergistic effects on increasing cell survival to insults such as osmotic stress and proinflammatory cytokines, and increasing gene expression for tasks such as proliferation, differentiation, and mitosis^{123, 124}. In addition to enhancing the downstream effects of Tβ4, IWP-2 activation of components of the noncanonical/Ca²⁺ pathway has cardiac implications. NF-AT, activated by calcineurin-mediated dephosphorylation in response to increases in intracellular Ca²⁺, is crucial for heart muscle growth and ongoing protection in vivo¹²⁵. PKC, particularly the alpha isoform increased as a response to a rise in intracellular Ca²⁺, is imperative for cardiomyocyte survival and cardiac remodeling after injury¹²⁶. In vivo and ex vivo proliferation of mature cardiomyocytes can be aided by the attenuation of β-catenin, either through gene knockout¹²⁷ or small molecule addition to culture¹²⁸. In light of the slow degradation of the factors from the nanoscaffold and the positive cardiac benefits of our system it can be hypothesized that translating these factors in vivo will contribute to improved cardiac function after MI.

The results obtained in this chapter suggest that Tβ4 is a hBMSC growth factor that, when present, significantly increases cell growth and differentiation. A

biocompatible and biodegradable nanoscaffold was successfully created from a PCL polymer and coated with activating concentrations of T β 4 and the WNT inhibitor IWP-2. This nanoscaffold provided a support system by which hBMSCs were successfully differentiated towards the cardiac lineage. While the regenerative effects of T β 4 and the modulatory effects of IWP-2 have been well documented, to our knowledge this is the first time a platform for combined T β 4 promotion/canonical WNT inhibition has been fully developed and tested to successfully differentiate hBMSCs. This platform may serve as a simple and effective solution to repair various impairments of damaged cardiac tissue through in vivo implantation.

Chapter 5

ASSESS THE RESPONSE OF A GIVEN INFARCT TO AN OPTIMIZED DIFFERENTIATED hBMSC/NANOSCAFFOLD DELIVERY PLATFORM

5.1 Abstract

Cell-based therapies as treatment for myocardial infarction (MI) have demonstrated safety in vivo but mixed efficacy. To determine a potential reason why, we developed an adjustable rat model of MI in which to test the therapeutic effectiveness of intracardiac injections of human bone marrow mesenchymal stem cells (hBMSCs) and cell culture media. hBMSCs primed on protein- and small molecule-coated nanoscaffolds increased cardiac biomarker expression and decreased canonical WNT signaling. Subcutaneous administration of isoproterenol resulted in dose dependent myocardial damage in a rat model of ischemic MI. After intracardiac injections, hBMSCs engrafted within the heart and provided increased ejection fraction (EF) and fractional shortening (FS), and decreased left ventricular end systolic volume (LVESV), in animals given low and medium/high cardiac damage, compared to control rats. Media-only injections increased EF in hearts receiving low-level cardiac damage, but provided greater benefit compared to hBMSCs in improving left ventricular size and volume after systole across all damage levels. These results demonstrate stem cell-based therapies are not conducive to all levels of MI severity, and future stem cell trials will be aided by tailoring regenerative therapies to a patient's current cardiac function.

5.2 Background

The declining but still worrisome rate of cardiovascular disease and death has led researchers to look beyond pharmaceutical standards of care to new cell-based therapies to benefit patients^{129, 130}.

One innovation is the use of stem cells as a regenerative medicine strategy to replace damaged cardiac tissue after traumatic ischemic events such as a heart attack^{131, 132}. For example, the advent of induced pluripotent stem cells (iPSCs) allows for the development of beating cardiac tissue in vitro^{91, 92}, stoking thoughts that these cells could replace scar tissue in a damaged heart. Though this is a promising step forward, particularly for in vitro drug toxicity studies¹³³, the time to induce full differentiation can be prohibitively long, and only recently has iPSC therapy been translated to higher animals^{59, 134, 135}.

These drawbacks, coupled with the ethical issues inherent in embryonic stem cells, have led researchers to turn to adult stem cells to heal cardiac damage^{136, 137}. Human mesenchymal stem cells, particularly from the bone marrow (hBMSCs), have been used in hundreds of clinical trials for treatment of cardiac damage^{138, 139}, though discrepancies in efficacy reporting and patient subgroup analysis have prevented the spread of FDA-approved stem cell therapies for myocardial infarction (MI)³⁷.

Recent research has demonstrated two advances in hBMSC therapy for cardiac healing: first, priming the cells in vitro for eventual transplantation aides cell survival and terminal differentiation once the cells are deposited to the ischemic myocardium^{41, 140}; and second, paracrine factors produced by hBMSCs while differentiating in culture can be captured in the cell culture media and used as a separate therapy^{141, 142}.

In an effort to provide some clarification on patient populations that would best benefit from these two regenerative therapies, we have developed an adjustable rat

model of MI in which to test primed hBMSCs against cell culture media over a range of cardiac damage. In this chapter, we show that hBMSCs primed to increase non-canonical/ Ca^{2+} WNT signaling significantly improve ejection fraction (EF) and fractional shortening (FS) in animals receiving low ($p < 0.001$) and medium/high ($p < 0.01$) cardiac damage. Similarly, cell culture media significantly improves left ventricular size (LVIDs) and volume (LVESV) after MI in all groups, but this did not translate to significant improvements in cardiac function (EF, FS). Here we describe the successful development of a new therapy for treating a range of ischemic MI, but the discrepancies in damage resolution shown demonstrate the need for targeted patient populations in cell-based therapies for MI.

5.3 Materials and Methods

5.3.1 PCL solution formulation

PCL tablets were purchased from Sigma Aldrich (Missouri, USA). Dichloromethane (DCM) and N,N-dimethylformamide (DMF) were purchased from Acros Organics (Geel, Belgium). PCL tablets weighing 1.5g were dissolved in a solvent mixture containing a 1:4 ratio of DCM to DMF. This combination was sonicated for 1hr to ensure tablets were fully dissolved.

5.3.2 Electrospinning of nanoscaffold

The DCM/DCF/PCL solution was suctioned into a syringe and attached to a flow rate controller (Thermo Fisher Scientific, Massachusetts, USA). The solution was pumped at a flow rate of 0.5mL/h. A Voltmeter lead was attached to the syringe needle and another lead was attached to a rolling drum (Oriental Motor, Tokyo, Japan) that housed an aluminum sheet. The rolling drum was mounted on an E7 Limo easy

linear motion controller (Oriental Motor) for linear and rotational fiber distribution. The Human Machine Interface (Omron, Kyoto, Japan) was set at a 3hr run time, a starting position of 105mm, and a rolling drum speed of 630RPM. A potential of 12kV was applied between the spinneret and grounded collector located 12cm below the spinneret to pull the solution from the syringe and accurately align the fibers to the rolling drum mounted on the E7 Limo.

5.3.3 Nanoscaffold preparation

Electrospun PCL nanoscaffolds were adhered to square 20mm² coverslips by adhesive silicon type A glue (NuSil Technology, California, USA). Cover slips with nanoscaffolds were transferred and attached to the base of 6- or 12-well culture plates (Thermo Fisher Scientific, Massachusetts, USA) with silicon glue. Nanoscaffolding and cover slip were then sanitized as follows: 1mL bleach wash for 5min, rinse with ultrapure water (Millipore, Massachusetts, USA), repeat; 1mL ethanol wash for 5min, rinse with ultrapure water, repeat; nanoscaffolding was left under UV light to dry.

Optimization experiments (May 2014-March 2015): 100μL of 2%, 4%, or 10% concentrations of Tβ4 stock in ultrapure water were mixed with either 100μL of 20μM, 40μM, or 100μM concentrations of CHIR99021 or IWP-2 stocks (StemCell Technologies, Vancouver, Canada) in ultrapure water. Resulting 200uL solutions were used to coat the nanoscaffolds and allowed one hour to dry.

5.3.4 Cell culture

Human bone marrow mesenchymal stem cells (hBMSCs) were purchased from StemCell Technologies (Vancouver, Canada) and passaged in MSC Basal Medium (StemCell Technologies) with MesenCult Stimulatory Supplements (StemCell

Technologies) to prevent differentiation. hBMSCs were seeded at a concentration of $7.5-10 \times 10^4$ cells/mL over nanoscaffolds coated with T β 4 and/or CHIR99021 or IWP-2, and covered with MSC Basal Medium (StemCell Technologies) without supplementation to allow differentiation. Cells were incubated in a Forma SteriCycle CO₂ Incubator (Thermo Fisher Scientific, Massachusetts, USA) at 36.5°C and 5.0% CO₂.

5.3.5 Nanoparticle preparation

0.5g Fe II was mixed with 1.0g Fe III in 6mL diH₂O and stirred for 1hr at 1200RPM. Supernatant was removed and particles washed in ethanol 3x. Ethanol was allowed to evaporate, particles were resuspended in PBS, and spun down. The supernatant was removed, particles were resuspended, and run through a 0.1 μ m filter. The filtrate was resuspended in 1-2mL PBS with a ratio of 1 μ L Lipofectamine:1mL of cell culture media. NP/PBS/Lipofectamine was added to cell culture flasks 24hrs prior to seeding on nanoscaffolds.

5.3.6 Microscopic analysis

An EvosFL Cell Imaging System (Life Technologies, Carlsbad, CA) was used to monitor cell growth and determine preliminary cell counts. Cells were washed and stained as described, and placed on the microscope stage. An image was taken, and the Toolbar function was used to place a hemocytometer grid on the screen for cell counts.

5.3.7 Animals

IACUC: Final protocol (AUP#1301) was approved in late March 2016; experiments began on 2month old female Sprague Dawley rats (Envigo, Maryland, USA) in April 2016. No protocol was long enough to necessitate eye drops or a

heating pad. No dietary manipulations were induced. Clinical parameters that necessitated euthanasia, including sluggishness that impedes eating or drinking, weight loss exceeding 20%, hunched posture, or serious infection, were used to determine if animals should not continue through the full course of experimentation.

Heart attack induction: Isoproterenol (ISO; Sigma Aldrich, Missouri, USA) was dissolved in PBS at concentrations ranging from 10mg ISO per kg rat body weight (mg/kg) to 100mg/kg, with lower concentrations corresponding to a less severe heart attack. ISO was dissolved in a sterile rubber capped vial at volumes dependent on number of animals in the protocol (no more than 5mL at any one time). Solutions were kept for no longer than 2weeks, as ISO is light sensitive. To induce the heart attack, rats were anesthetized with isoflurane through a nose cone, level 4 for induction, level 2 for maintenance. Injections of ~100uL (dependent on ISO concentration and rat weight) were made subcutaneously at the base of the neck. Long acting (72hr) buprenorphine was given directly following injection; short acting (24hr) buprenorphine was given as needed for the remaining protocol period. Rats were monitored for 1hr after injection to ensure no adverse effects; subsequent checkups occurred 3x daily for 1week.

Ultrasound: Rats were anesthetized with isoflurane through a nose cone, level 4 for induction, level 2 for maintenance. The left thoracic region was shaved to aid visualization. Ultrasound gel was placed on the shaved area and on the ultrasound probe. The probe was placed parallel to the ribs with the rat laying on its right side. Standard images were taken in M-mode; blood flow images were taken using the Doppler setting. Rats were monitored for 1hr following ultrasound to ensure no side effects from prolonged anesthesia. Left ventricular interior diameter during diastole

(LVIDd) and systole (LVIDs) were measured using ultrasound readouts. The following calculations were then performed to determine cardiac function (FS: fractional shortening; LVESV: left ventricular end systolic volume; LVEDV: left ventricular end diastolic volume; EF: ejection fraction):

$$FS\% = 100 * ((LVIDd - LVIDs) / LVIDs)$$

$$LVESV = (7 / (2.4 + LVIDs)) * (LVIDs^3)$$

$$EF\% = 100 * ((LVEDV - LVESV) / LVEDV)$$

Intra-cardiac injections: 48hrs after ISO injections, rats were anesthetized for standard ultrasound just prior to intra-cardiac injections. 1mL syringes (20-24G) were loaded with 100uL of either PBS, cell culture media only, or cell culture media + nanoscaffold containing hBMSCs. The heart was detected manually by feeling for the 4th intercostal space of a rat laying on its right side. Needle puncture occurred in the 2nd intercostal space and moved from the upper left hypochondriac region to the middle epigastric region to puncture the left ventricle of the rat heart. Aspiration of pumping blood prior to injection ensured placement within the left ventricle and not the body cavity. The syringe contents were then slowly dispensed into the left ventricle cavity and the needle removed from the body. Rats were monitored directly for 1hr after injection to ensure no immediate adverse effects; subsequent checkups occurred 3x daily for 1week.

Euthanization: After 2weeks animals were euthanized via intraperitoneal injection of Euthazol solution. Death was confirmed by tail and toe pinch, and lack of breathing. Animals were then necropsied, with heart removed. Other organs, such as kidneys, liver, and lungs, were also removed.

Tissue imaging: Hearts were flash frozen in liquid nitrogen and stored at -80°C. Frozen hearts were placed in a Leica 3050 Cryostat (Leica, Wetzlar, Germany), sliced at 10µm, and mounted on glass slides. Slides were stained for immunofluorescence as described above (fixed in PFA, washed in PBS, 1^o anti-SRY at 1:200, 2^o donkey anti-mouse at 1:200) and imaged via Zeiss 5 LIVE DUO Highspeed/Spectral Confocal microscope (Zeiss, Gena, Germany). Slides were stained for nanoparticles using proprietary reagents from HEMATOGNOST Fe® kit (Millipore, Massachusetts, USA). Slides were stained with H&E as per DBI protocol. H&E and nanoparticle slides were imaged using Axioplan 2 Upright Light Microscope (Zeiss, Gena, Germany) with top-mounted AxioCam camera and software (Zeiss).

5.3.8 Statistics

The statistical significance of the results was determined using analysis of variance (ANOVA) and a multiple means comparison function (t-test) in JMP/GraphPad Prism with an alpha level of 0.05. All error bars are reported in mean ± standard error from the mean. N is dependent on experimental protocol.

Animal numbers: The statistics and pilot studies indicate approximately 120 animals were needed to complete the initial experiment. Attrition in the pilot studies necessitated an increase in the number of animals per group; the statistics indicated $n=4/\text{sample}$ with 4 samples/group = 16 rats/group, but we elected to increase by 0.66 to ensure enough rats for statistical viability in the results.

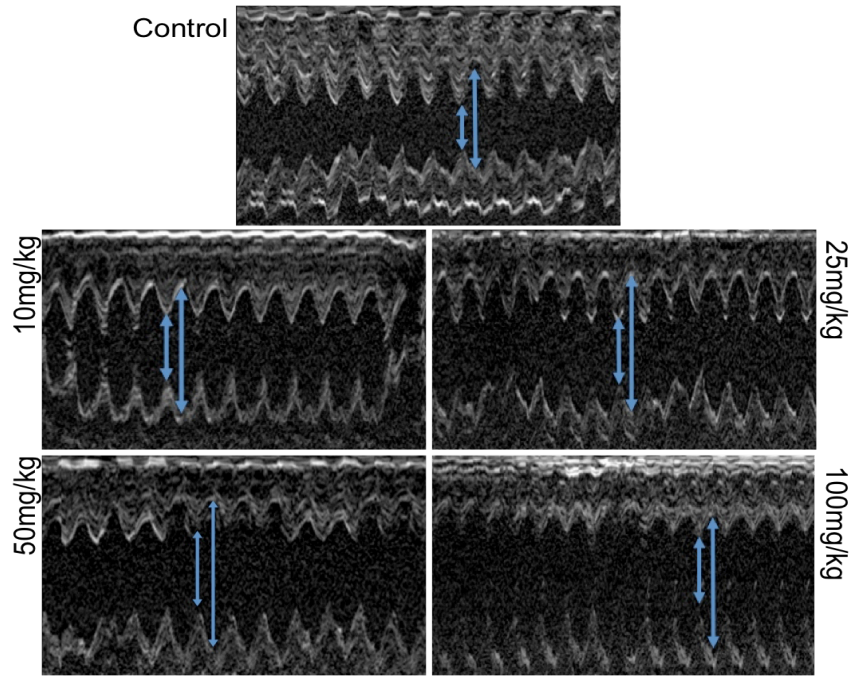


Figure 5.1: Representative ultrasounds. Arrows show left ventricular interior diameter during systole (small arrow) and diastole (large arrow), which are used to calculate cardiac metrics.

5.4 Results

5.4.1 Development of adjustable MI model

The beta-agonist isoproterenol induces a range of ischemic cardiomyopathy by forcing cells to outpace their use of oxygen and nutrients^{64, 75}. These variable effects are seen across studies, but have never been investigated together. We sought to develop an adjustable model of MI that would allow us to test the effects of multiple therapies over a range of cardiac damage (Fig 3.4, Fig 5.1). Isoproterenol caused notable changes in cardiac metrics compared to untreated controls, demonstrated by linear decreases in EF ($p=0.07$ vs $p<0.05$) and FS ($p=0.06$ vs $p<0.05$), and increased LVESV ($p<0.05$ vs $p<0.01$) in 10mg/kg to 100mg/kg, respectively. Histological images show intramuscular edema, characterized by wavy actin fibers and dissociation of linear contractile cell morphology (see Chapter 3, Figure 3.3). In the largest dose (100mg/kg), there is a complete dissociation of muscle fibers from their linear contractile alignment (see Chapter 3, Figure 3.3).

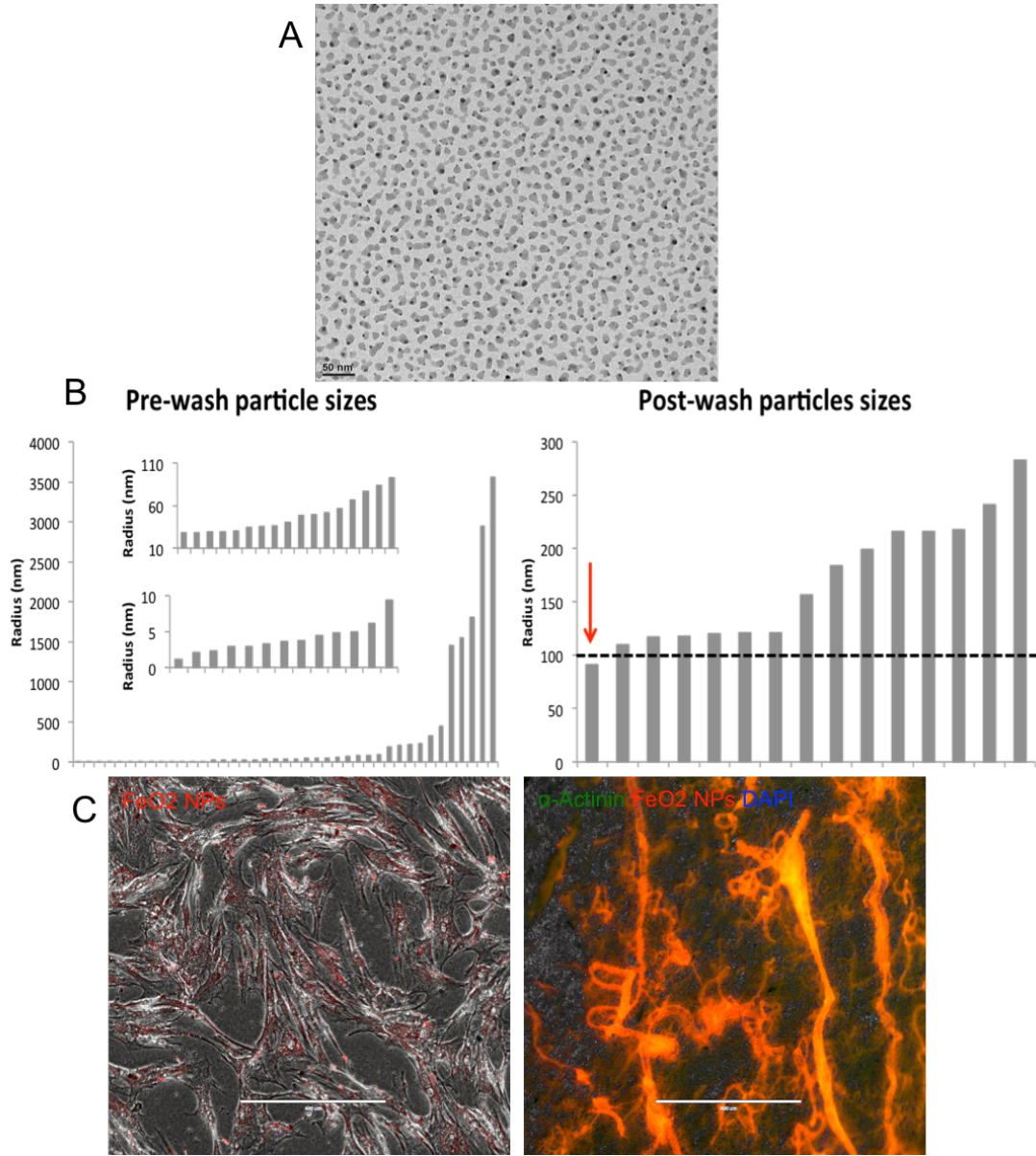


Figure 5.2: NP formulation and addition to cells. A. TEM of NPs showing uniform size. B. DLS graph(s) of NPs formulation. Washing and rinsing through 0.1um pore sized filters resulted in consistent sub-100nm particles. C. Rinsed nanoparticles were transfected to BMSCs in culture. No effect was seen on differentiation potential.

5.4.2 hBMSCs engraft to the myocardium

Either primed hBMSCs on nanoscaffolds, cell culture media, or PBS was injected into the LV of rat populations 48hrs after MI induction (Fig 5.3A). To enhance visualization and tracking of hBMSCs, FeO₂ nanoparticles (NPs) were synthesized and subsequently transfected to hBMSCs prior to seeding on nanoscaffolds (Fig 5.2). NP transfection to cells did not affect growth or differentiation in vitro (Fig 5.2C). We used male hBMSCS that were sex-mismatched to target animals, which allowed for staining of the SRY protein (Y chromosome) against the female rat background. Immunohistochemistry and iron oxide staining demonstrated successful engraftment of hBMSCs within the rat hearts, sustained over the 2week study period (Fig 5.3). Positive markers for hBMSCs were seen from the ventricular side to the epicardium (Fig 5.3B/C), indicating the cells were able to integrate throughout the ventricular myocardium.

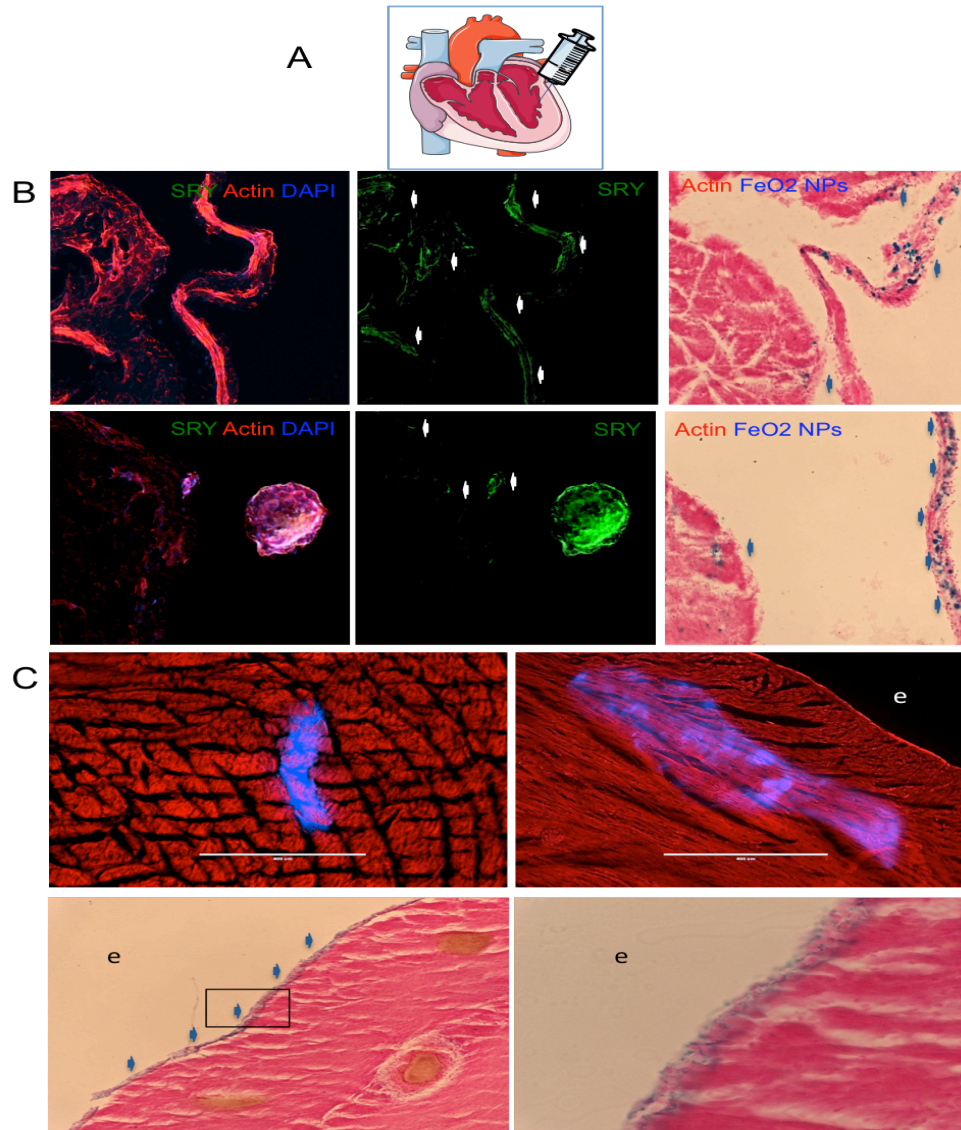


Figure 5.3: Cellular injections stayed in the heart after 2weeks. A. Schematic image demonstrating injection strategy. B. Positive staining for SRY protein (green, indicated by white arrowheads) and NPs (navy, indicated by blue arrowheads) in the same area shows cells stayed in the heart. C. Injected cells spread through spaces in myocardial tissue caused by increasing cardiac damage allowing collections of cells to be found beneath the epicardial membrane despite being injected into the ventricle. Blue, nanoparticles/cells; red, cardiac actinin; e, epicardium.

5.4.3 Therapeutic benefit of injections is dependent on cardiac damage

hBMSCs and cell culture media were injected to the left ventricle and compared to a sham PBS injection to determine the effect of primed therapies on improvement of cardiac metrics after 2 weeks (Table 1). No differences were seen in baseline cardiac measurements between any groups.

Cell media: Injections of cell culture media prevented left ventricular remodeling, demonstrated by significant decreases in size and volume of rat hearts post-MI for all damage levels compared to PBS injections, except 25mg/kg ($p=0.07$ for LVIDs; $p=0.08$ for LVESV; Fig. 5.4, Table 1). The therapeutic benefit increased in a linear fashion in direct correlation to an increase in cardiac damage, illustrating a damage-dependent healing effect (Fig 5.4, graphs). Cardiac function was only significantly improved in the hearts with the smallest damage (10mg/kg; $p=0.03$ for FS, $p<0.01$ for EF).

hBMSCs: hBMSC injections also significantly improved the size and volume of rat hearts post-MI for all damage levels except in the 25mg/kg group ($p=0.12$ for LVIDs; $p=0.13$ for LVESV), though the beneficial effect was noticeably less than the cell culture media alone (Fig. 5.4, Table 1). hBMSC injections proved much more beneficial in improving cardiac function, showing significant benefits in the small (10mg/kg) and medium/large (50mg/kg) MI groups. hBMSCs averaged an 11% increase in EF over PBS control ($p=0.09$) in the largest 100mg/kg group (Fig. 5.4, graphs).

		Week 0				NS	Week 1			NS	Week 2			NS
		CNTRL	PBS	MEDIA	MSCs		PBS	MEDIA	MSCs		PBS	MEDIA	MSCs	
Weight	10	228.3	212.0	218.0	213.0	NS	220.0	221.3	218.5	NS	228.5	226.8	228.0	NS
	25	228.3	215.3	212.0	212.0	NS	219.5	224.8	*214.25	NS	226.0	228.5	221.8	NS
	50	228.3	206.0	203.5	204.8	NS	211.5	208.0	215.8	NS	222.3	217.3	225.8	NS
	100	228.3	216.0	208.0	218.3	NS	228.3	215.8	219.0	NS	231.3	220.3	229.5	NS
LVIDd	10	3.2	2.7	3.1	3.1	NS	3.4	3.1	3.1	NS	3.6	*2.9	3.1	NS
	25	3.2	3.3	3.0	3.2	NS	3.3	3.1	*2.8	NS	3.3	3.0	3.1	
	50	3.2	3.4	2.8	3.0	NS	3.2	2.9	2.9	NS	3.5	**2.7	3.4	
	100	3.2	3.3	3.0	3.2	NS	3.3	3.1	*2.9	NS	3.4	**2.9	2.9	
LVIDs	10	1.4	1.3	1.6	1.6	NS	1.6	1.5	1.3	NS	2.3	***1.5	**1.4	NS
	25	1.4	1.7	1.4	1.6	NS	1.6	1.3	**1.1	NS	1.8	1.4	1.6	
	50	1.4	1.7	1.7	1.5	NS	1.6	1.4	1.3	NS	2.1	**1.3	*1.7	
	100	1.4	1.9	1.7	1.7	NS	1.8	1.3*	1.4	NS	2.0	*1.4	*1.4	
LVEDV	10	41.1	28.7	37.1	38.7	NS	48.4	39.2	38.7	NS	54.6	*31.8	39.0	NS
	25	41.1	45.7	34.1	42.1	NS	44.6	36.7	*29.6	NS	43.5	34.3	37.3	
	50	41.1	49.8	30.6	34.6	NS	42.1	32.4	31.5	NS	51.8	***27.5	46.6	
	100	41.1	44.9	35.6	39.6	NS	42.8	39.7	*32.9	NS	47.8	**31.6	32.7	
LVESV	10	5.1	5.0	8.0	7.7	NS	7.6	7.0	4.2	NS	17.4	**5.7	**5.6	NS
	25	5.1	8.4	5.4	7.9	NS	7.4	4.3	**2.5	NS	9.8	5.6	6.7	
	50	5.1	9.2	8.3	6.0	NS	7.3	4.7	4.3	NS	14.2	**5.0	*8.5	
	100	5.1	12.2	8.5	8.5	NS	10.7	4.0	4.9	NS	12.9	*4.7	*4.8	
FS	10	56%	51%	47%	51%	NS	54%	51%	58%	NS	38%	*48%	***54%	NS
	25	56%	51%	53%	50%	NS	51%	60%	61%	NS	45%	52%	50%	
	50	56%	51%	40%	52%	NS	52%	53%	55%	NS	41%	51%	*50%	
	100	56%	43%	45%	46%	NS	45%	58%	53%	NS	43%	53%	50%	
EF	10	87%	83%	79%	82%	NS	85%	83%	89%	NS	69%	*81%	***86%	NS
	25	87%	83%	85%	82%	NS	82%	89%	91%	NS	78%	84%	82%	
	50	87%	82%	70%	84%	NS	83%	86%	86%	NS	73%	82%	*82%	
	100	87%	75%	76%	79%	NS	76%	88%	85%	NS	74%	85%	85%	

Table 1.1: Animal measurements taken over the full 2week study period. No significance was noted at baseline in any animal group. N=4 animals per test; *p<0.05, **p<0.01, ***p<0.001, NS=no significance of samples compared to PBS control; data are mean±SEM. LVIDd, left ventricular internal diameter during diastole; LVIDs, left ventricular internal diameter during systole; LVEDV, left ventricular end diastolic volume; LVESV, left ventricular end systolic volume; FS, fractional shortening; EF, ejection fraction.

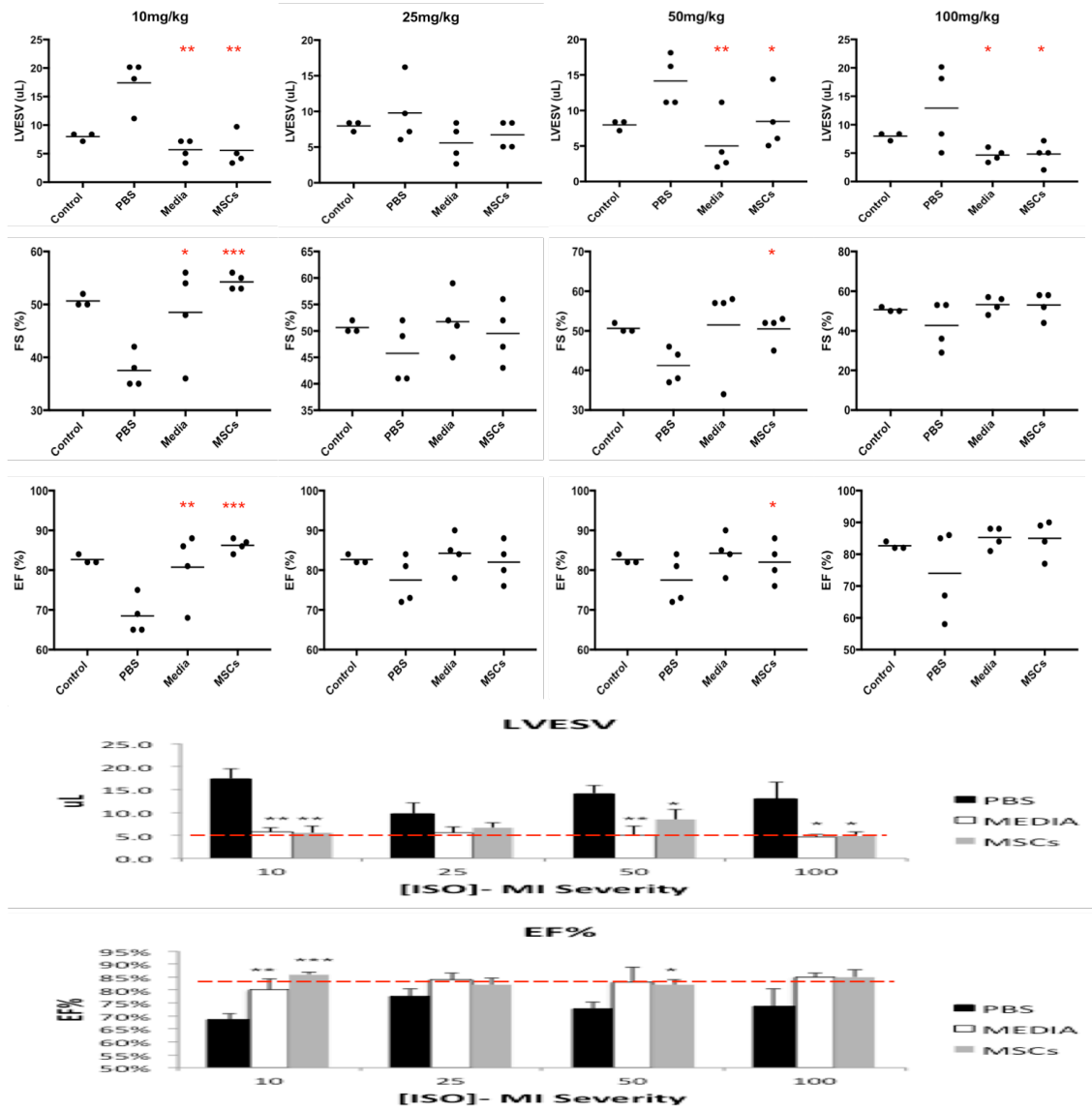


Figure 5.4: Therapeutic injections prevent LV remodeling and improve cardiac function. Despite lack of statistical significance, therapeutic injections increased FS and EF over PBS control in all cases (see graphs). N=4 animals per test; red line= control sample means; *p<0.05, **p<0.01, ***p<0.001 of samples compared to PBS control ; data are mean±SEM. LVESV, left ventricular end systolic volume; FS, fractional shortening; EF, ejection fraction.

5.5 Discussion

Despite the large number of clinical trials using hBMSCs as treatment for various cardiac disorders, there is still no consensus as to the effectiveness of treatment. This can be partially explained by the lack of sub-group analysis across studies. Indeed, the correlation between increased therapeutic benefit of cell therapy and increasing cardiac damage seen in patients is not without precedent. Two large clinical trials (POSEIDON¹³⁶ and REPAIR-AMI¹⁴³) demonstrated a marked improvement in patients receiving hBMSCs only when EF was <20% or <50%. In a two-year follow-up of the REPAIR-AMI cohort¹⁴⁴, this benefit was not borne out in patients with EF above a 30% threshold. Similarly, injections of factors from cell culture media were performed in a large PhIII trial (STEM-AMI OUTCOME¹⁴⁵), demonstrating notable improvement in LV remodeling over a 3year follow-up but no significant improvements in EF. We were able to corroborate outcomes from these clinical trials with data from this study.

Rat groups receiving therapeutic injections for small cardiac damage (10mg isoproterenol/kg body weight) demonstrated the largest improvements in all metrics, particularly in relation to PBS control groups. This can be partially explained by the presence of cardiac-specific resident cKit+ stem cells¹⁴⁶ in vivo. This niche cell population is released in response to ventricular damage to provide precursors to new cardiomyocytes^{27, 28}; this extensive repopulation and repair though is not seen in animals with more diffuse cardiac damage¹⁴⁷. With the large decrease in EF improvement between 10mg/kg and 25mg/kg seen in this study (-5% for Media only; -14% for MSCs), it can be concluded that cardiac damage using isoproterenol concentrations above 10mg/kg in this study resulted in a depletion of cKit+ therapeutic benefit, a conclusion bolstered by comparison to previous studies^{148, 149}.

Also, the large increase in EF seen when comparing our treatment with PBS control injections in the 10mg/kg cohort independently provides evidence for a synergistic effect of our therapy with native cardiac repair mechanisms. Future work will elucidate this interaction more fully.

Positive cardiac benefits seen from injections of cell culture media and hBMSCs are thought to result from the supposed “hit and run” paracrine effects of cellular factors^{30, 150}. These factors, released by hBMSCs into the culture media as they are growing or after the cells have been injected to the heart, are a combination of proteins, exosomes, small molecules, and other soluble factors that may impact cardiac function and/or improve recruitment of native cell populations (i.e- cKit+ stem cells)^{141, 142}. Our therapy also benefitted from integration of hBMSCs into the myocardium, which followed the wave-front phenomenon of ischemic cell death¹⁵¹ (sub-endocardial to epicardial damage). Increasing cardiac ischemia was correlated with greater cell integration and improvements in contractile metrics after hBMSC injection (mean EF above PBS control: 4% at 25mg/kg; 9% at 50mg/kg; 11% at 100mg/kg). We therefore conclude that more extensive integration of our cells provided continued therapeutic paracrine effects to the remodeling hearts.

The hBMSCs used in this study were primed on a polycaprolactone (PCL) nanoscaffold system. An electrospun PCL polymer is an ideal nanoscaffolding material for cardiac biological applications as it is both biocompatible and biodegradable^{109, 152} and is able to withstand the forces produced by contraction of a healthy adult heart¹⁵². hBMSCs in general are known to produce an extracellular matrix when grown on nanoscaffolding material of varying stiffness and polymer

composition^{153, 154}, and this could be contributing to the extensive nanoscaffold coverage we observe (see Chapter 4).

We confirmed previous results^{100, 111} showing T β 4 alone is sufficient to steer stem cells towards cardiac-like cells. T β 4 is an actin regulator, promoting polymerization and cell growth¹⁵⁵. To enhance cardiomygenic differentiation we included IWP-2, a small molecule inhibitor of the canonical WNT pathway. T β 4 and IWP-2 have synergistic effects on increasing cell survival to insults such as osmotic stress and proinflammatory cytokines, and increasing gene expression for tasks such as proliferation, differentiation, and mitosis^{123, 124}, potentially explaining why we saw robust in vivo hBMSC stability over the 2week monitoring period.

Limitations of this study were mainly due to the small number of animals available for each treatment group. For example, after one week statistically significant recordings were seen when measuring ventricular size in the 25mg/kg group, but these results were not borne out for the duration of the experiment (exception: LVIDs measurement for media-only injection, p=0.04 at 1week, p=0.03 at 2weeks). Similarly, p-values for EF among media-treated groups trended towards significance (p=0.07 for 25mg/kg; p=0.08 for 50mg/kg; p=0.07 for 100mg/kg), but outlier effects hid the fact that EF was improved 6-11% compared to PBS injections (Fig. 5.4, graphs). Future work will look to expand the number of included animals, and increase study duration to determine effects on prevention of heart failure.

To our knowledge this is the first study to perform side-by-side comparisons of hBMSC cell and culture media injections in a murine model to improve heart function over a wide range of cardiac damage. We were able to demonstrate a profound positive effect of hBMSC cell and media therapy on cardiac volumetric and contractile

performance compared to a PBS control, but the outcomes were specific to the extent of cardiac damage. These results, coupled with comparisons from clinical trials, leads to the conclusion that targeting of specific patient populations is crucial to determine which patients will receive the greatest benefit (if any) from hBMSC cell therapy.

Chapter 6

CONCLUSION AND FUTURE DIRECTIONS

6.1 Background

The burden of heart disease is a continual worldwide issue. Hallmark signs of heart disease (hypertension, atherosclerotic plaque buildup, and heart failure) often lead to myocardial infarctions (MI) and progression to heart failure (HF), decreasing left ventricular wall thickness and contraction force^{2,3}. The resulting ventricular remodeling leading to lack of contractile tissue is due to the extremely slow proliferation rate of cardiomyocytes⁵, necessitating research of regenerative cardiac therapies tested in proper animal models of MI.

In the preceding chapters, we have described the development of an *in vivo* regenerative medicine model used to test the efficacy of adult stem cells in healing the cardiac environment post-MI. We had measured success in differentiating our stem cells towards cardiac tissue and in determining the severity of cardiac damage that was healed best by our regenerative medicine strategy. This work will lay the foundation for future experiments in determining how best to heal MI damage using a stem cell/nanoscaffolding system.

6.2 Specific Aim 1

6.2.1 Conclusion

The induction of MI in rat models can be invasive or noninvasive. The hallmark MI model is the left anterior descending artery (LAD) ligation model, which was first used to prove efficacy of angiotensin II and ACE inhibitors¹⁶. This technique, along with electrocautery, relies on invasive surgeries to induce full thickness ventricular damage, which may account for less than half of the MI pathologies seen in a given clinic¹⁵⁶. Animals recovering from these surgeries then have to heal from both invasive surgery and MI, a pathology not seen in normal MI patients pretreatment. Meanwhile, studies allowing the animal to first recover from surgery before treatment run the risk of the animal developing an “old” infarct complete with noncontractile scar tissue development.

Isoproterenol, a beta agonist, is injected subcutaneously to induce diffuse myocardial damage, with cardiac damage directly correlated to dose¹⁵⁷. At higher concentrations and/or multiple injections (>200mg/kg; >3 injections), nonspecific damage to other organs and cardiac atria are observed¹⁵⁸, necessitating proper experimental setup. To combat these potential issues, we injected female Sprague Dawley rats with concentrations of isoproterenol ranging from 0mg isoproterenol per kg rat weight (mg/kg), to 150mg/kg, to test the potential toxicities and induction of cardiac damage. We were able to demonstrate reproducible dose-dependent damage within rat myocardium, with some animal death noted in concentrations above 100mg/kg. As far as we have found, this is the first instance in which a single protocol has used an extensive range of isoproterenol concentrations and compared the results within a single study. As mentioned in Chapter 3, many labs use single concentrations

to induce native cardiac stem cell release or promote extensive myocardial ischemia. By tailoring our concentrations, we have shown that isoproterenol can be used to induce a range of cardiac damage that better represents the full spate of ischemic MI seen clinically. Though further translation to higher animal models will require continued optimization, the data presented above provides a solid primer for future noninvasive ischemic MI models to build on.

6.2.2 Future directions

LAD ligation methods can be applied in mice, but extensive surgical expertise is needed as there is much less margin for error due to smaller organ size⁵³. Researchers working with mice though, compared to rats, have the added advantage of being able to choose from an extensive array of knockout models, including Cre¹⁵⁹ and FLP¹⁶⁰ recombinase systems, tetracycline-inducible (Tet) conditional gene targeting¹⁶¹, and more recently zinc fingers¹⁶² and TALENs¹⁶³ (techniques reviewed more extensively in Ref.¹⁶⁴). These models allow researchers to mimic HF following MI by selectively knocking out protein pathways or developing necrotic tissue by outright killing specific cardiomyocytes, potentially decreasing the need for invasive models. Although limited, genetic models do exist for rats. The Dahl salt-sensitive rat¹⁶⁵ and the McCune model¹⁶⁶ slowly develop HF and hypertension. These models are more clinically relevant than surgical methods, but can be expensive to house while waiting for disease to develop⁵³.

By combining these multiple methods to induce cardiac damage, researchers may be able to recapitulate congenital and environmental defects to test future regenerative strategies¹⁶⁴. For example, it is well known that stroke¹⁶⁷ and arrhythmias¹⁶⁸ are significantly more common in children and adults with congenital

heart defects; all three are easily recapitulated in separate animal models but have not been tested as comorbidities. Similarly, malformations in the protein phosphatase-1 catalytic subunit beta (PPP1CB) lead to congenital heart defects¹⁶⁹; inducing small, focal isoproterenol-induced ischemia in a PPP1CB knockout could provide a model for studying de novo repair in exercise-induced ischemia.

6.3 Specific Aim 2

6.3.1 Conclusion

Because of the controversy surrounding MSC differentiation to the cardiac lineage, we developed our own cardiac differentiation protocol for human derived bone marrow stem cells (hBMSCs). This protocol used a polycaprolactone nanoscaffold base housing two factors: the cardiac protein thymosin β 4 (T β 4); and the small molecule canonical WNT pathway inhibitor IWP-2. hBMSCs were then coated on top of this nanoscaffold and allowed to interact with the factors and nanoscaffolding material.

We were able to show robust differentiation and maturation of our stem cells towards the cardiac lineage, based on cardiac biomarker staining. This was also shown to be dependent on down regulation of the canonical WNT pathway, as cells grown on a nanoscaffold coated with CHIR99021, a canonical WNT promoter, failed to differentiate or thrive. Our nanoscaffold material was biocompatible, and slowly degraded over time, providing a satisfactory surface for hBMSCs to begin growing before laying their own extracellular matrix¹⁷⁰.

6.3.2 Future directions

In line with all published literature on MSC differentiation protocols, we did not observe beating cardiomyocytes on our nanoscaffold. In our model specifically, this could be for two reasons. First, the tensile modulus of the nanoscaffold may have been too high for the cells. Increasing stiffness of a given nanoscaffold material pushes hBMSCs towards other lineages (namely, osteogenic)^{171,172}. Even mature cardiomyocytes grown on stiffer nanoscaffolding decrease contractile function and increase production of stress fibers¹⁷³. This could explain our observed increase in positive staining for troponin I, an inhibitory portion of the contractile apparatus, compared to α -actinin, meaning our nanoscaffolding material may be too stiff to support contraction. By tweaking the stiffness of our nanoscaffold, perhaps by pre-incubating the material or using a different polymer, we may be able to increase contractile protein production.

Second, the cells may not have been incubated for a long enough period to begin transcription of the contractile machinery. The most robust differentiation of pluripotent stem cells to cardiomyocytes involves 14 days of incubation following weeks of preparation⁹², and previous attempts to differentiate hBMSCs to cardiomyocytes using nanofiber morphology required an experimental period of 56 days¹⁷³, which still did not yield mature, beating cardiomyocytes. To our knowledge no group has been able to produce beating cardiomyocytes from hBMSCs, but there is still confidence in their therapeutic potential, as evidenced by the plethora of clinical trials involving naïve hBMSCs. By taking our growth out past 1 week, we may be able to produce beating cardiomyocytes.

Synthetic contractility may be possible by targeting the interaction between the sarco/endoplasmic reticulum Ca^{2+} -ATPase (SERCA) and phospholamban (PLB). It is

well known that PLB inhibits SERCA activity by decreasing the Ca^{2+} ion concentration, preventing refilling of the sarcoplasmic reticulum and delaying the next heart contraction^{174, 175}. What has also been shown is the relationship between β -adrenergic signaling and PLB inhibition, whereby β -adrenergic agonists such as epinephrine or isoproterenol can activate protein kinase A (PKA) which increases phosphorylation, and thus inhibition, of PLB^{176, 177}. In all, this leads to increased SERCA activity and Ca^{2+} trafficking, promoting increased contraction and stroke volume (in vivo). To this end, addition of exogenous Ca^{2+} and a β -adrenergic agonist such as epinephrine or isoproterenol to our in vitro culture may block the effects of PLB, flooding the cell with Ca^{2+} and inducing contractility. This would be further enhanced on our nanoscaffold platform because of IWP-2's effects of NF-AT and PKC, two proteins important for cardiac cell protection and growth that are activated by increased intracellular Ca^{2+} ^{125, 178}. Further investigation into the expression of cell surface L-type Ca^{2+} channels, and proper cell regulation of Na^+ and K^+ flow, would also be beneficial.

The development of a biocompatible therapy to treat the ischemic MI model described above is of crucial importance. The range of therapies that have been previously attempted is enormous, stretching from acellular hydrogels¹⁰² and synthetic nanoscaffolds^{101, 179}, to fully biologically-based scaffolds^{52, 180}, and even plain cells^{181, 182}. While moderate success has been found in animal models, the translation to clinical trials has been slow and plagued by controversy³⁷.

In recent decades, there has been a shift towards including stem cells in the regenerative medicine process for repairing infarcted myocardium. This sea change resulted from discoveries concerning the immune system interaction with adult stem

cells (i.e- there is very little³⁰), that there are resident stem cells within the heart¹⁴⁶, and the discovery/development of induced pluripotent stem cells (iPSCs)¹⁸³. These iPSCs are produced from fibroblast precursors through the actions of OCT4, SOX2, KLF4, and MYC (called OSKM factors)¹⁸³. Differentiation of cardiac fibroblasts to cardiomyocytes with an iPSC precursor only requires OSK, decreasing the potential for in vivo oncogenic transformation¹⁸⁴ that can plague researchers injecting undifferentiated iPSCs. This process uses cells directly isolated from the patient, eliminating the potential for transplant rejection, but the timeline from bench-to bedside is so far too lengthy to prevent extensive remodeling of the myocardium, though the timeline has been decreasing recently⁵⁹.

Many other groups have shown the potential of mesenchymal stem cells (MSCs) to differentiate towards the cardiac lineage^{41, 141, 185}, which was partly brought on by the moratorium on embryonic stem cell research and the long timelines and mixed safety of iPSC differentiation. In vitro and in vivo differentiation of MSCs occur at much faster rates than iPSCs¹⁰⁰, but controversy in the field over whether MSCs fully differentiate to cardiomyocytes, therefore providing replacements to lost tissue, clouds many conclusions¹⁸⁶. The use of nanoscaffolds and gels to house MSCs for cardiac therapies allows researchers to better control the cardiac tissue microenvironment, aiding in vivo repair¹⁸⁷. Successful nanoscaffolds for growth and/or differentiation of cardiomyocytes include PCL⁴⁹, PLGA/carbon nanofiber blends¹⁸⁸, chitosan/carbon nanofiber blends¹⁷⁹, and gold particle composite nanofibers¹⁸⁹. While nanofiber gels of fibrin and fibrinogen, and pericardial ECM¹⁸⁰ can be injected into the heart without exacerbation of MI symptoms, the addition of cells to these injectable gel molds has yet to be realized. What has been added to those

nanoscaffold gels are small molecules¹⁹⁰ or other factors^{191, 192} that enhance angiogenesis and endogenous stem cell migration to the damaged cardiac tissue. Many studies have laid synthetic nanoscaffolds directly on to the myocardial infarct area¹⁹¹, or fully capped the heart to aid beating¹⁹³, with promising results. Most of these techniques though involve invasive surgical procedures to implant, decreasing their utility post-MI. There needs to be extensive further research into the best methods for cell growth and retention within the myocardium and, as demonstrated herein, which patients or MI types benefit from a given therapy.

6.4 Specific Aim 3

6.4.1 Conclusion

The main goal of these experiments was to produce a regenerative medicine cell therapy that could be injected to an infarcted heart to determine the extent of healing. Because of the controversy behind therapeutic injections for MI, specifically with the involvement of stem cells, we used multiple levels of cardiac damage to ensure we tested our therapy in as many clinically relevant hearts as possible. We were able to successfully inject 54 rats with our nanoscaffold system over a range of 5 heart attacks (with 3 controls). The advantage of our system was in the non-invasive delivery mechanism, whereby the heart position was determined via ultrasound and the injection made to the ventricular cavity as opposed to the muscle tissue. After two weeks there was demonstrated improvement in major cardiac metrics, including ejection fraction, fractional shortening, and left ventricular volume during systole.

6.4.2 Future directions

Our results added strength to hypotheses that hBMSC therapies may not be right for every patient¹⁹⁴. Timelines for cardiac healing after MI in the rat is significantly shorter than that for a human⁶, therefore our 2week protocol can lead to general conclusions that because of the improvement seen after ~10-14days, we had set the stage for decreasing risk of HF progression. Future protocols would benefit from significantly longer timelines ranging from 6months to 1year post-therapy to confirm that HF symptoms were ameliorated in addition to MI repair.

There would also be a future benefit in probing the extent of molecular and cellular engraftment of our therapy within the hearts. We demonstrated significant staying power of the nanoscaffold and cells lasting the full 2week experiment, and it would bolster the regenerative argument for hBMSCs if we show whether those cells contributed to the formation of new cardiomyocytes. Molecular staining of cellular signaling between injected and native cells, whether Connexin43- or calcium channel-mediated, will go a long way in determining the level of cellular incorporation.

Injection localization could also be optimized to induce a more robust healing potential. We opted to inject directly into the left ventricle not only for ease of delivery but also because there is a profound stem cell niche on the epicardial side of the heart^{195,196}. The hypothesis was that our stem cell injections would seed the ventricle side, while the epicardial stem cells, activated after an ischemic event, would repopulate the outer myocyte layer(s). Our stem cells successfully wove throughout the heart so we did not probe for cKit+ cardiac progenitors of epicardial origin, but future work may be able to use less hBMSCs if the in vivo progenitor pool is efficiently activated to aid repair. Other work in critical limb ischemia¹⁹⁷ and cardiac disorders¹⁹⁸⁻²⁰⁰ shows that site of cell or factor injection can have a profound effect on

healing potential. The thought is that paracrine mechanisms cannot diffuse out much farther from where they are injected, isolating the injection site as the primary area of healing. For a larger MI then, direct injection of our therapy to the muscle may further enhance payload delivery, and thus myocardial repair.

Additions of cells and factors to murine models and to individuals in clinical trials have been performed using IV injections²⁰¹, intracoronary infusion²⁰², transendocardial catheters²⁰³, transc coronary vein injections²⁰⁴ (BMSCs and MSCs), systemic addition²⁰⁵ (SCF and SDF-1), and direct myocardial injection²⁰⁶ (cells and factors). The primary stem cells may initially grow in standard culture plates as a monolayer, or peeled off culture plates using their own ECM matrix as a scaffold (“cell sheet” engineering)²⁰⁷; regardless of method, the cells get collected in a syringe and injected to the patient. Many of the clinical therapies, despite reporting positive results, are rife with ethical and methodological errors²⁰⁸, which may explain the lack of stem cell-based cardiac therapies on the market. For example, only 1-5% of cells injected through the vasculature home and adhere to the damaged myocardium²⁰¹, a painfully small and ineffective number of cells. Additional work is being performed to enhance this effect³⁶. For example, the upregulation of monocyte chemoattractant protein-1 (MCP-1)³⁸ and/or stem cell antigen-1 (Sca1)²⁰⁹ on hBMSCs pre-injection can significantly enhance their homing to sites of inflammation. These cells can be tracked in vivo^{185, 210} to measure the efficacy of homing, and the eventual contribution to new cardiomyocytes.

This pretreatment of stem cells is a new advancement that will significantly aid the field. In our analysis we found that pretreated cells greatly enhanced expression of cardiomyocyte contractile proteins, and ion channels such as Connexin43 that will aid

communication with the native myocardium. Other studies have also found that pretreatment of MSCs, whether using in vitro coculture with native cardiomyocytes²¹¹, cyclical strain/mechanical stretch on the nanoscaffold carrier^{212, 213}, or simple molecule addition to culture¹⁴⁰ can aid in their differentiation and gene expression in vivo. The in vitro cellular transformation induces release of different exosomes, proteins, and small molecules (termed the “secretome”)¹⁴¹ into the cell culture media. Following the discovery of these factors, numerous studies have used cell media for cardiac healing, with mixed results^{134, 142, 145, 214}. Unfortunately many of these factors are unknown, and current research is investigating high throughput approaches to uncover which proteins and small molecules may best heal various tissues²¹⁵, and what pretreatment factors may best induce robust secretome enhancement²¹⁶.

This is not to say that stem cells and nanoscaffolds are the only way to heal a heart attack. Genetic approaches in murine models have recently been applied as treatment: a novel method involves the use of miRNAs, specifically in conjunction with targeting single nucleotide polymorphisms²¹⁷. Existing heart tissue can be targeted and protein production blocked by miRNAs to enhance cardiomyocyte differentiation from fibroblasts, speeding up repair before remodeling occurs^{218, 219}. Common pathways targeted include PI3K, various CDKs, Hippo, IGF, and WNT. Delivery of targeted miRNAs can be accomplished by direct injection into the myocardium, or conjugation to or encapsulation within nanoparticles and liposomes²²⁰. Also, miRNA specificity allows for a varied array of positive effects, including promoting cardiomyocyte reentry into the cell cycle, reducing scar formation, and improving cardiac function after cardiomyocyte loss following injury¹⁸⁴. miRNAs also lend themselves well to high throughput screening, and have

much higher gene manipulation capabilities compared to siRNAs¹⁹². Downsides include several miRNA genes with related predicted specificities at multiple loci²²¹, which can be overcome using longer and more specific synthetic miRNAs. Nucleic acid-based therapies also cannot be used to repair damage after remodeling (i.e. for heart failure treatment²²²), and do not stop the progression of ischemia through the heart during MI recovery. Their main advantage is converting infiltrating fibroblasts to cardiomyocytes in the hopes that this will increase contractile cells and decrease scar formation²²³.

6.5 Overall conclusion:

The research goal for cardiac therapies should be a combination of a number of the above approaches, coupled with increased transparency in clinical studies. For smaller infarcts with decreased chance of ventricular rupture, direct cell injections alone to the myocardium may provide a therapeutic benefit, while larger infarcts may need the mechanical support provided by a thicker hydrogel scaffold to prevent significant remodeling and ventricular rupture. As mentioned, there are defined processes for differentiating iPSCs and MSCs to the cardiac lineage, successful ways to recruit stem cells to damaged cardiac tissue, genetic ways to increase and decrease cell proliferation, and novel ways to add scaffolds into the necrotic area. There seems to be an issue though in merging these methods. New approaches, such as seeding cells and factors on scaffolds prior to implantation as described here, will provide both mechanical and biological benefits to the damaged myocardium. Also, keeping frozen stocks of differentiated, HLA-typed allogeneic iPSCs and MSCs available in the clinic will significantly decrease transplant rejection and bench-to-bedside time. The ability

to connect the salient points from each of these (and many other) studies will define the success of future cardiac therapies.

REFERENCES

1. Cirino, A. L. & Ho, C. in *GeneReviews(R)* (ed Pagon, R. A. et al.) (University of Washington, Seattle, Seattle (WA), 1993).
2. Murphy, S. L., Xu, J. & Kochanek, K. D. Deaths: final data for 2010. *Natl. Vital Stat. Rep.* **61**, 1-117 (2013).
3. Writing Group Members *et al.* Heart Disease and Stroke Statistics-2016 Update: A Report From the American Heart Association. *Circulation* **133**, e38-360 (2016).
4. Lassen, J. F., Botker, H. E. & Terkelsen, C. J. Timely and optimal treatment of patients with STEMI. *Nat. Rev. Cardiol.* **10**, 41-48 (2013).
5. Bergmann, O. *et al.* Evidence for cardiomyocyte renewal in humans. *Science* **324**, 98-102 (2009).
6. Holmes, J. W., Borg, T. K. & Covell, J. W. Structure and mechanics of healing myocardial infarcts. *Annu. Rev. Biomed. Eng.* **7**, 223-253 (2005).
7. Fishbein, M. C., Maclean, D. & Maroko, P. R. The histopathologic evolution of myocardial infarction. *Chest* **73**, 843-849 (1978).
8. Mallory, G. K., White, P. D. & Salcedo-Salgar, J. The speed of healing of myocardial infarction: a study of the pathologic anatomy in seventy-two cases. *American Heart Journal* **18**, 647-648-671 (1959).
9. Hood, W. B., Jr, Bianco, J. A., Kumar, R. & Whiting, R. B. Experimental myocardial infarction. IV. Reduction of left ventricular compliance in the healing phase. *J. Clin. Invest.* **49**, 1316-1323 (1970).
10. Whittaker, P., Boughner, D. R. & Kloner, R. A. Analysis of healing after myocardial infarction using polarized light microscopy. *Am. J. Pathol.* **134**, 879-893 (1989).

11. Gupta, K. B., Ratcliffe, M. B., Fallert, M. A., Edmunds, L. H., Jr & Bogen, D. K. Changes in passive mechanical stiffness of myocardial tissue with aneurysm formation. *Circulation* **89**, 2315-2326 (1994).
12. Holmes, J. W., Yamashita, H., Waldman, L. K. & Covell, J. W. Scar remodeling and transmural deformation after infarction in the pig. *Circulation* **90**, 411-420 (1994).
13. Sun, Y., Kiani, M. F., Postlethwaite, A. E. & Weber, K. T. Infarct scar as living tissue. *Basic Res. Cardiol.* **97**, 343-347 (2002).
14. Frank, C., McDonald, D., Wilson, J., Eyre, D. & Shrive, N. Rabbit medial collateral ligament scar weakness is associated with decreased collagen pyridinoline crosslink density. *J. Orthop. Res.* **13**, 157-165 (1995).
15. Connelly, C. M. *et al.* Effects of reperfusion after coronary artery occlusion on post-infarction scar tissue. *Circ. Res.* **57**, 562-577 (1985).
16. Pfeffer, M. A. *et al.* Myocardial infarct size and ventricular function in rats. *Circ. Res.* **44**, 503-512 (1979).
17. Robinson, J. G. *et al.* Efficacy and safety of alirocumab in reducing lipids and cardiovascular events. *N. Engl. J. Med.* **372**, 1489-1499 (2015).
18. Blom, D. J. *et al.* A 52-week placebo-controlled trial of evolocumab in hyperlipidemia. *N. Engl. J. Med.* **370**, 1809-1819 (2014).
19. Ponikowski, P. *et al.* 2016 ESC Guidelines for the diagnosis and treatment of acute and chronic heart failure: The Task Force for the diagnosis and treatment of acute and chronic heart failure of the European Society of Cardiology (ESC). Developed with the special contribution of the Heart Failure Association (HFA) of the ESC. *Eur. J. Heart Fail.* **18**, 891-975 (2016).
20. Hunt, S. A. *et al.* 2009 Focused update incorporated into the ACC/AHA 2005 Guidelines for the Diagnosis and Management of Heart Failure in Adults A Report of the American College of Cardiology Foundation/American Heart Association Task Force on Practice Guidelines Developed in Collaboration With the International Society for Heart and Lung Transplantation. *J. Am. Coll. Cardiol.* **53**, e1-e90 (2009).

21. Dickstein, K. *et al.* ESC guidelines for the diagnosis and treatment of acute and chronic heart failure 2008: the Task Force for the diagnosis and treatment of acute and chronic heart failure 2008 of the European Society of Cardiology. Developed in collaboration with the Heart Failure Association of the ESC (HFA) and endorsed by the European Society of Intensive Care Medicine (ESICM). *Eur. J. Heart Fail.* **10**, 933-989 (2008).
22. Townsend, N. *et al.* Cardiovascular disease in Europe: epidemiological update 2016. *Eur. Heart J.* **37**, 3232-3245 (2016).
23. Lo, B. & Parham, L. Ethical issues in stem cell research. *Endocr. Rev.* **30**, 204-213 (2009).
24. Medvedev, S. P., Shevchenko, A. I. & Zakian, S. M. Induced Pluripotent Stem Cells: Problems and Advantages when Applying them in Regenerative Medicine. *Acta Naturae* **2**, 18-28 (2010).
25. Bassetti, B., Capogrossi, M. C. & Pompilio, G. Power Is Nothing Without Control: The Enduring Search for the Best Cell in Cardiac Cell Therapy at a Crossroads. *Circ. Res.* **119**, 988-991 (2016).
26. Goichberg, P. Current Understanding of the Pathways Involved in Adult Stem and Progenitor Cell Migration for Tissue Homeostasis and Repair. *Stem Cell. Rev.* **12**, 421-437 (2016).
27. Orlic, D. *et al.* Bone marrow cells regenerate infarcted myocardium. *Nature* **410**, 701-705 (2001).
28. Ellison, G. M. *et al.* Adult c-kit(pos) cardiac stem cells are necessary and sufficient for functional cardiac regeneration and repair. *Cell* **154**, 827-842 (2013).
29. Squillaro, T., Peluso, G. & Galderisi, U. Clinical Trials With Mesenchymal Stem Cells: An Update. *Cell Transplant.* **25**, 829-848 (2016).
30. Ankrum, J. A., Ong, J. F. & Karp, J. M. Mesenchymal stem cells: immune evasive, not immune privileged. *Nat. Biotechnol.* **32**, 252-260 (2014).
31. Ma, S. *et al.* Immunobiology of mesenchymal stem cells. *Cell Death Differ.* **21**, 216-225 (2014).
32. Williams, A. R. & Hare, J. M. Mesenchymal stem cells: biology, pathophysiology, translational findings, and therapeutic implications for cardiac disease. *Circ. Res.* **109**, 923-940 (2011).

33. Maureira, P. *et al.* Repairing chronic myocardial infarction with autologous mesenchymal stem cells engineered tissue in rat promotes angiogenesis and limits ventricular remodeling. *J. Biomed. Sci.* **19**, 93-0127-19-93 (2012).
34. Abdel-Latif, A. *et al.* Adult bone marrow-derived cells for cardiac repair: a systematic review and meta-analysis. *Arch. Intern. Med.* **167**, 989-997 (2007).
35. Beitnes, J. O., Lunde, K., Brinchmann, J. E. & Aakhus, S. Stem cells for cardiac repair in acute myocardial infarction. *Expert Rev. Cardiovasc. Ther.* **9**, 1015-1025 (2011).
36. Li, S. H. *et al.* Tracking cardiac engraftment and distribution of implanted bone marrow cells: Comparing intra-aortic, intravenous, and intramyocardial delivery. *J. Thorac. Cardiovasc. Surg.* **137**, 1225-33.e1 (2009).
37. Nowbar, A. N. *et al.* Discrepancies in autologous bone marrow stem cell trials and enhancement of ejection fraction (DAMASCENE): weighted regression and meta-analysis. *BMJ* **348**, g2688 (2014).
38. Karp, J. M. & Leng Teo, G. S. Mesenchymal stem cell homing: the devil is in the details. *Cell. Stem Cell.* **4**, 206-216 (2009).
39. Mortensen, L. J. *et al.* Quantification of Mesenchymal Stem Cell (MSC) delivery to a target site using in vivo confocal microscopy. *PLoS One* **8**, e78145 (2013).
40. Eisenberg, C. A., Burch, J. B. & Eisenberg, L. M. Bone marrow cells transdifferentiate to cardiomyocytes when introduced into the embryonic heart. *Stem Cells* **24**, 1236-1245 (2006).
41. Rota, M. *et al.* Bone marrow cells adopt the cardiomyogenic fate in vivo. *Proc. Natl. Acad. Sci. U. S. A.* **104**, 17783-17788 (2007).
42. Reinecke, H., Poppa, V. & Murry, C. E. Skeletal muscle stem cells do not transdifferentiate into cardiomyocytes after cardiac grafting. *J. Mol. Cell. Cardiol.* **34**, 241-249 (2002).
43. Rose, R. A. *et al.* Bone marrow-derived mesenchymal stromal cells express cardiac-specific markers, retain the stromal phenotype, and do not become functional cardiomyocytes in vitro. *Stem Cells* **26**, 2884-2892 (2008).

44. Zhang, Y. *et al.* Fractalkine promotes chemotaxis of bone marrow-derived mesenchymal stem cells towards ischemic brain lesions through Jak2 signaling and cytoskeletal reorganization. *FEBS J.* **282**, 891-903 (2015).
45. Gnecci, M., Zhang, Z., Ni, A. & Dzau, V. J. Paracrine mechanisms in adult stem cell signaling and therapy. *Circ. Res.* **103**, 1204-1219 (2008).
46. Cho, D. I. *et al.* Mesenchymal stem cells reciprocally regulate the M1/M2 balance in mouse bone marrow-derived macrophages. *Exp. Mol. Med.* **46**, e70 (2014).
47. Ziadloo, A. *et al.* Enhanced homing permeability and retention of bone marrow stromal cells by noninvasive pulsed focused ultrasound. *Stem Cells* **30**, 1216-1227 (2012).
48. Kuyumcu-Martinez, M. N. & Bressan, M. C. Rebuilding a broken heart: lessons from developmental and regenerative biology. *Development* **143**, 3866-3870 (2016).
49. Pok, S., Myers, J. D., Madhally, S. V. & Jacot, J. G. A multilayered scaffold of a chitosan and gelatin hydrogel supported by a PCL core for cardiac tissue engineering. *Acta Biomater.* **9**, 5630-5642 (2013).
50. Li, Z. & Guan, J. Hydrogels for Cardiac Tissue Engineering. *Polymers* **3**, 740-741-761 (2011).
51. Mathieu, E. *et al.* Intramyocardial delivery of mesenchymal stem cell-seeded hydrogel preserves cardiac function and attenuates ventricular remodeling after myocardial infarction. *PLoS One* **7**, e51991 (2012).
52. Reis, L. A., Chiu, L. L., Feric, N., Fu, L. & Radisic, M. Biomaterials in myocardial tissue engineering. *J. Tissue Eng. Regen. Med.* **10**, 11-28 (2016).
53. Patten, R. D. & Hall-Porter, M. R. Small animal models of heart failure: development of novel therapies, past and present. *Circ. Heart Fail.* **2**, 138-144 (2009).
54. Nikolova, S., Ting-Yim Lee, T. & Bartha, R. The Severity of Ischemia Varies in Sprague-Dawley Rats from Different Vendors. *ISRN Stroke* 2014, **1** (2014).

55. Galankina, I. E. & Topchiian, G. S. Mechanisms of the development of hemorrhagic myocardial infarction and the criteria of angiographic diagnosis. *Kardiologiia* **30**, 20-23 (1990).
56. Xu, Z., Alloush, J., Beck, E. & Weisleder, N. A murine model of myocardial ischemia-reperfusion injury through ligation of the left anterior descending artery. *J. Vis. Exp.* **(86)**. doi, 10.3791/51329 (2014).
57. Gao, E. *et al.* A novel and efficient model of coronary artery ligation and myocardial infarction in the mouse. *Circ. Res.* **107**, 1445-1453 (2010).
58. Quijada, P. *et al.* Cardiac Stem Cell Hybrids Enhance Myocardial Repair. *Circ. Res.* **117**, 695-706 (2015).
59. Shiba, Y. *et al.* Allogeneic transplantation of iPS cell-derived cardiomyocytes regenerates primate hearts. *Nature* **538**, 388-391 (2016).
60. Wallukat, G. The beta-adrenergic receptors. *Herz* **27**, 683-690 (2002).
61. Saroff, J. & Wexler, B. C. Isoproterenol-induced myocardial infarction in rats. Distribution of corticosterone. *Circ. Res.* **27**, 1101-1109 (1970).
62. Herrmann, J. E. *et al.* Isoproterenol effects evaluated in heart slices of human and rat in comparison to rat heart in vivo. *Toxicol. Appl. Pharmacol.* **274**, 302-312 (2014).
63. Zhang, J., Knapton, A., Lipshultz, S. E., Weaver, J. L. & Herman, E. H. Isoproterenol-induced cardiotoxicity in sprague-dawley rats: correlation of reversible and irreversible myocardial injury with release of cardiac troponin T and roles of iNOS in myocardial injury. *Toxicol. Pathol.* **36**, 277-278 (2008).
64. Brady, S. *et al.* Cardiac troponin I in isoproterenol-induced cardiac injury in the Hanover Wistar rat: studies on low dose levels and routes of administration. *Toxicol. Pathol.* **38**, 287-291 (2010).
65. Calvano, J. *et al.* Evaluation of microRNAs-208 and 133a/b as differential biomarkers of acute cardiac and skeletal muscle toxicity in rats. *Toxicol. Appl. Pharmacol.* **312**, 53-60 (2016).
66. Iwai, M. & Shimazu, T. Exaggeration of acute liver damage by hepatic sympathetic nerves and circulating catecholamines in perfused liver of rats treated with D-galactosamine. *Hepatology* **23**, 524-529 (1996).

67. Carll, A. P., Willis, M. S., Lust, R. M., Costa, D. L. & Farraj, A. K. Merits of non-invasive rat models of left ventricular heart failure. *Cardiovasc. Toxicol.* **11**, 91-112 (2011).
68. Ram, R., Mickelsen, D. M., Theodoropoulos, C. & Blaxall, B. C. New approaches in small animal echocardiography: imaging the sounds of silence. *Am. J. Physiol. Heart Circ. Physiol.* **301**, H1765-80 (2011).
69. Prendiville, T. W. *et al.* Ultrasound-guided transthoracic intramyocardial injection in mice. *J. Vis. Exp.* **90**, e51566. doi, e51566 (2014).
70. Rymer, C. C. & Sims-Lucas, S. In utero intra-cardiac tomato-lectin injections on mouse embryos to gauge renal blood flow. *J. Vis. Exp.* **96**. doi, 10.3791/52398 (2015).
71. Lohse, M. J., Engelhardt, S. & Eschenhagen, T. What is the role of beta-adrenergic signaling in heart failure? *Circ. Res.* **93**, 896-906 (2003).
72. Zbinden, G. & Bagdon, R.E. Isoproterenol-Induced Heart Necrosis, an Experimental Model for the Study of Angina Pectoris and Myocardial Infarct. *Rev. Can. Biol.* **22**, 257-263 (1963).
73. Yang, J. H. & Saucerman, J. J. Phospholemman is a negative feed-forward regulator of Ca²⁺ in beta-adrenergic signaling, accelerating beta-adrenergic inotropy. *J. Mol. Cell. Cardiol.* **52**, 1048-1055 (2012).
74. Kuehl, M. & Stevens, M. J. Cardiovascular autonomic neuropathies as complications of diabetes mellitus. *Nat. Rev. Endocrinol.* **8**, 405-416 (2012).
75. Rahmathulla, S. B. M. & Devi, K. L. Origination and Development of Isoproterenol-induced Myocardial Infarction in Male Wistar Rats. *Int. Res. J. Pharm* **4**, 26 (2013).
76. Kuloglu, T. *et al.* Irisin: a potentially candidate marker for myocardial infarction. *Peptides* **55**, 85-91 (2014).
77. Sinner, M. F. *et al.* Completion of guideline-recommended initial evaluation of atrial fibrillation. *Clin. Cardiol.* **35**, 585-593 (2012).
78. Xu, J. *et al.* Protective role of AT₂ and B₁ receptors in kinin B₂-receptor-knockout mice with myocardial infarction. *Clin Sci (Lond)* **124**, 87-88-96 (2013).

79. Protti, A., Dong, X., Sirker, A., Botnar, R. & Shah, A. M. MRI-based prediction of adverse cardiac remodeling after murine myocardial infarction. *Am. J. Physiol. Heart Circ. Physiol.* **303**, H309-14 (2012).
80. Dong, H. *et al.* Integrated wall stress: a new methodological approach to assess ventricular workload and myocardial contractile reserve. *J. Transl. Med.* **11**, 183-5876-11-183 (2013).
81. Bock-Marquette, I., Saxena, A., White, M. D., Dimaio, J. M. & Srivastava, D. Thymosin beta4 activates integrin-linked kinase and promotes cardiac cell migration, survival and cardiac repair. *Nature* **432**, 466-472 (2004).
82. Segers, V. F. & Lee, R. T. Stem-cell therapy for cardiac disease. *Nature* **451**, 937-942 (2008).
83. Gajzer, D. C., Balbin, J. & Chaudhry, H. W. Thymosin beta4 and cardiac regeneration: are we missing a beat? *Stem Cell. Rev.* **9**, 303-312 (2013).
84. Smart, N. *et al.* Myocardial regeneration: expanding the repertoire of thymosin beta4 in the ischemic heart. *Ann. N. Y. Acad. Sci.* **1269**, 92-101 (2012).
85. Hinkel, R. *et al.* Thymosin beta4 is an essential paracrine factor of embryonic endothelial progenitor cell-mediated cardioprotection. *Circulation* **117**, 2232-2240 (2008).
86. Srivastava, D., Ieda, M., Fu, J. & Qian, L. Cardiac repair with thymosin beta4 and cardiac reprogramming factors. *Ann. N. Y. Acad. Sci.* **1270**, 66-72 (2012).
87. Zhou, B. *et al.* Thymosin beta 4 treatment after myocardial infarction does not reprogram epicardial cells into cardiomyocytes. *J. Mol. Cell. Cardiol.* **52**, 43-47 (2012).
88. Kraehenbuehl, T. P., Ferreira, L. S., Zammaretti, P., Hubbell, J. A. & Langer, R. Cell-responsive hydrogel for encapsulation of vascular cells. *Biomaterials* **30**, 4318-4324 (2009).
89. Kawaguchi, N., Hatta, K. & Nakanishi, T. 3D-culture system for heart regeneration and cardiac medicine. *Biomed. Res. Int.* 2013, 895967 (2013).
90. Minami, I. *et al.* A small molecule that promotes cardiac differentiation of human pluripotent stem cells under defined, cytokine- and xeno-free conditions. *Cell. Rep.* **2**, 1448-1460 (2012).

91. Lian, X. *et al.* Robust cardiomyocyte differentiation from human pluripotent stem cells via temporal modulation of canonical Wnt signaling. *Proc. Natl. Acad. Sci. U. S. A.* **109**, E1848-57 (2012).
92. Lian, X. *et al.* Directed cardiomyocyte differentiation from human pluripotent stem cells by modulating Wnt/beta-catenin signaling under fully defined conditions. *Nat. Protoc.* **8**, 162-175 (2013).
93. Kim, W. H., Jung, D. W. & Williams, D. R. Making cardiomyocytes with your chemistry set: Small molecule-induced cardiogenesis in somatic cells. *World J. Cardiol.* **7**, 125-133 (2015).
94. Yang, G. *et al.* Mesenchymal TGF-beta signaling orchestrates dental epithelial stem cell homeostasis through Wnt signaling. *Stem Cells* **32**, 2939-2948 (2014).
95. Rao, T. P. & Kuhl, M. An updated overview on Wnt signaling pathways: a prelude for more. *Circ. Res.* **106**, 1798-1806 (2010).
96. Clevers, H. & Nusse, R. Wnt/beta-catenin signaling and disease. *Cell* **149**, 1192-1205 (2012).
97. Doll, T. A., Raman, S., Dey, R. & Burkhard, P. Nanoscale assemblies and their biomedical applications. *J. R. Soc. Interface* **10**, 20120740 (2013).
98. Prabu, P. & Kim, K. W. Antimicrobial Drug Release Scaffolds of Natural and Synthetic Biodegradable Polymers. *Macromolecular Research* **16**, 303-304-307 (2008).
99. Liu, T., Xu, J., Chan, B. P. & Chew, S. Y. Sustained release of neurotrophin-3 and chondroitinase ABC from electrospun collagen nanofiber scaffold for spinal cord injury repair. *J. Biomed. Mater. Res. A.* **100**, 236-242 (2012).
100. Kumar, A., Patel, A., Duvalsaint, L., Desai, M. & Marks, E. D. Thymosin beta4 coated nanofiber scaffolds for the repair of damaged cardiac tissue. *J. Nanobiotechnology* **12**, 10-3155-12-10 (2014).
101. Mihic, A. *et al.* A Conductive Polymer Hydrogel Supports Cell Electrical Signaling and Improves Cardiac Function After Implantation into Myocardial Infarct. *Circulation* **132**, 772-784 (2015).

102. Serpooshan, V. *et al.* The effect of bioengineered acellular collagen patch on cardiac remodeling and ventricular function post myocardial infarction. *Biomaterials* **34**, 9048-9055 (2013).
103. Capkin, M. *et al.* Random/aligned electrospun PCL/PCL-collagen nanofibrous membranes: comparison of neural differentiation of rat AdMSCs and BMSCs. *Biomed. Mater.* **7**, 045013-6041/7/4/045013. Epub 2012 Jun 1 (2012).
104. Kai, D., Prabhakaran, M. P., Jin, G. & Ramakrishna, S. Guided orientation of cardiomyocytes on electrospun aligned nanofibers for cardiac tissue engineering. *J. Biomed. Mater. Res. B. Appl. Biomater.* **98**, 379-386 (2011).
105. Baker, B. M. *et al.* Sacrificial nanofibrous composites provide instruction without impediment and enable functional tissue formation. *Proc. Natl. Acad. Sci. U. S. A.* **109**, 14176-14181 (2012).
106. Bettinger, C. J., Langer, R. & Borenstein, J. T. Engineering substrate topography at the micro- and nanoscale to control cell function. *Angew. Chem. Int. Ed Engl.* **48**, 5406-5415 (2009).
107. Vasita, R. & Katti, D. S. Nanofibers and their applications in tissue engineering. *Int. J. Nanomedicine* **1**, 15-30 (2006).
108. Murphy, C. M., Haugh, M. G. & O'Brien, F. J. The effect of mean pore size on cell attachment, proliferation and migration in collagen-glycosaminoglycan scaffolds for bone tissue engineering. *Biomaterials* **31**, 461-466 (2010).
109. Bakhshandeh, B., Soleimani, M., Ghaemi, N. & Shabani, I. Effective combination of aligned nanocomposite nanofibers and human unrestricted somatic stem cells for bone tissue engineering. *Acta Pharmacol. Sin.* **32**, 626-636 (2011).
110. Gupta, D. *et al.* Aligned and random nanofibrous substrate for the in vitro culture of Schwann cells for neural tissue engineering. *Acta Biomater.* **5**, 2560-2569 (2009).
111. Marks, E. D. & Kumar, A. Thymosin beta4: Roles in Development, Repair, and Engineering of the Cardiovascular System. *Vitam. Horm.* **102**, 227-249 (2016).

112. Cooke, J. P. & Losordo, D. W. Nitric oxide and angiogenesis. *Circulation* **105**, 2133-2135 (2002).
113. Forstermann, U. & Munzel, T. Endothelial nitric oxide synthase in vascular disease: from marvel to menace. *Circulation* **113**, 1708-1714 (2006).
114. Freeman, K. W., Bowman, B. R. & Zetter, B. R. Regenerative protein thymosin beta-4 is a novel regulator of purinergic signaling. *FASEB J.* **25**, 907-915 (2011).
115. de Rivero Vaccari, J. P. *et al.* P2X4 receptors influence inflammasome activation after spinal cord injury. *J. Neurosci.* **32**, 3058-3066 (2012).
116. Shen, J. B., Pappano, A. J. & Liang, B. T. Extracellular ATP-stimulated current in wild-type and P2X4 receptor transgenic mouse ventricular myocytes: implications for a cardiac physiologic role of P2X4 receptors. *FASEB J.* **20**, 277-284 (2006).
117. Qian, L. *et al.* In vivo reprogramming of murine cardiac fibroblasts into induced cardiomyocytes. *Nature* **485**, 593-598 (2012).
118. Smart, N. *et al.* Thymosin beta4 induces adult epicardial progenitor mobilization and neovascularization. *Nature* **445**, 177-182 (2007).
119. Tateishi, K., Takehara, N., Matsubara, H. & Oh, H. Stemming heart failure with cardiac- or reprogrammed-stem cells. *J. Cell. Mol. Med.* **12**, 2217-2232 (2008).
120. Qiu, F. Y., Song, X. X., Zheng, H., Zhao, Y. B. & Fu, G. S. Thymosin beta4 induces endothelial progenitor cell migration via PI3K/Akt/eNOS signal transduction pathway. *J. Cardiovasc. Pharmacol.* **53**, 209-214 (2009).
121. Grant, D. S. *et al.* Thymosin beta4 enhances endothelial cell differentiation and angiogenesis. *Angiogenesis* **3**, 125-135 (1999).
122. Sanger, J. M. *et al.* Increasing intracellular concentrations of thymosin beta 4 in PtK2 cells: effects on stress fibers, cytokinesis, and cell spreading. *Cell Motil. Cytoskeleton* **31**, 307-322 (1995).
123. Wei, C., Kumar, S., Kim, I. K. & Gupta, S. Thymosin beta 4 protects cardiomyocytes from oxidative stress by targeting anti-oxidative enzymes and anti-apoptotic genes. *PLoS One* **7**, e42586 (2012).

124. Cargnello, M. & Roux, P. P. Activation and function of the MAPKs and their substrates, the MAPK-activated protein kinases. *Microbiol. Mol. Biol. Rev.* **75**, 50-83 (2011).
125. Schulz, R. A. & Yutzey, K. E. Calcineurin signaling and NFAT activation in cardiovascular and skeletal muscle development. *Dev. Biol.* **266**, 1-16 (2004).
126. Paoletti, R. *et al.* Protein kinase C θ is required for cardiomyocyte survival and cardiac remodeling. *Cell. Death Dis.* **1**, e45 (2010).
127. Kerkela, R. *et al.* Deletion of GSK-3 β in mice leads to hypertrophic cardiomyopathy secondary to cardiomyoblast hyperproliferation. *J. Clin. Invest.* **118**, 3609-3618 (2008).
128. Tseng, A. S., Engel, F. B. & Keating, M. T. The GSK-3 inhibitor BIO promotes proliferation in mammalian cardiomyocytes. *Chem. Biol.* **13**, 957-963 (2006).
129. Cicha, I., Garlich, C. D. & Alexiou, C. Cardiovascular therapy through nanotechnology – how far are we still from bedside? **6**, 63 (2014).
130. Pearson-Stuttard, J. *et al.* Modeling Future Cardiovascular Disease Mortality in the United States: National Trends and Racial and Ethnic Disparities. *Circulation* **133**, 967-978 (2016).
131. Jeevanantham, V. *et al.* Adult bone marrow cell therapy improves survival and induces long-term improvement in cardiac parameters: a systematic review and meta-analysis. *Circulation* **126**, 551-568 (2012).
132. Prowse, A. B. *et al.* Transforming the promise of pluripotent stem cell-derived cardiomyocytes to a therapy: challenges and solutions for clinical trials. *Can. J. Cardiol.* **30**, 1335-1349 (2014).
133. Zhao, Y., Korolj, A., Feric, N. & Radisic, M. Human pluripotent stem cell-derived cardiomyocyte based models for cardiotoxicity and drug discovery. *Expert Opin. Drug Saf.* **15**, 1455-1458 (2016).
134. Khan, M. *et al.* Embryonic stem cell-derived exosomes promote endogenous repair mechanisms and enhance cardiac function following myocardial infarction. *Circ. Res.* **117**, 52-64 (2015).

135. Chong, J. J. & Murry, C. E. Cardiac regeneration using pluripotent stem cells--progression to large animal models. *Stem Cell. Res.* **13**, 654-665 (2014).
136. Hare, J. M. *et al.* Comparison of allogeneic vs autologous bone marrow-derived mesenchymal stem cells delivered by transendocardial injection in patients with ischemic cardiomyopathy: the POSEIDON randomized trial. *JAMA* **308**, 2369-2379 (2012).
137. Makkar, R. R. *et al.* Intracoronary cardiosphere-derived cells for heart regeneration after myocardial infarction (CADUCEUS): a prospective, randomised phase 1 trial. *Lancet* **379**, 895-904 (2012).
138. Clifford, D. M. *et al.* Stem cell treatment for acute myocardial infarction. *Cochrane Database Syst. Rev.* (2):**CD006536**. doi, CD006536 (2012).
139. Cong, X. Q., Li, Y., Zhao, X., Dai, Y. J. & Liu, Y. Short-Term Effect of Autologous Bone Marrow Stem Cells to Treat Acute Myocardial Infarction: A Meta-Analysis of Randomized Controlled Clinical Trials. *J. Cardiovasc. Transl. Res.* **8**, 221-231 (2015).
140. Kuster, G. M. & Liao, R. Fortune Favors the Prepared: Safety and Efficacy of Allogeneic Hypoxia Preconditioned Mesenchymal Stromal Cells in Primates. *Circ. Res.* **118**, 908-910 (2016).
141. Ranganath, S. H., Levy, O., Inamdar, M. S. & Karp, J. M. Harnessing the mesenchymal stem cell secretome for the treatment of cardiovascular disease. *Cell. Stem Cell.* **10**, 244-258 (2012).
142. Timmers, L. *et al.* Human mesenchymal stem cell-conditioned medium improves cardiac function following myocardial infarction. *Stem Cell. Res.* **6**, 206-214 (2011).
143. Schachinger, V. *et al.* Intracoronary bone marrow-derived progenitor cells in acute myocardial infarction. *N. Engl. J. Med.* **355**, 1210-1221 (2006).
144. Assmus, B. *et al.* Clinical outcome 2 years after intracoronary administration of bone marrow-derived progenitor cells in acute myocardial infarction. *Circ. Heart Fail.* **3**, 89-96 (2010).
145. Achilli, F. *et al.* Granulocyte-colony stimulating factor for large anterior ST-elevation myocardial infarction: rationale and design of the prospective randomized phase III STEM-AMI OUTCOME trial. *Am. Heart J.* **170**, 652-658.e7 (2015).

146. Nadal-Ginard, B., Ellison, G. M. & Torella, D. The cardiac stem cell compartment is indispensable for myocardial cell homeostasis, repair and regeneration in the adult. *Stem Cell. Res.* **13**, 615-630 (2014).
147. van Berlo, J. H. *et al.* C-Kit⁺ Cells Minimally Contribute Cardiomyocytes to the Heart. *Nature* **509**, 337-341 (2014).
148. Tang, X. L. *et al.* Long-Term Outcome of Administration of c-kit(POS) Cardiac Progenitor Cells After Acute Myocardial Infarction: Transplanted Cells Do not Become Cardiomyocytes, but Structural and Functional Improvement and Proliferation of Endogenous Cells Persist for at Least One Year. *Circ. Res.* **118**, 1091-1105 (2016).
149. Di Siena, S. *et al.* Activated c-Kit receptor in the heart promotes cardiac repair and regeneration after injury. *Cell. Death Dis.* **7**, e2317 (2016).
150. de Witte, S. F., Franquesa, M., Baan, C. C. & Hoogduijn, M. J. Toward Development of iMesenchymal Stem Cells for Immunomodulatory Therapy. *Front. Immunol.* **6**, 648 (2016).
151. Reimer, K. A., Lowe, J. E., Rasmussen, M. M. & Jennings, R. B. The wavefront phenomenon of ischemic cell death. 1. Myocardial infarct size vs duration of coronary occlusion in dogs. *Circulation* **56**, 786-794 (1977).
152. Yeo, M., Lee, H. & Kim, G. Three-dimensional hierarchical composite scaffolds consisting of polycaprolactone, beta-tricalcium phosphate, and collagen nanofibers: fabrication, physical properties, and in vitro cell activity for bone tissue regeneration. *Biomacromolecules* **12**, 502-510 (2011).
153. Xie, L. *et al.* In vitro mesenchymal trilineage differentiation and extracellular matrix production by adipose and bone marrow derived adult equine multipotent stromal cells on a collagen scaffold. *Stem Cell. Rev.* **9**, 858-872 (2013).
154. Chan, B. P. & Leong, K. W. Scaffolding in tissue engineering: general approaches and tissue-specific considerations. *Eur. Spine J.* **17 Suppl 4**, 467-479 (2008).
155. Goldschmidt-Clermont, P. J. *et al.* The control of actin nucleotide exchange by thymosin beta 4 and profilin. A potential regulatory mechanism for actin polymerization in cells. *Mol. Biol. Cell* **3**, 1015-1024 (1992).

156. McManus, D. D. *et al.* Recent trends in the incidence, treatment, and outcomes of patients with STEMI and NSTEMI. *Am. J. Med.* **124**, 40-47 (2011).
157. Rona, G., Chappel, C.I., Balazs, T., & Gaudry, R. An infarct-like myocardial lesion and other toxic manifestations produced by isoproterenol in the rat. *AMA Archives of Pathology* **67**, 443-455 (1959).
158. Teerlink, J. R., Pfeffer, J. M. & Pfeffer, M. A. Progressive ventricular remodeling in response to diffuse isoproterenol-induced myocardial necrosis in rats. *Circ. Res.* **75**, 105-113 (1994).
159. Sohal, D. S. *et al.* Temporally regulated and tissue-specific gene manipulations in the adult and embryonic heart using a tamoxifen-inducible Cre protein. *Circ. Res.* **89**, 20-25 (2001).
160. Dymecki, S. M. Flp recombinase promotes site-specific DNA recombination in embryonic stem cells and transgenic mice. *Proc. Natl. Acad. Sci. U. S. A.* **93**, 6191-6196 (1996).
161. Schonig, K. & Bujard, H. Generating conditional mouse mutants via tetracycline-controlled gene expression. *Methods Mol. Biol.* **209**, 69-104 (2003).
162. Geurts, A. M. *et al.* Knockout rats via embryo microinjection of zinc-finger nucleases. *Science* **325**, 433 (2009).
163. Tesson, L. *et al.* Knockout rats generated by embryo microinjection of TALENs. *Nat. Biotechnol.* **29**, 695-696 (2011).
164. Doetschman, T. & Azhar, M. Cardiac-specific inducible and conditional gene targeting in mice. *Circ. Res.* **110**, 1498-1512 (2012).
165. Inoko, M., Kihara, Y., Morii, I., Fujiwara, H. & Sasayama, S. Transition from compensatory hypertrophy to dilated, failing left ventricles in Dahl salt-sensitive rats. *Am. J. Physiol.* **267**, H2471-82 (1994).
166. McCune, S., Park, S., Radin, M. & Jurin, R. in *Mechanisms of Heart Failure* (eds Singal, P., Dixon, I., Beamish, R. & Dhalla, R.) 91-106 (Kluwer Academic Publishers, Netherlands, 1995).
167. Lanz, J. *et al.* Stroke in Adults With Congenital Heart Disease: Incidence, Cumulative Risk, and Predictors. *Circulation* **132**, 2385-2394 (2015).

168. Walsh, E. P. & Cecchin, F. Arrhythmias in adult patients with congenital heart disease. *Circulation* **115**, 534-545 (2007).
169. Ma, L. *et al.* De novo missense variants in PPP1CB are associated with intellectual disability and congenital heart disease. *Hum. Genet.* **135**, 1399-1409 (2016).
170. Simpson, D. G. *et al.* Modulation of cardiac myocyte phenotype in vitro by the composition and orientation of the extracellular matrix. *J. Cell. Physiol.* **161**, 89-105 (1994).
171. Polini, A., Pisignano, D., Parodi, M., Quarto, R. & Scaglione, S. Osteoinduction of human mesenchymal stem cells by bioactive composite scaffolds without supplemental osteogenic growth factors. *PLoS One* **6**, e26211 (2011).
172. Zhao, C., Tan, A., Pastorin, G. & Ho, H. K. Nanomaterial scaffolds for stem cell proliferation and differentiation in tissue engineering. *Biotechnol. Adv.* **31**, 654-668 (2013).
173. Rockwood, D. N., Akins, R. E., Jr, Parrag, I. C., Woodhouse, K. A. & Rabolt, J. F. Culture on electrospun polyurethane scaffolds decreases atrial natriuretic peptide expression by cardiomyocytes in vitro. *Biomaterials* **29**, 4783-4791 (2008).
174. Periasamy, M., Bhupathy, P. & Babu, G. J. Regulation of sarcoplasmic reticulum Ca²⁺ ATPase pump expression and its relevance to cardiac muscle physiology and pathology. *Cardiovasc. Res.* **77**, 265-273 (2008).
175. Akin, B. L., Hurley, T. D., Chen, Z. & Jones, L. R. The structural basis for phospholamban inhibition of the calcium pump in sarcoplasmic reticulum. *J. Biol. Chem.* **288**, 30181-30191 (2013).
176. Brittsan, A. G. & Kranias, E. G. Phospholamban and cardiac contractile function. *J. Mol. Cell. Cardiol.* **32**, 2131-2139 (2000).
177. Dash, R. *et al.* Interactions between phospholamban and beta-adrenergic drive may lead to cardiomyopathy and early mortality. *Circulation* **103**, 889-896 (2001).
178. Paoletti, R. *et al.* Protein kinase C θ is required for cardiomyocyte survival and cardiac remodeling. *Cell. Death Dis.* **1**, e45 (2010).

179. Martins, A. M. *et al.* Electrically conductive chitosan/carbon scaffolds for cardiac tissue engineering. *Biomacromolecules* **15**, 635-643 (2014).
180. Seif-Naraghi, S. B., Salvatore, M. A., Schup-Magoffin, P. J., Hu, D. P. & Christman, K. L. Design and characterization of an injectable pericardial matrix gel: a potentially autologous scaffold for cardiac tissue engineering. *Tissue Eng. Part A*. **16**, 2017-2027 (2010).
181. Liao, B., Zhang, D. & Bursac, N. Functional cardiac tissue engineering. *Regen. Med.* **7**, 187-206 (2012).
182. Anversa, P., Kajstura, J., Rota, M. & Leri, A. Regenerating new heart with stem cells. *J. Clin. Invest.* **123**, 62-70 (2013).
183. Takahashi, K. & Yamanaka, S. Induction of pluripotent stem cells from mouse embryonic and adult fibroblast cultures by defined factors. *Cell* **126**, 663-676 (2006).
184. Xin, M., Olson, E. N. & Bassel-Duby, R. Mending broken hearts: cardiac development as a basis for adult heart regeneration and repair. *Nat. Rev. Mol. Cell Biol.* **14**, 529-541 (2013).
185. Amsalem, Y. *et al.* Iron-oxide labeling and outcome of transplanted mesenchymal stem cells in the infarcted myocardium. *Circulation* **116**, I38-45 (2007).
186. Murry, C. E. *et al.* Haematopoietic stem cells do not transdifferentiate into cardiac myocytes in myocardial infarcts. *Nature* **428**, 664-668 (2004).
187. Arnal-Pastor, M., Chachques, J., Pradas, M. & Vallés-Lluch, A. in ***Regenerative Medicine and Tissue Engineering*** (ed Andrades, J. A.) 275-323 (InTech Open Access, 2013).
188. Meng, X. *et al.* Novel injectable biomimetic hydrogels with carbon nanofibers and self assembled rosette nanotubes for myocardial applications. *J. Biomed. Mater. Res. A*. **101**, 1095-1102 (2013).
189. Fleischer, S., Shevach, M., Feiner, R. & Dvir, T. Coiled fiber scaffolds embedded with gold nanoparticles improve the performance of engineered cardiac tissues. *Nanoscale* **6**, 9410-9414 (2014).
190. Godier-Furnemont, A. F. *et al.* Composite scaffold provides a cell delivery platform for cardiovascular repair. *Proc. Natl. Acad. Sci. U. S. A.* **108**, 7974-7979 (2011).

191. Ventrelli, L., Ricotti, L., Menciacchi, A., Mazzolai, B. & Mattoli, V. Nanoscaffolds for Guided Cardiac Repair: The New Therapeutic Challenge of Regenerative Medicine. *Journal of Nanomaterials* **2013**, 1-16 (2013).
192. Mercola, M. Cardiovascular biology: A boost for heart regeneration. *Nature* **492**, 360-362 (2012).
193. Roche, E. T. *et al.* Soft robotic sleeve supports heart function. *Sci. Transl. Med.* **9**, 10.1126/scitranslmed.aaf3925 (2017).
194. Caplan, A. I. in *Stem Cells in Regenerative Medicine: Science, Regulation and Business Strategies* (eds Vertes, A. A., Qureshi, N., Caplan, A. I. & Babiss, L. E.) 415-422 (John Wiley & Sons, USA, 2015).
195. Leri, A., Rota, M., Hosoda, T., Goichberg, P. & Anversa, P. Cardiac stem cell niches. *Stem Cell. Res.* **13**, 631-646 (2014).
196. Chong, J. J. *et al.* Adult cardiac-resident MSC-like stem cells with a proepicardial origin. *Cell. Stem Cell.* **9**, 527-540 (2011).
197. Annex, B. H. Therapeutic angiogenesis for critical limb ischaemia. *Nat. Rev. Cardiol.* **10**, 387-396 (2013).
198. Hou, J. *et al.* Cardiac stem cells and their roles in myocardial infarction. *Stem Cell. Rev.* **9**, 326-338 (2013).
199. Ichim, T. E. *et al.* Combination stem cell therapy for heart failure. *Int. Arch. Med.* **3**, 5-7682-3-5 (2010).
200. Windmolders, S. *et al.* Mesenchymal stem cell secreted platelet derived growth factor exerts a pro-migratory effect on resident Cardiac Atrial appendage Stem Cells. *J. Mol. Cell. Cardiol.* **66**, 177-188 (2014).
201. Barbash, I. M. *et al.* Systemic delivery of bone marrow-derived mesenchymal stem cells to the infarcted myocardium: feasibility, cell migration, and body distribution. *Circulation* **108**, 863-868 (2003).
202. Chen, S. L. *et al.* Effect on left ventricular function of intracoronary transplantation of autologous bone marrow mesenchymal stem cell in patients with acute myocardial infarction. *Am. J. Cardiol.* **94**, 92-95 (2004).
203. Fuchs, S. *et al.* Catheter-based autologous bone marrow myocardial injection in no-option patients with advanced coronary artery disease: a feasibility study. *J. Am. Coll. Cardiol.* **41**, 1721-1724 (2003).

204. Thompson, C. A. *et al.* Percutaneous transvenous cellular cardiomyoplasty. A novel nonsurgical approach for myocardial cell transplantation. *J. Am. Coll. Cardiol.* **41**, 1964-1971 (2003).
205. Askari, A. T. *et al.* Effect of stromal-cell-derived factor 1 on stem-cell homing and tissue regeneration in ischaemic cardiomyopathy. *Lancet* **362**, 697-703 (2003).
206. Psaltis, P. J., Zannettino, A. C., Gronthos, S. & Worthley, S. G. Intramyocardial navigation and mapping for stem cell delivery. *J. Cardiovasc. Transl. Res.* **3**, 135-146 (2010).
207. Wang, C. C. *et al.* Direct intramyocardial injection of mesenchymal stem cell sheet fragments improves cardiac functions after infarction. *Cardiovasc. Res.* **77**, 515-524 (2008).
208. Munsie, M. & Hyun, I. A question of ethics: selling autologous stem cell therapies flaunts professional standards. *Stem Cell. Res.* **13**, 647-653 (2014).
209. Smart, N. & Riley, P. R. The stem cell movement. *Circ. Res.* **102**, 1155-1168 (2008).
210. Wu, J. M. *et al.* Circulating cells contribute to cardiomyocyte regeneration after injury. *Circ. Res.* **116**, 633-641 (2015).
211. Xu, M. *et al.* Differentiation of bone marrow stromal cells into the cardiac phenotype requires intercellular communication with myocytes. *Circulation* **110**, 2658-2665 (2004).
212. Liang, C., Li, Y. & Luo, J. A Novel Method to Detect Functional microRNA Regulatory Modules by Bicliques Merging. *IEEE/ACM Trans. Comput. Biol. Bioinform* **13**, 549-556 (2016).
213. Huang, Y. *et al.* Effect of cyclic strain on cardiomyogenic differentiation of rat bone marrow derived mesenchymal stem cells. *PLoS One* **7**, e34960 (2012).
214. Kinnaird, T. *et al.* Local delivery of marrow-derived stromal cells augments collateral perfusion through paracrine mechanisms. *Circulation* **109**, 1543-1549 (2004).
215. Parekkadan, B. *et al.* Mesenchymal stem cell-derived molecules reverse fulminant hepatic failure. *PLoS One* **2**, e941 (2007).

216. Nguyen, B. K. *et al.* Improved function and myocardial repair of infarcted heart by intracoronary injection of mesenchymal stem cell-derived growth factors. *J. Cardiovasc. Transl. Res.* **3**, 547-558 (2010).
217. Cordes, K. R. & Srivastava, D. MicroRNA regulation of cardiovascular development. *Circ. Res.* **104**, 724-732 (2009).
218. Liu, N. & Olson, E. N. MicroRNA regulatory networks in cardiovascular development. *Dev. Cell.* **18**, 510-525 (2010).
219. Small, E. M. & Olson, E. N. Pervasive roles of microRNAs in cardiovascular biology. *Nature* **469**, 336-342 (2011).
220. van Rooij, E., Marshall, W. S. & Olson, E. N. Toward microRNA-based therapeutics for heart disease: the sense in antisense. *Circ. Res.* **103**, 919-928 (2008).
221. Griffiths-Jones, S., Grocock, R. J., van Dongen, S., Bateman, A. & Enright, A. J. miRBase: microRNA sequences, targets and gene nomenclature. *Nucleic Acids Res.* **34**, D140-4 (2006).
222. Katz, M. G., Fagnoli, A. S., Kendle, A. P., Hajjar, R. J. & Bridges, C. R. Gene Therapy in Cardiac Surgery: Clinical Trials, Challenges, and Perspectives. *Ann. Thorac. Surg.* **101**, 2407-2416 (2016).
223. Hodgkinson, C. P., Kang, M. H., Dal-Pra, S., Mirotsov, M. & Dzau, V. J. MicroRNAs and Cardiac Regeneration. *Circ. Res.* **116**, 1700-1711 (2015).

Appendix

**INSTITUTIONAL ANIMAL CARE AND USE COMMITTEE PROTOCOL
APPROVAL**

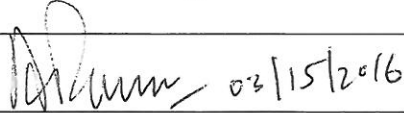
University of Delaware
Institutional Animal Care and Use Committee
Application to Use Animals in Application to use animals in Research
(New and 3-Yr submission)

Title of Protocol: Intraventricular nanoscaffold injections for repair of damaged cardiac tissue after MI	
AUP Number: 1301-2016-0	← (4 digits only — if new, leave blank)
Principal Investigator: Arun Kumar	
Common Name (Strain/Breed if Appropriate): White rat	
Genus Species: Rattus norvegicus	
Date of Submission: March 18, 2016	

Official Use Only
IACUC Approval Signature: _____
Date of Approval: _____

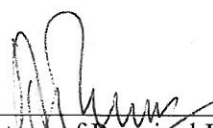
NAMES OF ALL PERSONS WORKING ON THIS PROTOCOL

I certify that I have read this protocol, accept my responsibility and will perform only those procedures that have been approved by the IACUC.

Name	Signature
1. Arun Kumar	
2. Edward D. Marks	
3. Click here to enter text.	
4. Click here to enter text.	
5. Click here to enter text.	
6. Click here to enter text.	
7. Click here to enter text.	
8. Click here to enter text.	
9. Click here to enter text.	
10. Click here to enter text.	

If after hours participation is required by students on project involving **agricultural animals**, please describe how this is handled and the times and days that students may be on site
Click here to enter text.

Principal Investigator Assurance

1. I agree to abide by all applicable federal, state, and local laws and regulations, and UD policies and procedures.	
2. I understand that deviations from an approved protocol or violations of applicable policies, guidelines, or laws could result in immediate suspension of the protocol and may be reportable to the Office of Laboratory Animal Welfare (OLAW).	
3. I understand that the Attending Veterinarian or his/her designee must be consulted in the planning of any research or procedural changes that may cause more than momentary or slight pain or distress to the animals.	
4. I declare that all experiments involving live animals will be performed under my supervision or that of another qualified scientist. All listed personnel will be trained and certified in the proper humane methods of animal care and use prior to conducting experimentation.	
5. I understand that emergency veterinary care will be administered to animals showing evidence of discomfort, ailment, or illness.	
6. I declare that the information provided in this application is accurate to the best of my knowledge. If this project is funded by an extramural source, I certify that this application accurately reflects all currently planned procedures involving animals described in the proposal to the funding agency.	
7. I assure that any modifications to the protocol will be submitted to by the UD-IACUC and I understand that they must be approved by the IACUC prior to initiation of such changes.	
8. I understand that the approval of this project is for a maximum of one year from the date of UD-IACUC approval and that I must re-apply to continue the project beyond that period.	
9. I understand that any unanticipated adverse events, morbidity, or mortality must be reported to the UD-IACUC immediately.	
10. I assure that the experimental design has been developed with consideration of the three Rs: reduction, refinement, and replacement, to reduce animal pain and/or distress and the number of animals used in the laboratory.	
11. I assure that the proposed research does not unnecessarily duplicate previous experiments. <i>(Teaching Protocols, including cooperative extension demonstrations, Exempt)</i>	
12. I understand that by signing, I agree to these assurances.	
 _____ Signature of Principal Investigator	<u>03/15/2016</u> Date

The Animal Use Protocol form has been developed to facilitate review of requests for specific research, teaching, or biological testing projects. The review process has been designed to communicate methods and materials for using animals through administrative officials and attending veterinarians to the Institutional Animal Care and Use Committee (IACUC). This process will help assure that provisions are made for compliance with the Animal Welfare Act, the Public Health Service Policy on Humane Care and Use of Laboratory Animals and the Guide for the Care and Use of Laboratory Animals.

Please read this form carefully and fill out all sections. Failure to do so may delay the review of this application. Sections that do not apply to your research must be marked "NA" for "Not Applicable."

This application form must be used for all NEW or THREE-YEAR RENEWAL protocols.

All answers are to be completed using Arial 12 size font.

All questions must be answered in their respective boxes and NOT as attachments at the end of this form.

Please complete any relevant addenda:

- Hybridoma/Monoclonal Antibodies ("B")
- Polyclonal Antibodies ("C")
- Survival Surgery ("D")
- Non-Survival Surgery ("E")
- Wildlife Research ("F")

If help is needed with these forms, contact the IACUC Coordinator at extension 2616, the Facility Manager at extension 2400 or the Attending Veterinarian at extension 2980.

1. Principal Investigator Information:	
a. Name:	Arun Kumar
b. University/Company:	University of Delaware
c. Department:	Medical Laboratory Sciences
d. Building/Room:	Willard Hall Room 305
e. Office Phone:	302-831-4552
f. Lab Phone(s):	302-831-3367
g. Home Phone:	Click here to enter text.
h. Mobile Phone:	Click here to enter text.
i. E-Mail Address:	arunk@udel.edu
2. Protocol Status:	
a. <input checked="" type="checkbox"/> New Protocol OR <input type="checkbox"/> Re-submission due to three (3) completed years. If re-submission, enter Protocol Number: Click here to enter text.	
b. <input checked="" type="checkbox"/> Research OR <input checked="" type="checkbox"/> Teaching or Cooperative Extension	
c. <input checked="" type="checkbox"/> Laboratory Animals OR <input checked="" type="checkbox"/> Wildlife OR <input type="checkbox"/> Agricultural Animals If "Wildlife" please complete Addendum "F" For agricultural animal protocols, please list the name and contact information for veterinarian who is on-call. A copy of the protocol should be shared with the veterinarian Click here to enter text.	
d. Proposed Start Date: April 15 th 2016	
e. Proposed Completion Date: May 31 st 2019	
f. Funding Source: COBRE grant	
g. Award Number if applicable: CHEM175269	

3. Non-Scientific Summary: In language understandable to a *high-school senior, very briefly describe* the goals and significance of this study.

- a. Specific Scientific Goals: To effectively treat heart attacks by replacing the damaged tissue with a dissolvable scaffold gel containing cells and growth factors. This gel will aid in removing the damaged tissue and repairing the injured areas of the heart.

- b. Significance of this Research or Teaching/Cooperative Extension Demonstration (including the possible benefits to human and/or animal health, the advancement of scientific knowledge, or the betterment of society): Cardiovascular disease (CVD) is the leading cause of death in the world, representing almost a third of all deaths. Moderate to severe cardiac events stemming from CVD, including heart attack, stroke, and coronary artery disease, significantly alter the heart in shape and function due to necrotic, and thus nonfunctioning, tissue. This deformation results in poor cardiovascular functionality, increasing the likelihood of a second cardiac event and ultimately death. By replacing the damaged tissue with new heart muscle cells delivered via our injectable scaffold, the heart will be able to repair the damage, something it is unable to do without outside intervention. This replacement heart muscle will decrease post-injury heart muscle remodeling, improve heart functionality measures, and decrease or eliminate the patient's lifetime dependence on pharmacological intervention, such as beta-blockers. The scaffold will also be applied to the damaged area using a minimally invasive orthoscopic procedure to decrease the intense scarring and additional healing time indicative of open heart surgery. Additionally, all injectable elements and surgical strategies are directly translatable to the human case, meaning successful completion of this procedure will lead us one step closer towards clinical trials.

4. Experimental Design: Explain the experimental design. This description should allow the IACUC to understand fully the experimental course of an animal or group of animals from its entry into the experiment to the endpoint of the study.

The inclusion of flow charts, diagrams, and/or tables are greatly encouraged to explain experimental design or sequential events.

Be sure to include all animal events and related details, i.e.,

- **All Procedures**—bleedings, injections, identification methods, genotyping methods, physiological measurements, surgical procedures, euthanasia, etc.
- **Procedural details**—number of animals involved in procedure, approximate animal weight, if relevant (for injections, bleeding, etc.), route, frequency, volume, etc.
- **Pharmaceutical-grade and non-pharmaceutical grade compounds** – Identify any drugs, biologics, or reagents that will be administered to animals.
- **Vaccines and organisms used for challenge** – Identify any experimental or commercial vaccines and/or microorganisms used for challenge of the animals.
- **Federal or other permits** – Identify any federal or other permits needed to obtain vaccines or organisms used in animal studies.

- **Names of surgical procedures** (but reserve the surgical details for the proper Surgical Addenda)

(Describe):

	Treatment Option				
[ISO] mg/kg	Sham	Cell Media	MSCs	Scaffold	MSC+scaffold
0	6	6	6	6	6
10	6	6	6	6	6
50	6	6	6	6	6
100	6	6	6	6	6
Totals	24	24	24	24	24
Total	120				

Table 1. Experimental plan for control and test animals. Concentration in the left column represent isoproterenol concentrations corresponding to increasing severity of cardiac damage. Top row are injections that will be given to the animals; explanations can be found in the text.

Procedural details:

Animal details:

The statistics and pilot studies indicate approximately 120 animals will be needed to complete the initial experiment. Attrition in the pilot studies has necessitated an increase in the number of animals per group; the statistics indicated n=4/sample with 4 samples/group = 16 rats/group, but we elected to increase by 0.66 to ensure enough rats for statistical viability in the results. The animals will be 3month old Sprague Dawley rats, most likely purchased from Envigo, weighing ~325-375 grams.

ISO injections:

All animals (except those in the 0mg/kg group) will be given an injection to begin the experiment (T0). The injection is isoproterenol (from Sigma), a pharmaceutical grade beta-agonist that induces cardiac damage akin to a heart attack (Rona et al., Arch Pathol 67,443–55; Ellison et al., Cell 154, 827–42). We have performed these injections in two pilot studies so far, using concentrations from 0mg/kg-150mg/kg. Because of distress to the animal and risk of death, we have chosen to use concentrations not exceeding 100mg/kg.

After injection, animals will receive subcutaneous long-acting buprenorphine in accordance with SOP#A-104. We have received prior amendment approval for buprenorphine administration. Buprenorphine will be administered once after ISO injection, as it lasts up to 72hrs.

Animals will be monitored 3x a day (morning, midday, night) after isoproterenol injections to ensure proper recovery and survival. Sluggishness in animals receiving higher concentrations is expected and normal. These animals will be monitored for 48-72hours before therapeutic injection.

Treatment:

As per Table 1, the animals will receive one treatment for cardiac damage 48-72hrs

after induction of heart attack; this timeline will ensure inflammation has decreased to a point that likelihood of stem cell survival and therapeutic efficacy is increased (Frangogiannis, Nat Rev Cardiology 11, 255–265). Human mesenchymal stem cells can be placed into an animal model because they are described as “immunoprivileged”, meaning they do not contain major histocompatibility complexes (MHCs) on their surface, a target for immune cells and the cause of most organ rejections (Ankrum et al. Nat Biotech 32, 2014). For this reason allogeneic mesenchymal stem cells have been used in many animal tests and human clinical trials with no adverse safety events (Abdel-Latif et al. Arch Intern Med 167, 2007). The treatments, described below, will be administered via a 20G or 22G needle into the left ventricle (LV) of the rat’s heart. Experimenters have received training on intraventricular injections. Previous studies (Yoshimitsu et al. Circ J. 70, 2006; Barbash et al. Circulation 108, 2003; Ranganath et al. Cell Stem Cell 10, 2012) have shown intraventricular injections to be safe and effective for delivering a therapeutic payload. The volume of injection will not exceed 200uL including vehicle and treatment. The animals will be under isoflurane anesthesia during the injection, and will be tested via toe pinch. The animals will receive a SC buprenorphine injection after intraventricular injection to alleviate potential distress.

All treatment modalities will be injected into the LV of each rat given ISO. The treatment descriptions are as follows: sham, will receive PBS injection; Cell media, MSC-free cell culture media injection; scaffold, injection of sterilized but unseeded polycaprolactone nanoscaffold free in cell culture media; MSCs, injection of bone marrow mesenchymal stem cells in cell culture media; MSCs + scaffold, injection of MSCs attached to the polycaprolactone nanoscaffold free in cell culture media.

Recently, we performed intraventricular injections of the nanoscaffold (without cells) using a 20G and a 22G needle. In both instances there was no emboli formation or excess bleeding, and the animals maintained proper breathing and heart rate for the monitoring period (15-30min post-injection). The biodegradable nanoscaffolds are chopped into fine pieces prior to injection, decreasing if not eliminating the risk of emboli formation.

Bleeding:

Tail vein or sublingual bleeds will be performed on a subset of animals (as per Table in SOP PRO-001, Survival Bleed Volumes). We will be measuring cardiac troponin, a common protein increased after cardiac damage and a standard measure in the field of cardiology to measure extent of cardiac damage (Shah et al., BMJ 350, g7873).

	Month		
	April 18-May 5	May 2-May 19	May 13-May 30
Animals beginning	16	16	16
Animals euthanized	all	all	all

Table 2. Proposed timeline for initial experimental completion. Animals beginning are when the 3month old Sprague Dawleys will be purchased. Animals euthanized are those that will be euthanized at the end of the 2week period.

Monitoring:

All animals will be monitored for two weeks. Full cardiac remodeling occurs two weeks after symptom onset (Holmes, et al. Annu. Rev. Biomed. Eng. 7, 223–53), so full therapeutic efficacy will be determined as the heart is healing. Weight will be taken before surgeries. Animals will be assessed every day for survival and removed forthwith if deceased. Clinical

parameters that necessitate euthanasia, including sluggishness that impedes eating or drinking, weight loss exceeding 20%, signs of severe organ dysfunction, or serious infection, will be assessed each day.

The animals will have their heart function and size monitored via ultrasound. Edward and Dr. Kumar have received a year of training on the ultrasound machine. The machine is a noninvasive approach to measure LV diameter and wall thickness (both at the end of systole and diastole), rate of blood flow, and heart sounds. The animals will be anesthetized with 4% isoflurane and maintained at 2%, and will be shaved around the left ribs and shoulder. While we don't expect the procedure to take more than a few minutes, eye drops and a heating pad will be on hand to ensure animal comfort, should the procedure take longer. Readings will be taken every 48hrs.

Euthanization:

After 2weeks animals will be euthanized via IP injection of Euthasol solution. Death will be confirmed by tail and toe pinch, and lack of breathing. Animals will then be necropsied, with heart removed. Other organs, such as kidneys, liver, and lungs, may also be removed.

5. Administration of compounds

Drug name or class of drug	Volume	Dose or range of doses	Route (IP, IV, SC, IM, PO)	Frequency	Duration	Pharma-grade Yes or No
Isoproterenol	100-500uL	25-100 mg/kg	SC	Once per animal	Single injection	No
Long-acting Buprenorphine	500uL	1.0 mg/kg	SC	After ISO;	Single injection	Yes
Regular buprenorphine	300 uL	0.01-0.05 mg/kg	SC	After intra-cardiac injection	Single injection	Yes
Euthasol	1mL	>150 mg/kg	IP	Terminal	Single injection	Yes

If non-pharmaceutical grade compounds are used, they must be justified (such as pharmaceutical-grade not available) and the method to ensure appropriate preparation must be described: (for example: pharmaceutical grade drugs are not available. Chemical-grade isoproterenol is used to make the drug in the appropriate concentrations. Sterile saline will be used as a vehicle and the solution will be sterile-filtered. [Click here to enter text.](#)

6. Does this work involve surgery or antibody production Yes No

If yes, please complete Addendum B for hybridoma/monoclonal antibody production, Addendum C for polyclonal antibody production, Addendum D for survival surgery and Addendum E for terminal surgery

REFINEMENT, REDUCTION & REPLACEMENT

When using animals for research, it is important to consider the three Rs: reduction, refinement, and replacement to reduce both animal distress and the number of animals used in the laboratory.

Reduction: Minimizing the number of animals used

Refinement: Using techniques and procedures to reduce pain and distress

Replacement: Using non-animal methods or lower phylogenetic organisms

7. **Justification for the Use of Animals** (instead of *in vitro* methods)
(Check all that apply and explain):

a. The complexity of the processes being studied cannot be duplicated or modeled in simpler systems: *(Explain):* Many simpler model systems do not contain adequate cardiovascular features to allow for proper study of this phenomena. Simpler organisms with hearts, such as the zebrafish, also have regeneration capabilities that will skew the data and not allow for accurate study.

b. There is not enough information known about the processes being studied to design non-living models: *(Explain):* Click here to enter text.

c. Other: *(Explain):* Click here to enter text.

8. **Justification for Species Appropriateness:**
(Check all that apply and explain):

a. A large database exists, allowing comparisons with previous data: *(Explain):* Many heart treatment studies have used rats, as they are the simplest system that still can provide clinically relevant information of physiology and function.

b. The anatomy or physiology is uniquely suited to the study proposed: **(Explain)**: Rats contain all the parts of the heart a human does. Also, the heart and animal are both bigger than a mouse, making the outcomes more clinically relevant.

c. This is the lowest species on the phylogenic scale suitable to the proposed study: **(Explain)**: Mice have been used, with mixed results. Difficulty in study design and data analysis for clinical relevancy while using mice necessitate rat usage. Pigs, dogs, and rabbits have also been used but they are higher on the phylogenetic scale and therefore not justifiable for the work at this time.

d. Other: **(Explain)**: Click here to enter text.

9. Justification for Number of Animals Requested: (Note: numbers should include animals used for breeding and all animals born)

a. Pilot study or preliminary project where group variances are unknown at the present time. Describe the information used to estimate how many animals will be needed: (Only a limited number of animals will be permitted.)

(Explain): We have performed multiple pilot studies within the last year to optimize our protocol. Initial statistical tallies indicated over 600 rats were needed, because of uncertainties in the protocol. By using small pilot studies we were able to decrease the number of rats used and increase the efficiency of our whole system.

b. Group sizes are determined statistically. Describe the statistical analysis used to estimate the number (N) of animals needed: N may be estimated from a power analysis for the most important measurement in the study, usually based on the expected size of the treatment effect, the standard error associated with the measurement, and the desired statistical power (e.g. $P < 0.05$). Data analysis methods should not be submitted unless directly applicable to the estimate of N.

An online calculator may be found at: <http://www.math.uiowa.edu/~rlenth/Power/> or a stand-alone calculator that can be downloaded from

<http://www.psych.uni-duesseldorf.de/abteilungen/aap/gpower3>

(Explain): The statistics and pilot studies indicate approximately 120 animals will be needed to complete the initial experiment. Attrition in the pilot studies has necessitated an increase in the number of animals per group; the statistics indicated $n=4/\text{sample}$ with 4 samples/group = 16 rats/group, but we elected to increase by 0.66 to ensure enough rats for statistical viability in the results. Please see table in Experimental Design section (Q4).

c. Group sizes are based on the quantity of harvested cells or the amount of tissue required for *in vitro* studies. Explain how much tissue is needed based on the number of experiments to be conducted and

the amount of tissue you expect to obtain from each animal (e.g., 10g of tissues are needed: Each animal can provide 2g. $10g / 2g \text{ per animal} = 5 \text{ animals needed.}$) **(Explain):** [Click here to enter text.](#)

d. Teaching or cooperative extension demonstration protocol. Specify the number of students in the class, the student to animal ratio and how that ratio was determined: Animal numbers should be minimized to the fullest extent possible without compromising the quality of the hands-on teaching experience for students or the health and welfare of the animals. **(Explain):** [Click here to enter text.](#)

e. Study involving feral or wild animals. Animals will be captured and released in an attempt to maximize the sample size within logistical constraints. Describe the process by which you estimate these numbers and estimate the precision needed: **(Explain):** [Click here to enter text.](#)

f. Observational, non-manipulative study. Animals will not be captured, their behavior will not be interfered with, and exact animal numbers cannot be predicted: **(Explain):** [Click here to enter text.](#)

g. Product testing. The number of animals needed is based on FDA or USDA guidelines. Provide the citation from the regulations, the IND tracking number, or relevant FDA or USDA correspondence: **(Explain):** [Click here to enter text.](#)

h. Other. Elaborate, indicating the method used to determine the group size. **(Explain):** [Click here to enter text.](#)

10. Animals Requested:

Common Name	Genus and Species	Total Number of Animals for Three Years
1. White rat	Rattus norvegicus	120
2. Click here to enter text.	Click here to enter text.	Click here to enter text.
3. Click here to enter text.	Click here to enter text.	Click here to enter text.
4. Click here to enter text.	Click here to enter text.	Click here to enter text.
5. Click here to enter text.	Click here to enter text.	Click here to enter text.

<p>11. Where will animals be obtained and are there any special shipping requirements? Envigo delivery, no special instructions</p> <p>If these are privately owned animals please attach an owner consent form</p> <p>Are agricultural animals obtained from a non-traditional source such as poultry from a commercial production company or swine from commercial herd? <input type="checkbox"/> Yes <input type="checkbox"/> No</p> <p>If yes, please describe how the animals are tested and determined to be free of diseases which could potentially infect other animals on site, and any special precautions, such as quarantine isolation housing that is required. Click here to enter text.</p>		
<p>12. Where will animals be housed (or captured for wildlife)? Life Sciences Research Facility</p>		
<p>13. Will any untreated or non-manipulated animals be humanely euthanized, to obtain tissue, cells, etc.? <input checked="" type="checkbox"/> Yes <input type="checkbox"/> No</p> <p>If Yes, list types of tissue, etc: Cardiac muscle, whole hearts; possible kidneys and livers</p>		
<p>14. Dietary Manipulations <input type="checkbox"/> Yes <input checked="" type="checkbox"/> No</p> <p>If Yes, list and explain (Note: if food or fluid will be restricted, describe method for assessing the health and wellbeing of the animals. Body weights must be recorded at least weekly. Amount earned (if animals work for food or fluid) during testing and amount freely given must be recorded. A scientific justification must be provided for departures from the recommendations of the Guide.) Click here to enter text.</p>		

15. **Environmental Stress (e.g. cold, prolonged restraint, forced exercise, shock)** Yes No
If Yes, list and explain: [Click here to enter text.](#)

16. **Special Study Requirements or Exceptions to Standards:** Please describe any special study requirements such as single housing of the animals, exemption from environmental enrichment, or special caging [Click here to enter text.](#)

17. **Will any animal undergo anesthesia for any reason other than surgery?** Yes No

If Yes,

a. List Procedures and Reason(s) for using anesthesia: Ultrasound will be performed to measure cardiac metrics.

b. Check the type of anesthesia to be used.

Isoflurane

Injectable (*For injectable, complete the following*):

Drug: [Click here to enter text.](#)

Dose: [Click here to enter text.](#)

Route: [Click here to enter text.](#)

HAZARDOUS AGENTS

18. **Administration of Hazardous Chemicals, Drugs, Toxins, or Nanoparticles**

Yes CAS#_5984-95-2_ No

If Yes, describe hazards posed to personnel: Iso: Minimal- is a potent beta-adrenergic agonist, but at concentrations hundreds of times higher than what will be used in this procedure

Nanoparticles: Minimal- they are trapped within the injected cells, are easily excreted by the animal, and are used clinically as MRI contrast agents as they pose no risk to the patient.

Methods to control exposure: Using sub-toxic concentrations

Methods of Disposal of Animals and Bedding: No special treatment required

We are describing two materials. The first is isoproterenol, which is used to induce the MI. We are using sub-lethal doses on the animals, meaning the chemical would have to be thousands of times more potent to cause any damage in a human. For the nanoparticles, they are made of ferric oxide (Fe₂O₃) in water, and are sequestered within the stem cells. They cause no damage to cells (eukaryotic or prokaryotic), are easily secreted, and are used in clinics to provide a non-toxic MRI contrast for those allergic or intolerant to normal radioactive dyes (Amselem et al. Circulation 116, 2007; Cicha et al. Eur. J. Nanomed 6, 2014).

Describe hazards posed to personnel: Minimal- these are human cells suspended within a microtube and attached to a nanoscaffold

Methods to control exposure: Standard PPE

Methods of Disposal of Animals and Bedding: No special treatment required

Approval received from UD- Institutional Biosafety Committee, and if required, the UD-Select Agent Committee? Yes No Pending

Please attach a copy of any approvals or provide the approval number. [Click here to enter text.](#)

22. Will tumor cells, tissue, sera, viral vectors or other biologics of RODENT origin – other than those isolated from rodents already housed in the facility – be administered to animals?

Yes No

If Yes, this material must be tested for rodent pathogens and test results must be attached (Please contact the Attending Veterinarian for details).

23. Use of Genetically Engineered (GEM, transgenic, knockout) Animals

Yes No

If Yes, please describe any anticipated phenotypes that may cause pain or distress and any special care or monitoring that the animals will require.

[Click here to enter text.](#)

Does the proposed work involve creating new genetically modified animals, or involve crossing two genetically modified animals to produce offspring with a new genotype.

Yes No

Approval received from UD- Institutional Biosafety Committee?

Yes No Pending Exempt (breeding of two lines of genetically-modified rodents is exempt if 1) both parents can be housed under BL1 containment and 2) neither parent strain incorporates more than one half of the genome of an exogenous eukaryotic virus or incorporates a transgene under the control of a gammaretroviral long terminal repeat and 3) the rodent that results from the breeding is not expected to contain more than one half of an exogenous viral genome)

Please attach a copy of any approvals or provide the approval number.

_____ [Click here to enter text.](#) _____

Potential Pain and Distress

24. Pain Category: (please mark one)

USDA PAIN CATEGORY: (Note change of categories from previous form)	
Category	Description
<input type="checkbox"/> B	Breeding or holding where NO research is conducted
<input type="checkbox"/> C	Procedure involving momentary or no pain or distress
<input checked="" type="checkbox"/> D	Procedure where pain or distress is alleviated by appropriate means (analgesics, tranquilizers, euthanasia etc.)
<input type="checkbox"/> E	Procedure where pain or distress cannot be alleviated, as this would adversely affect the procedures, results or interpretation

25. If animals may experience pain or distress, (for example, animal challenge studies using a pathogenic disease agent) please include how they will be monitored, frequency of observation, and potential treatments (note: for survival surgery procedures this will be described in addendum D and does not need to be repeated here): Animals receiving isoproterenol will also be given long-acting buprenorphine, and will be checked 3x a day for 72hours (the time course for MI induction and healing) After the intracardiac injections, rats will be administered one dose of regular buprenorphine, then checked in 4 to 6 hours

26. Please describe criteria for when an animal will be euthanized (humane endpoints – possible examples include 20% weight loss, ulceration of subcutaneous tumors, difficulty ambulating, hunched posture);

Animals will be assessed every day. Clinical parameters that necessitate euthanasia include sluggishness that impedes eating or drinking, weight loss exceeding 20%, hunched posture, or serious infection.

Alternatives to Pain and Distress

27. If you have indicated that animals in your study experience pain or distress (category D or E), even if it will be fully alleviated, please mark the appropriate check boxes below and fill in the requested information for each item marked. (Note: If the pain category is B or C, please skip to question 28)

You must conduct at least two (2) searches.

I have considered alternatives to the use of animals in my study. Alternatives refer to methods or approaches which result in refinement of procedures which lessen pain and/or distress; reduction in numbers of animals required; or replacement of animals with non-whole-animal systems or

replacement of one animal species with another, particularly if the substituted species is non-mammalian or invertebrate. I have used the following methods and sources to search for alternatives:

Note: You may need to do more than one search per database to look for alternatives if there are multiple procedures that may cause pain and/or distress.

Database Used:

- | | |
|--|---|
| <input checked="" type="checkbox"/> Medline | <input type="checkbox"/> Agricola |
| <input type="checkbox"/> Toxline | <input type="checkbox"/> CAB Abstracts |
| <input type="checkbox"/> Biosis | <input type="checkbox"/> Other (<i>Specify</i>): Click here to enter text. |

Date of Search: 02/15/2016

Years Covered: all years

Keywords Used (must include the word *alternative*): animal "heart failure model" alternative

Number of Papers Found: 6

Discussion of the Relevancy of the Papers Found: We are using an animal in this study to see how great of an effect our tissue engineered scaffold has on an in vivo test subject that has a heart structure that is comparable to a human's. Many of the papers discuss novel techniques that induce specific kinds of heart failure, such as blocking of vascular endothelial growth factor. Other models included ligating specific parts of the heart or injections with substances such as doxorubicin. The reason that the direct injection of isoproterenol will be better than any of these models is that this method will cause a localized injury of predictable size and severity. Rat, pig, dog, and mouse models are used for various different types of experiments. The rat model will work best for our experiment because this species is affordable to obtain and store in large numbers and is less delicate and easier to work with than other small rodents, such as mice. For example, the rat heart has about 10 times greater myocardial mass than the mouse heart.

Database Used:

- | | |
|---|---|
| <input type="checkbox"/> Medline | <input type="checkbox"/> Agricola |
| <input type="checkbox"/> Toxline | <input type="checkbox"/> CAB Abstracts |
| <input checked="" type="checkbox"/> Biosis | <input type="checkbox"/> Other (<i>Specify</i>): Click here to enter text. |

Date of Search: 02/15/2016

Years Covered: all years

Keywords Used (must include the word *alternative*): animal "heart failure model" alternative

Number of Papers Found: 3

Discussion of the Relevancy of the Papers Found: Discussed in paragraph above; the 3 papers found were also found in the PubMed database search.

--

Unnecessary Duplication of Work.

28. Activities involving animals must not unnecessarily duplicate previous experiments performed by you or others. Provide a written narrative that assures that the activities of this project comply with this requirement and support this assurance by performing a literature search.

The search should return, at minimum, the related previous work from your laboratory.

You must conduct at least two (2) searches.

(NOT REQUIRED FOR TEACHING PROTOCOLS)

Note: You may need to do more than one search per database to look for duplication of work, especially if you are doing more than one experiment.

Database Used:

- | | |
|---|--|
| <input type="checkbox"/> Medline | <input type="checkbox"/> Agricola |
| <input type="checkbox"/> Toxline | <input type="checkbox"/> CAB Abstracts |
| <input checked="" type="checkbox"/> Biosis | <input type="checkbox"/> Other (Specify): Click here to enter text. |

Date of Search: 02/15/2016

Years Covered: all years

Keywords Used: **alternative*animal* treatment* cardiac* infarction* tissue* engineering***

Number of Papers Found: 78

Discussion of the Relevancy of the Papers Found: Similar tissue engineering based experiments have already been performed. Many of these experiments did not actually culture the cells on a nanofiber in vitro before introducing them to the site of infarction. Our experiment differs from the previous experiments that did use this tissue engineering approach in a few key ways. These include the coating of the nanofiber scaffold with thymosin B4, varying times of delivery, and the injection method.

Database Used:

- | | |
|--|--|
| <input checked="" type="checkbox"/> Medline | <input type="checkbox"/> Agricola |
| <input type="checkbox"/> Toxline | <input type="checkbox"/> CAB Abstracts |
| <input type="checkbox"/> Biosis | <input type="checkbox"/> Other (Specify): Click here to enter text. |

Date of Search: 02/15/2016

Years Covered: all years

Keywords Used: **alternative animal model for treatment of cardiac infarction tissue engineering**

Number of Papers Found: 44

Discussion of the Relevancy of the Papers Found: Similar to the previous search, although many have looked into using nanofiber scaffolds as a treatment for cardiac infarctions, our experiment differs in the few key aspects listed above.

--

Disposition of Animals

29. What is the expected disposition of animals at the end of the experiments?

(Check all that apply):

Euthanized - If an infectious disease studies - carcasses decontaminated by incineration
 composting other [Click here to enter text.](#)

Maintained

Released (*Wildlife Only*)

Other (*Specify*): [Click here to enter text.](#)

30. Euthanasia*

Select methods that will be used in case of emergency and/or at the end of the procedure/experiment.

***NOTE:**

- Methods must be approved by the AVMA or must be scientifically justified.
- A “Primary” and “Secondary” method must be selected (UD Double Kill Policy).
- **If different methods will be used for different groups** of animals, indicate the group after the procedure (e.g., write “Neonates” after Decapitation, “Adults” after CO₂, “Terminal Surgery Animals” after Isoflurane Anesthesia Overdose, etc.).

Animals will NOT be under anesthesia when euthanasia is performed.

Animals will be under anesthesia when euthanasia is performed. (*Check drug used below*):

Isoflurane

Injectable (*Complete the following*):

Drug: [Click here to enter text.](#)

Dose: [Click here to enter text.](#)

Route: [Click here to enter text.](#)

PRIMARY method(s) of euthanasia

CO₂ by compressed gas cylinder (*Not for animals already under anesthesia or neonates*)

Barbiturate Euthanasia Solution - Injectable $\geq 150\text{mg/kg}$ (*Check route below*):

IV

IP

IC

Isoflurane Anesthesia Overdose - Inhalant

Cervical Dislocation (*acceptable with anesthesia, or for poultry, without anesthesia if personnel are trained*)

Decapitation (*only under anesthesia or neonates*)

<input type="checkbox"/> Exsanguination or Perfusion (<i>only under anesthesia</i>)
<input type="checkbox"/> Incision of Chest Cavity – Bilateral Pneumothorax (<i>only under anesthesia</i>)
<input type="checkbox"/> Pithing – (<i>only under anesthesia</i>) (<i>amphibians, reptiles only</i>)
<input type="checkbox"/> Removal of Vital Organ(s) (<i>only under anesthesia</i>) (<i>Check all that apply</i>): <input type="checkbox"/> Brain <input type="checkbox"/> Kidneys <input type="checkbox"/> Heart <input type="checkbox"/> GI Tract <input type="checkbox"/> Liver <input type="checkbox"/> Lungs <input type="checkbox"/> Other Vital Organ(s) – (<i>Specify</i>): Click here to enter text.
<input type="checkbox"/> Other Method of Euthanasia: (<i>Describe and Scientifically Justify</i>):
SECONDARY method(s) of euthanasia that will be used to ensure that the animal does not survive:
<input type="checkbox"/> Cervical Dislocation
<input type="checkbox"/> Decapitation
<input type="checkbox"/> Exsanguination or Perfusion
<input type="checkbox"/> Incision of Chest Cavity – Bilateral Pneumothorax
<input type="checkbox"/> Barbiturate Euthanasia Solution - Injectable $\geq 150\text{mg/kg}$ (<i>Check route below</i>): <input type="checkbox"/> IV <input type="checkbox"/> IP <input type="checkbox"/> IC
<input type="checkbox"/> Pithing – Double pithing required (<i>fish, amphibians, reptiles only</i>)
<input type="checkbox"/> Monitor for lack of respiration and heart beat (Agricultural animals only)
<input checked="" type="checkbox"/> Removal of Vital Organ(s): (<i>Check all that apply</i>): <input type="checkbox"/> Brain <input type="checkbox"/> Kidneys <input checked="" type="checkbox"/> Heart <input type="checkbox"/> GI Tract <input type="checkbox"/> Liver <input type="checkbox"/> Lungs <input type="checkbox"/> Other Vital Organ(s) – (<i>Specify</i>): Click here to enter text.
<input type="checkbox"/> Other Method of Euthanasia: (<i>Describe and Scientifically Justify</i>): Click here to enter text.

Personnel and Training

31. Personnel involved in Protocol (*Include Principal Investigator*):

Status: Indicate Prof, Post-Doc, Grad Student, Lab Manager, Research Assistant, Technician, etc.

Qualifications: Include **procedures this person is proficient in performing** on proposed species and the time they have been doing the procedure.

Be specific (e.g. sub-mandibular bleeding on mice-2yrs, performing castrations on mice and rats-1yr, tail-vein injections on mice-2yrs, etc.) **(If no experience, list who will train.)**

Responsibilities: Include **all responsibilities** this person will have with live animals on this protocol, including euthanizing animals.

Name	E-mail	Office phone number	Home/Cell phone number	Received IACUC required training Yes <input checked="" type="checkbox"/> No <input type="checkbox"/>
Arun Kumar	arunk@udel.edu	302-831-4552	Click here to enter text.	

Status: Assistant professor

Qualifications: Extensive experience in medical college performing surgeries and injections on small and large animals; training with OLAM specific practice for 3years including injections, surgeries, ultrasound, and sutures

Responsibilities: Injections (SC and intracardiac); minor surgery; ultrasound; laparoscopy

Name	E-mail	Office phone number	Home/Cell phone number	Received IACUC required training Yes <input checked="" type="checkbox"/> No <input type="checkbox"/>
Edward D. Marks	edmarks@udel.edu	302-831-3367	908-448-9771	

Status: PhD candidate

Qualifications: Small animal injections for 3years; OLAM specific practice with Gwen Talham for 2years, including major and minor surgery, suturing, SC and IP injections, ultrasound, and tail and sublingual bleeding

Responsibilities: Injections (SC and intracardiac); minor surgery; suturing; ultrasound;

checking on animals; laparoscopy

Name	E-mail	Office phone number	Home/Cell phone number	Received IACUC required training
Lauren DelMaestro	ldel@udel.edu	Click here to enter text.	908-635-1146	Yes <input checked="" type="checkbox"/> No <input type="checkbox"/>

Status: Undergraduate – junior year

Qualifications: Lauren has been volunteering in OLAM for one month, and has received training from Dr. Talham on rat handling.

Responsibilities: Lauren will be assisting Edward Marks with the procedures and potentially handling animals, but will not be doing any injections or euthanasia.

Name	E-mail	Office phone number	Home/Cell phone number	Received IACUC required training
Click here to enter text.	Click here to enter text.	Click here to enter text.	Click here to enter text.	Yes <input type="checkbox"/> No <input type="checkbox"/>

Status: Click here to enter text.

Qualifications: Click here to enter text.

Responsibilities: Click here to enter text.